Behavioural analysis of two novel mouse models of rare neurodevelopmental disorders

Hannah Wai Yiu Ng

Submitted in accordance with the requirements for the degree of Master of Science by Research

The University of Leeds

School of Biomedical Sciences

September 2020

The candidate confirms that the work submitted is her own and that appropriate credit has been given where reference has been made to the work of others.

This copy has been supplied on the understanding that it is copyright material and that no quotation from the thesis may be published without proper acknowledgement.

Acknowledgements

I would first like to express my sincere gratitude to the Ethel & Gwynne Morgan Charitable Trust for providing the funding for this important research.

I would like to give a big thank you to my supervisor, Dr Steven Clapcote, for the opportunity to work on this interesting research and for his guidance and support throughout.

I am very grateful to have worked alongside Dr Paul Armstrong and Dr Clare Tweedy, postdoctoral researchers in Clapcote lab. Thank you for making such a fun work environment! I would particularly like to thank Paul for patiently teaching me the different behavioural tests and statistics and Clare for her support and encouragement.

I would also like to extend my thanks to members of our research team, Tim Munsey for doing the genotyping, Kirstie Goodchild for scoring the jumping behaviour in PDZD8KO mice, and Dr Jamie Johnston, Jennifer Ogbeta, and Andreea Pantiru for their help and insightful discussions at our lab meetings.

Despite COVID-19 disrupting my project, I have learned so much during my Master's and it has been an invaluable and enjoyable research experience thanks to everyone mentioned above.

Abstract

Background. Heterozygous missense mutations in *ATP1A3* and homozygous nonsense mutations in *PDZD8* have been associated with alternating hemiplegia of childhood (AHC) and syndromic intellectual disability (ID) respectively. AHC is characterised by hemiplegic episodes, motor deficits, developmental delay, and cognitive impairments. ID is characterised by significant limitations both in intellectual functioning and in adaptive behaviour. Studying the *in-vivo* effects of such mutations is important for understanding the mechanisms of these neurodevelopmental disorders and developing efficacious treatments. To this end, we behaviourally characterised novel mouse models with mutation D923Y of *Atp1a3* (*Atp1a3*$^{D923Y/+}$) and null mutation of *Pdzd8* (PDZD8KO) respectively in comparison with wild type (WT) littermates.

Methods. Male and female *Atp1a3*$^{D923Y/+}$ mice aged 2-6 months underwent a range of behavioural tests including open field, elevated plus maze (EPM), elevated minus maze (EMM), delay and trace fear conditioning, and forced swimming. Female PDZD8KO mice aged 2.5 months underwent continual trial novel object recognition, spatial novelty preference, Barnes maze, social interaction, and trace fear conditioning.

Results. *Atp1a3*$^{D923Y/+}$ mice travelled more in the open field, appeared less anxious in the EPM and EMM, froze less in trace (but not delay) fear conditioning, and were less immobile in the forced swim test. Together, these results suggest that *Atp1a3*$^{D923Y/+}$ mice are hyperactive, have learning and memory impairments, and an anxiolytic-like phenotype. PDZD8KO mice displayed autistic-like features such as repetitive jumping behaviour and showed spatial memory deficits in the Barnes maze.

Conclusion. Our results reveal that mice heterozygous for the *Atp1a3*-D923Y mutation or homozygous for null mutation of *Pdzd8* replicate certain features seen in AHC or ID patients respectively, therefore establishing their validity as models for investigating disease mechanisms and novel treatments.

Table of Contents

List of Figures and Tables

Figures

Tables

Abbreviations

ADHD	Attention deficit/hyperactivity disorder
AHC	Alternating Hemiplegia of Childhood
ASD	Autism spectrum disorder
CAPOS	Cerebellar ataxia, areflexia, pes cavus, optic atrophy, and sensorineural hearing loss
CS	Conditioned stimulus
CTNOR	Continual trial novel object recognition
DSM-5	Diagnostic and Statistical Manual of Mental Disorders, Fifth Edition
ID	Intellectual disability
EEIE	Early infantile epileptic encephalopathy
EMM	Elevated minus maze
EPM	Elevated plus maze
FIPWE	Fever-induced paroxysmal weakness and encephalopathy
FMR1	Fragile X mental retardation 1
FST	Forced swim test
ITI	Intertrial interval
MAM	Mitochondrial associated membrane
MCS	Mitochondrial contact site
Mdm12	mitochondrial distribution and morphology protein 12
Mdm34	mitochondrial distribution and morphology protein 34
Mdm10	mitochondrial distribution and morphology protein 10
Mmm1	maintenance of mitochondrial morphology protein 1
NDD	Neurodevelopment disorders
NKA	Na^+,K^+-ATPase
OCD	Obsessive Compulsive Disorder
OF	Open field
PDZD8	PDZ domain containing 8
RECA	Relapsing encephalopathy with cerebellar ataxia
RDP	Rapid-onset dystonia parkinsonism
SMP	Synaptotagmin-like mitochondrial lipid-binding proteins
SUDEP	Sudden unexpected death from epilepsy
TULIP	Tubular lipid-binding protein
US	Unconditioned stimulus
XLID	X-linked intellectual disability

Chapter 1

The use of *Atp1a3* mutant mice to model Alternating Hemiplegia of Childhood

1.1 Introduction

1.1.1 Alternating Hemiplegia of Childhood – an overview

Alternating hemiplegia of childhood (AHC; OMIM # 614820) is an early onset neurodevelopmental disorder first described in 1971 (1). The defining characteristic of AHC is paroxysmal episodes of hemiplegia, in which the body undergoes temporary paralysis that can alternate between both sides of the body (1). Duration and frequency of attacks are variable, lasting from a few minutes to several days and occurring once or many times a day (2). Other manifestations that occur in isolation or alongside hemiplegia attacks include dystonia, ataxia, abnormal eye movements, and seizures (2). These paroxysmal events are commonly associated with triggers that precede or cause the attack such as stress, excitement, extreme temperatures, bathing, physical activities, and lighting changes (3). A characteristic feature of AHC is that all motor symptoms disappear with sleep (3), however atypical cases of AHC have been reported in which hemiplegic attacks arise from sleep without the association of developmental and cognitive decline, known as benign familial nocturnal alternating hemiplegia of childhood (4).

In addition to paroxysmal episodes, AHC patients often present with neurological abnormalities such as developmental delay and intellectual disability, both of which become more apparent with age (5). These cognitive symptoms can be easily overlooked as paroxysmal attacks are immediately more noticeable. In a recent study of neuropsychological profiles of 25 AHC patients, 72% had deficits in intellectual functioning and 60% had neuropsychiatric diagnoses, based on DSM-5 classification (6). The degree of severity was variable amongst patients and of those diagnosed with neuropsychiatric disorders, the majority had attention deficit hyperactivity disorder (ADHD).

The name of the disorder, “alternating hemiplegia of childhood”, suggests that patients are affected solely during childhood. However, symptoms of AHC patients present throughout the course of patients’ lives; abnormal ocular movements and hypotonia

regress, but do not disappear, into adulthood (7). It is not clear whether AHC is a progressive disorder but abrupt stepwise deterioration (8) and progressive brain atrophy in AHC patients have been reported (9, 10). AHC patients present with variable symptoms and severity of disease, with some experiencing mild symptoms (11), whereas others have died from seizures, known as sudden unexpected death from epilepsy (SUDEP) (12).

In the great majority of cases, AHC is caused by a mutation in the gene *ATP1A3* which encodes the α3 subunit of Na^+,K^+-ATPase (NKA), a pump essential for the maintenance of Na^+ and K^+ gradients across plasma membranes in all animal cells (13). Very rare familial cases of AHC, with autosomal dominant inheritance and causal *ATP1A3* mutations identified, have also been reported (14, 15). Onset is within 18 months of birth and affects an estimated 1:1,000,000 children (16), although one recent publication has since reported the incidence as 1:100,000 (17). Phenotypic variability and lack of disease awareness, leading to the underdiagnosis and misdiagnosis of AHC, are likely the reasons behind the range of incidences. Moreover, epilepsy is comorbid with AHC in 50% of AHC patients (16), which has also resulted in diagnostic difficulties.

No current treatments are able to cure AHC, but there are treatments that can control some symptoms. Given that symptoms disappear upon sleep in AHC patients, sleep-inducing agents such as benzodiazepines have been used (18). However, the most commonly used treatment is flunarizine, a selective Ca^{2+} entry blocker. Although not effective in all patients, anecdotal reports suggest that flunarizine reduces the severity, duration and frequency of paralytic episodes (19). It is hypothesised that flunarizine blocks the entry of Ca^{2+} into neurons via voltage-gated Ca^{2+} channels and thus reduces neuronal hyperexcitability (19). There still remains a high demand for more effective treatments but several barriers to creating specific therapeutic strategies exist: the course of the disease is highly variable, there has been a lack of longitudinal follow-up, and knowledge regarding the aetiology of AHC is limited.

1.1.2 Na^+/K^+-ATPase

1.1.2.1 Structure and function

The NKA is a transmembrane protein that hydrolyses ATP to allow for the exchange of three Na^+ for two K^+ ions across the cell membrane against their concentration gradient. This process is essential as the resultant gradients created are required for the resting membrane potential, action potentials, and secretion of neurotransmitters (20, 21). NKA is expressed throughout the brain and consumes approximately 50% of the energy of ATP hydrolysis in the CNS (22).

The pump is composed of a complex containing α-subunit, β-subunit and γ-subunit (Fig. 1). Mammals express four NKA α-isoforms: α1 is expressed ubiquitously, α2 in glial cells, α3 in neurons, and α4 in testis (20). The α-subunit of the NKA has three cytoplasmic domains – nucleotide binding (N), phosphorylation (P), and actuator (A) – and a transmembrane region consisting of ten transmembrane helices (M1-M10) and extracellular loops (13, 23). The exact location of the ouabain (NKA inhibitor) binding site is unknown, but it is thought to be mainly found in the M5-M6 extracellular loop (24). There are three Na^+ binding sites (sites I, II, III), located offset to the M4 and M5 region (25). Mammals also express three β and seven γ-subunit isoforms. The β and γ-subunit are in contact with α-subunit transmembrane helices M7/M10 and M9, respectively, and both have a modulatory effect by altering the affinity of Na^+ and K^+ to NKA, and help stabilise the enzyme (13, 26).

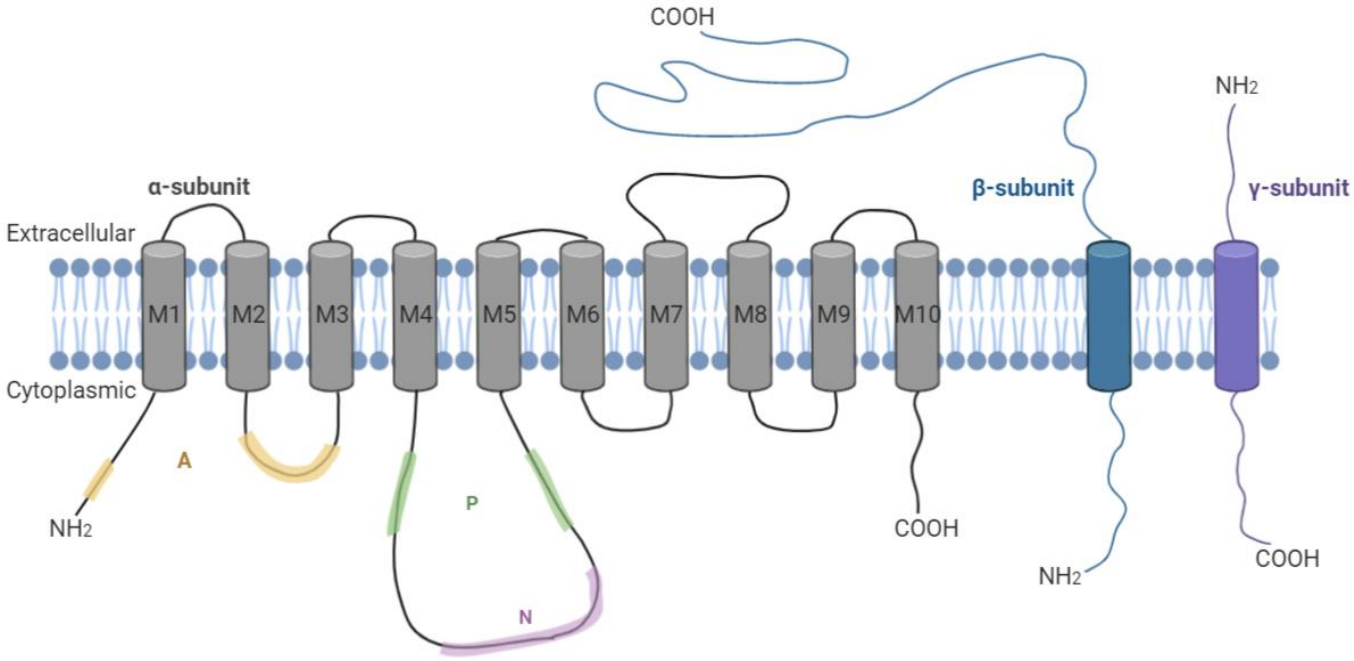

Figure 1. Structure of NKA. The enzyme consists of a complex made up of α-subunit, β-subunit, and γ-subunit. The α-subunit has three cytoplasmic domains, nucleotide binding (N), phosphorylation (P), and actuator (A), and one transmembrane region consisting of 10 transmembrane helices and extracellular loops. The ouabain binding site is thought to be located in the M5-M6 extracellular loop.

The exchange of ions occurs through the transitioning of major conformational states which can be described by the post-Albers model (Fig. 2), E_1 and E_1P (high affinity for Na^+, facing intracellular side) and E_2 and E_2P (high affinity for K^+, not Na^+, facing extracellular side) (13). E_1 binds Na^+ ions at three different sites; crystal structures predict they first bind the Na^+ site III, and then sites I and II (25). This leads to E_1P phosphorylation by ATP and allows the release of three Na^+ ions onto the extracellular side, resulting in E_2P conformation which has a high affinity for K^+. Two K^+ ions will then bind to E_2P, Pi will be hydrolysed, and the ions will become occluded (E_2 state). ATP will then bind and accelerate the disocclusion of K^+.

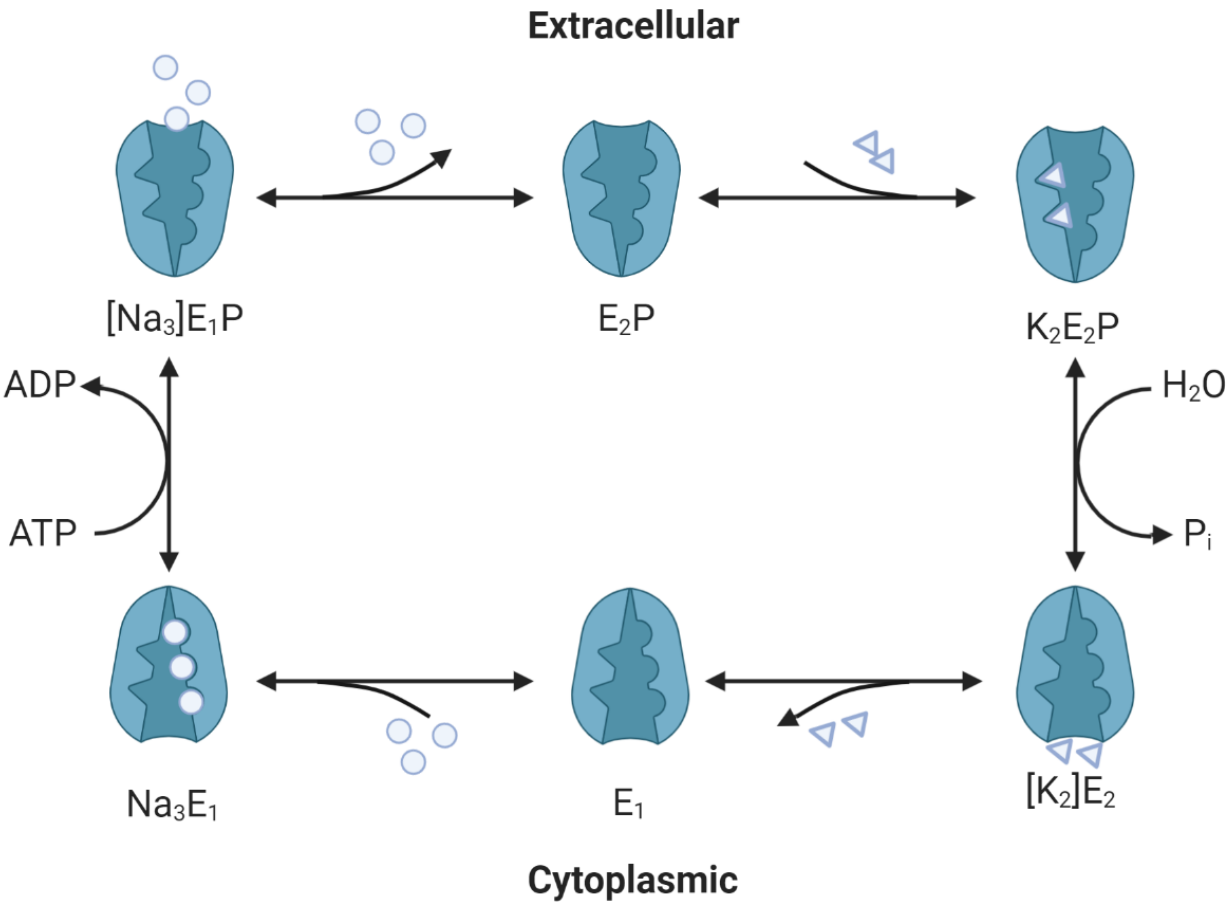

Figure 2. Post-Albers Na^+/K^+-ATPase reaction cycle. E_1 represents the conformation of NKA which has a high affinity for Na^+ ions. This allows three Na^+ ions to bind NKA from the cytoplasmic side. This results in the phosphorylation of NKA by bound ATP. Three Na+ ions are released into the extracellular side and two K+ ions bind. NKA auto-dephosphorylates by hydrolysis, and the two K+ ions are released. Diagram modified from (21, 27).

1.1.2.2 α3-isoform mutations

The *ATP1A3* gene on chromosome 19q13.2 encodes the α3 subunit of the NKA (21). Alternative splicing of *ATP1A3* can result in different transcript variants, of which distribution and function are unknown. In humans, there are three transcripts: variant 1/isoform 1 (1,013 aa), variant 2/isoform 2 (1,024 aa), variant 3/isoform 3 (1,026 aa). In mice there are two transcripts: variant 1/isoform 1 (1,026 aa) and transcript variant 2/isoform 2 (1,013 aa).

Mutations in the α3 isoform result in a phenotypic continuum of neurological disorders including alternating hemiplegia of childhood (AHC), rapid-onset dystonia parkinsonism (RDP, also known as DYT12), CAPOS (Cerebellar ataxia, Areflexia, Pes cavus, Optic atrophy, and Sensorineural hearing loss) syndrome, relapsing encephalopathy with cerebellar ataxia (RECA), early infantile epileptic encephalopathy (EEIE), fever-induced paroxysmal weakness and encephalopathy (FIPWE), and intermediate phenotypes (20). AHC was previously thought to be caused by a missense mutation in *ATP1A2*, due to a reported familial case (28), but mutation analysis in classic sporadic AHC patients and in an additional five kindreds failed to identify additional mutations in *ATP1A2* (29). There is now substantial evidence that *de novo* heterozygous mutations in the *ATP1A3* gene are the primary cause of AHC (12, 15, 30).

Most AHC mutations are concentrated in the ten transmembrane helices of NKA, which contrasts DYT12 where most mutations are distributed throughout the protein (15). Many AHC-causing mutations affect ion binding sites, therefore suggesting ion binding and transport are affected in AHC (31). Next generation sequencing of patients with AHC have identified *ATP1A3* mutations, and of those the most frequently occurring are D801N, E815K and G947R (Fig. 3) (12, 15, 32). These mutations result in different severities of clinical features in humans with AHC and also have differential effects on NKA structure and function (Table 1) (12, 20, 33).

The precise mechanism of how an α3 subunit mutation causes neurological dysfunction is unclear, but it is hypothesised that mutations in the *ATP1A3* gene impair Na^+ and K^+ transport across neuronal plasma membranes, consequently causing the imbalance of electrochemical gradients. Perturbed NKA activity may cause Na^+ to accumulate intracellularly as less is pumped out of the cell, causing the resultant ion gradient to prevent the influx of Na^+ via the Na^+/Ca^{2+} exchanger (17). Subsequently, less Ca^{2+} is exchanged for Na^+ which causes the increase of intracellular Ca^{2+} within the neuron, which

may eventually lead to cell death. Signalling pathways downstream of NKA are also affected, such as phospho-activation of ERK, as seen in mania models (34).

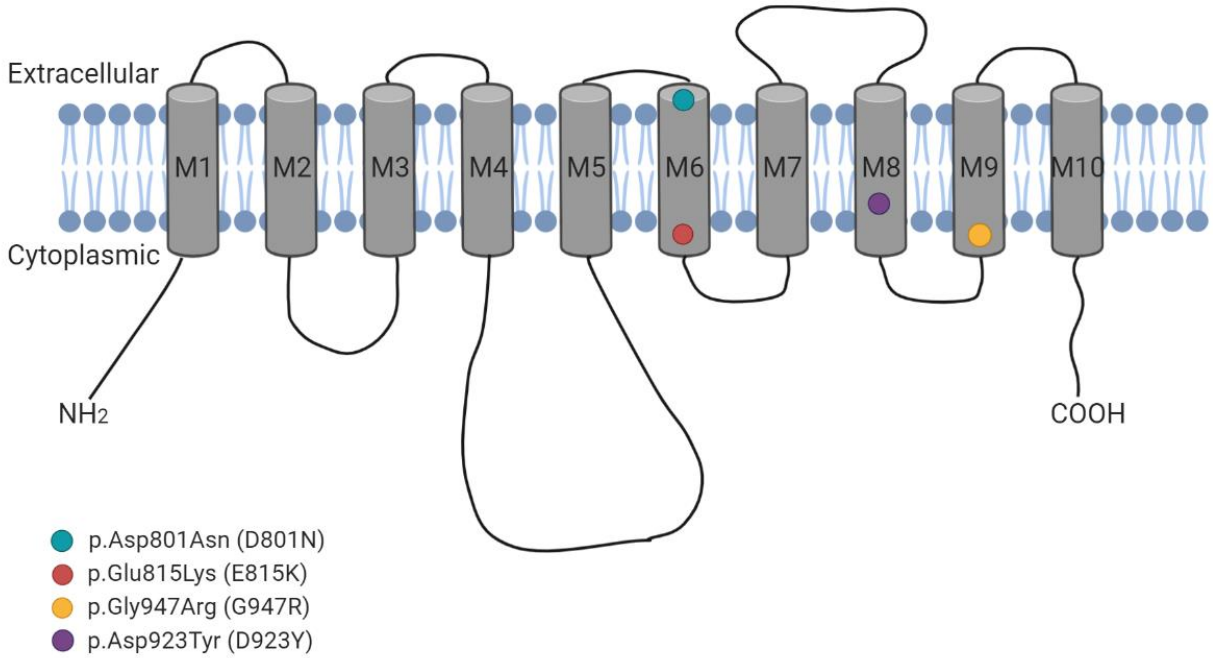

Figure 3. Diagram showing the α3 subunit transmembrane region consisting of 10 transmembrane helices, with the location of the three most common mutations and the mutant D923Y. p.Asp801Asn and p.Glu815Lys are located in M6, p.Gly947Arg is located in M9, and p.Asp923Tyr is located in M8.

AHC-causing mutation	Clinical features			Relative severity	Effect on NKA α3 structure and function	References
	Intellectual disability	Motor disability	Epilepsy frequency and seizure onset			
p.Asp801Asn (D801N)	Moderate	Severe dystonia	Less frequent Occurs later in life (median 5 years)	Moderate	Loss of electrostatic interaction between 2 K^+ ions, which results in the blocking of the K^+ pore and the passage of Na^+ and K^+	(15, 33)
p.Glu815Lys (E815K)	Severe	Mild dystonia	More frequent Occurs earlier in life (during first year of life)	Severe	Disrupts hydrogen bonding network between loops of the transmembrane domains and affects Na^+ affinity of site III	(20)
p.Gly947Arg (G947R)	Mild	Least dystonic	Less frequent (than D801N) Occurs earlier in life (earlier than E815K)	Mild	Disrupts Na^+ site III binding site of NKA through the destabilisation of Y768, caused by the arginine residue	(20, 35)

Table 1. Table showing the three most common AHC-causing mutations, the severity of clinical features relative to each other, and their known effects on NKA α3 structure and function.

1.1.2.3 Ouabain and Rostafuroxin

Endogenous ouabain is a cardiotonic steroid hormone released from the hypothalamus that binds the NKA α-subunit and inhibits its activity (36). The release of ouabain has been associated with stressor stimuli such as physical exercise and swim stress (37, 38). Therefore, stress-induced release of ouabain and consequent inhibition of NKA might be involved in the triggering of hemiplegic episodes in AHC patients. Although immunoneutralisation of ouabain can be achieved via intracerebroventricular injection using anti-ouabain antibodies (39), this is an invasive method when considering translatability to AHC patients. Alternatively, oral administration of rostafuroxin, a synthetic steroid with a similar structure to ouabain, can antagonise and displace ouabain without inhibiting NKA (40). In addition, one study has suggested that rostafuroxin can antagonise effects of ouabain in the brain, as it prevented the augmentation of glutamate-evoked Ca^{2+} signals in primary cultured rat hippocampal neurons (41). Rostafuroxin has also been tested on *Atp1a3*-I810N (*Myshkin*) mice, in which chronic treatment reduced mania-like behaviours. Together, these findings highlight rostafuroxin as a potential treatment for AHC.

1.1.3 Genetically-altered mouse models of AHC

Animal models have been indispensable in advancing our knowledge of diseases, but it is ultimately impossible to find an animal model that recapitulates all the symptoms of a particular disease – especially neurological diseases which encapsulate a range of motor, cognitive and psychiatric symptoms. Mice are useful models given the ease with which their genome can be manipulated and their genomic similarity to humans – the mouse orthologue *Atp1a3* has 99.6% protein and 90.8% identity relative to human *ATP1A3* (HomoloGene:113729*)*. Since the discovery of AHC, *Atp1a3* knock-out and knock-in models have been created (Table 2).

Mouse Model	Genetic background strain	Genetic Alteration	Behavioural Observations	Investigations		References
				Genotype difference	No genotype difference	
Atp1a3^{Myk}, *Atp1a3*^{I810N}, *Myshkin*	C57BL/6NCr	Missense I810N mutation	Increased locomotor activity Manic-like behaviours Low body weight Motor deficits Learning and memory deficits Social behaviour deficits Increased sensitivity to amphetamine Altered circadian rhythms Seizures SUDEP	Open field Balance beam Gait analysis Tail suspension Rotarod* Morris water maze Contextual fear conditioning Conditioned taste aversion Novel object recognition Hole-board test Elevated plus maze Light/dark box Y maze T maze Social recognition**	Grip strength	(33, 34, 42-45)

				Nest building Pup retrieval Three-chamber social approach Forced swim		
Atp1a3^{tm1Ling}	129/Black Swiss	Point mutation in intron 4 of *Atp1a3*	Increased locomotor activity Motor deficits Learning and memory deficits Increased sensitivity to amphetamine	Open field Morris water maze Balance beam*** Rotarod*** Elevated zero maze Novel object recognition Grip strength	Elevated zero maze Novel object recognition Grip strength	(46-48)
Atp1a3^{tm2Kwk}	C57BL/6J	Deletion of exons 2-6 of *Atp1a3* (KO)	Increased locomotor activity Stress-induced motor deficits Increased sensitivity to kainate-induced dystonia	Open field Rotarod**** Balance beam****		(49)

Atp1a3^{E815K}, Matoub, Matb	C57BL/6J	E815K mutation	Hemiplegic episodes Dystonia Reduced locomotor activity Reduced exploratory behaviour Low body weight Motor deficits Learning and memory deficits Seizures	Open field Balance beam Gait analysis Tail suspension test Rotarod Novel object recognition Forced swim	Grip strength	(50)
Atp1a3^{D801N}, Mashlool,	C57BL/6	D801N mutation	Hemiplegic episodes Dystonia Increased locomotor activity Increased exploratory behaviour Low body weight Learning and memory deficits	Open field Balance beam Gait analysis Morris water maze***** Novel object recognition	Grip strength Rotarod Fear conditioning	(51)

			Motor deficits			
Atp1a3^{D801Y}, $\alpha_3^{+/D801Y}$	C57BL/6JRj	D801Y mutation	Hypothermia induced dystonia Increased locomotor activity Learning and memory deficits Hypothermia induced motor deficits No spontaneous seizures but reduced seizure threshold	Open field Elevated plus maze Barnes maze Passive avoidance Forced swimming in 5-10°C cold water	Gait analysis	(52, 53)

*significant on the first day, not the following 4 days
**significant in 2 minute observation, not in 10 minute observation
***in females, not males
****enhanced performances compared with WT
*****not considered reliable enough to assess spatial memory

Table 2. Table summarising behavioural assays and observations researched in current mouse models of AHC.

1.1.3.1 Modelling hemiplegic episodes and dystonia

Hemiplegic episodes are a debilitating symptom of AHC that can last from minutes to days (2). During these episodes, patients may experience weakness and paralysis, which can alternate in laterality (hemiplegia) or affect the whole body (quadriplegia) (3). It would be valuable to find a mouse model that replicates hemiplegic episodes seen in humans to aid the development of potential AHC therapeutics, as the most common treatment currently is flunarizine, which reduces hemiplegic episodes in some patients (19).

Despite hemiplegia being an inherent symptomatic feature of AHC, surprisingly few mouse models have been tested for it. Of the six AHC mouse models currently published, only two, Mashl (D801N) and Matb (E815K), have characterised hemiplegia (50, 51). Hemiplegia was observed in Mashl and Matb from 8 weeks and at the time of weaning, respectively, in response to stress such as the forced swim test. This is consistent with what is seen in AHC patients, as exposure to water can induce hemiplegia (3). Less stressful triggers such as handling and introduction of mice to a new cage also induced episodes, suggesting these models have a high sensitivity to stress. Moreover, flunarizine-treated Matb mice experienced fewer hemiplegic attacks compared to vehicle-treated mice (50), which is similar to reported data in AHC patients, further suggesting that Matb mice have a phenotype similar to AHC patients with the E815K mutation.

As the name of the disease states, hemiplegia can alternate between both sides of the body. Only Mashl mice are reported to display hemiplegia with this feature, where stress-induced hemiplegia began unilaterally and alternated between sides within the same episode (51). Whilst Matb mice displayed hemiplegia, it is not mentioned whether it alternated within each episode.

Although hemiplegia has not been reported in *Myshkin* (I810N) mice, they do exhibit hemiplegic episodes (S. Clapcote, personal communication) and have other severe motor deficits that replicate aspects of the AHC phenotype (33). *Myshkin* mice have a total NKA activity reduction of ~42% and display splayed hind limbs when moving (33). This can be likened to diplegia found in humans, which is paralysis that affects symmetrical sides of the body (such as arms or legs), and is different to hemiplegia which affects one side of the body (right or left). Moreover, hind-limb clasping was evident in *Myshkin* mice when suspended by their tails, which is indicative of motor dysfunction (54). This may mimic dystonic episodes seen in AHC patients.

Atp1a3^{D801Y} mice exhibited hypothermia-induced dystonia characterised by hyper-extension of limbs and abnormal postures in response to forced swimming in 5-10°C water (53). Interestingly, other stressors such as forced swim in warm water, hyperthermia, restraining, and foot shocks did not cause dystonia. Nevertheless, this observation is similar to the abrupt onset of motor impairments seen in AHC patients that can be caused by temperature changes.

1.1.3.2 Modelling cognitive disturbances

Most AHC patients present with developmental delay and intellectual disability (6, 7). The neuropsychological profile of AHC ranges widely amongst patients, so characterisation is essential to plan for appropriate interventions. In rodent studies, there are several cognitive paradigms that can be used to assess mutant mice. The phenotype of mutant mice is often heterogeneous, so it is crucial to assess different aspects of cognition such as learning, memory, and attention. Besides the *Atp1a3*^{tm2Kwk} mouse model, all AHC models are reported to have learning and memory deficits.

1.1.3.2.1 Fear memory

Myshkin (*Atp1a3*^{I810N}) mice have reduced fear memory, which was tested via fear conditioning and passive avoidance (33, 43, 52). Fear conditioning assesses the ability of an animal to learn and remember an association between an environment and foot shock (contextual fear conditioning), or between an auditory tone and foot shock (cued fear conditioning) (55). Consequently, mice freeze in response to the context or cue alone. In delay fear conditioning, the tone cue (or conditioned stimulus, CS) is immediately followed by the foot shock (or unconditioned stimulus, US). In trace fear conditioning, there is an interval between the end of the CS and beginning of the US.

In both delay and trace fear conditioning, *Myshkin* mice froze less than WT mice to the CS, suggesting potential cognitive impairment (33, 43). However, it is crucial to account for any baseline freezing to interpret the results wholly. In trace fear conditioning, *Myshkin* mice showed less baseline freezing than WT mice during conditioning (43). Therefore, the results of the cue test may be confounded by the hyperactive phenotype of *Myshkin* mice (34). Despite this, during the cue test, *Myshkin* mice froze significantly more in response to the CS, indicating intact fear memory (43). It is interesting that no significant difference in baseline freezing was observed in delay fear conditioning (33), indicating that low baseline freezing is not observed across different types of fear conditioning. Nevertheless,

Kirshenbaum et al. (5) tested and found a deficit in another form of associative learning, conditioned taste aversion, which cannot be confounded by hyperactivity.

1.1.3.2.2 Recognition memory

Unlike *Myshkin* mice, fear conditioning was normal in Mashl mutants (51). Instead, these mice had deficits in novel object recognition. The time taken for mice to explore a novel object relative to a familiar object provides an indication of recognition memory (56). 24 hrs after exposure to identical objects, also known as the intertrial interval (ITI), Mashl mice did not show a preference for the novel object over the familiar object and also spent less time exploring it compared to WT mice (51). Fear conditioning and novel object recognition test different aspects of memory (fear and recognition memory, respectively) which may explain these discrepancies between both AHC mouse models (55, 56). Moreover, longer ITIs such as 24 h, seemingly reveal deficits in recognition memory in some AHC mouse models compared to shorter ITIs. One study of *Atp1a3*$^{tm1Ling/+}$ mice found no significant preference for the novel object compared to their WT counterparts with a 1h intertrial interval (ITI) (46). However, in a separate study with a 24h ITI and chronic variable stress protocol, *Atp1a3*$^{tm1Ling/+}$ mice spent equal time exploring both the novel and familiar object (48). Similarly, Matb mice did not show a preference for the novel object over the familiar object with a 24h ITI (50). Together, these findings suggest that disruption in NKA may result in long term memory deficits in the novel object recognition task.

1.1.3.2.3 Spatial memory

The hippocampus is essential for the generation of long-term memory and spatial learning (57). The Barnes maze and Morris water maze are often used to test spatial memory in rodents, and both function to measure the ability of rodents to learn and locate a target zone by using spatial cues (58). The Barnes maze consists of one circular platform with holes around the circumference with an escape box underneath one of the holes, and mice are given training trials to locate the escape hole. On the test day, also known as the probe trial, the escape box is removed, and the time spent by mice in the target zone is measured.

Atp1a3$^{D801Y/+}$ mice were tested on the Barnes maze and were able locate the escape box, but took significantly longer than WT mice to enter, which was thought to be a result of the stressful environment of the Barnes maze (52). Strategy analysis was also measured during training and the probe trial; serial strategies are described as mice chaining along

the holes, and direct strategies describe focal or direct movement to the target hole. During training, strategy analysis revealed that serial and direct strategies were equally used between genotypes, however at day 12 (probe trial), more *Atp1a3*$^{D801Y/+}$ mice used a serial strategy than direct, therefore suggesting potential long-term memory impairment, but intact short-term memory. This is consistent with the results of AHC mouse models on the novel object recognition task, in which long term memory rather than short term memory is thought to be affected.

Mashlool and *Atp1a3*^{tm1Ling} mice were tested on the Morris water maze, and *Myshkin* mice (43, 46, 51). Similar to the Barnes maze, mice are given training trials, in which they must swim and learn to locate a platform. Mashlool and *Atp1a3*^{tm1Ling} mice located the platform slower than WT mice in the probe test, therefore suggesting that they have deficits in spatial memory however the results of Mashlool mice were considered not reliable enough to assess spatial memory. *Myshkin* mice were also tested on an apparatus similar to the Morris water maze, known as the visible platform water maze, which is not a spatial test as it involves mice locating a visible platform rather than a hidden one. Instead, the Y-maze was used to assess short term spatial memory in *Myshkin* mice, in which mice are allowed to freely explore the three arms. Mice have a tendency to enter the least recently visited arm, therefore resulting in alternation between the three arms (59). The percentage of alternation in *Myshkin* mice did not significantly exceed chance level (50%). Together, these suggest that NKA dysfunction may affect spatial memory.

1.1.3.3 Modelling motor disturbances

To characterise dysfunction in motor co-ordination and balance, mice have been tested on the balance beam, a horizontal wooden dowel that the mice traverse. *Myshkin*, *Atp1a3*^{tm1Ling}, Matb and Mashl mice displayed an increased latency to cross the beam with increased foot slips compared to their WT littermates (33, 47, 50, 51). The *Myshkin* and Mashl models were the only ones to report tremors, ataxia or hind-limb dragging (33, 51). Restraint-stressed female *Atp1a3*^{tm1Ling} mice similarly exhibited deficits in beam walking, and displayed a 2.5-fold increase in hind limb slips compared with non-stressed female *Atp1a3*^{tm1Ling} mice (47). However, this difference was not replicated in *Atp1a3*^{tm1Ling} males, suggesting a potential sex difference – sensitivity to restraint stress is known to be sex dependent (60).

The rotarod test, which is also a measure of motor abnormality, has shown more contradictory results. Average latency to fall off the rod was shorter in Matb, *Atp1a3*^{tm2Kwk}

and *Atp1a3*^{tm1Ling} mice than respective WTs (47, 49, 50). Matb had 3 trials each day for 3 days; *Atp1a3*^{tm2Kwk} mice were tested on consecutive three days after 4 days of training (one trial each day); and *Atp1a3*^{tm1Ling} had 3 trials every day for 2 days. *Myshkin* mice fell off quicker on the first day, but not on the following four days, suggesting intact motor learning (33). This is surprising given that *Myshkin* mice showed learning and memory impairments in fear conditioning and novel object recognition (33, 43). However, it has previously been shown that rodents with lesioned hippocampi show no impairments in motor learning but impairments in memory tasks (61). Another reason for this difference may be due to the brain areas affected by the mutation – neuropathology of *Myshkin* hippocampus shows histological sequela of seizures (42). *Myshkin* mice are also notably smaller in size (62). Mouse weight can be a confound of the rotarod test; mutations which result in weight loss may offset motor disability as small mice tend to perform better than heavier mice (63).

Motor impairments were seemingly more apparent in the balance beam compared to the rotarod. This pattern has been similarly noted in mouse models of dystonia (64, 65). Whilst the rotarod and balance beam are similar, the rotarod test focuses more on gross motor skills whereas the balance beam tests fine motor skills (66). Therefore, the balance beam is more likely to detect subtle motor deficits than the rotarod. Motor dysfunction was shown to be caused by neurological deficits and not muscle weakness, as grip strength was found to be intact in all AHC mouse models tested (*Myshkin*, *Atp1a3* ^{tm1Ling}, Matb and Mashl) (33, 47, 50, 51).

In contrast, *Atp1a3*^{tm2Kwk} mice performed significantly better than their WT littermates on the balance beam and rotarod (49). They required less time to traverse the beam to reach the escape box and took longer to fall off the rotarod. It is unclear whether and how these results have clinical relevance. *Atp1a3*^{tm2Kwk} are heterozygous KO and seem to have milder phenotypic deficits than heterozygous missense mice. Moreover, this difference is unlikely related to age differences as the other mouse models also performed behavioural tests around the same age (post-natal week 8-14). Sex differences may have an influence as this behavioural assay was only performed on males, whereas the majority of the other AHC mouse models investigated both sexes. In the *Atp1a3*^{tm1Ling} model, stressed females displayed motor deficits but not in males, again revealing a potential sex difference (47). To date, there has been no published sex difference in disease prevalence, but there is unpublished anecdotal evidence from carers that male AHC patients tend to have a more

severe clinical phenotype than females. Nevertheless, research inclusive of both sexes is more useful.

1.1.3.4 Modelling neuropsychiatric symptoms

1.1.3.4.1 Mania

NKA α subunit genes are associated with bipolar disorder but the role of individual subunits in the pathophysiology of the disease is unclear (45). Bipolar disorder is a mood disorder characterised by characterised by periods of depression and periods of abnormally elevated mood (mania) (34). A NKA α3 mutation has also been found in a patient with schizophrenia (67). AHC patients are prone to psychiatric symptoms and exhibit mania-like symptoms, in particular, episodes of hyperactivity (45). This is a common symptom of AHC patients and is likened to manic episodes experienced by those with bipolar disorder.

The majority of AHC mouse models exhibit increased locomotor activity in the open field, which is indicative of hyperactivity (34, 46, 49, 51, 52). Matb mice, which carry the E815K mutation, are the only ones not to follow this trend, and instead are hypoactive (50). They move less and show an increased latency to begin locomotion. This contrast in locomotor activity could be explained by the severity of AHC phenotypes. There is a phenotypic spectrum of the disease as patients with the E815K mutation tend to have a more severe form of AHC than D810N, the most commonly occurring mutation in AHC (30). Symptom onset is earlier, motor and cognitive functions are more severely impaired, and patients have an increased likelihood of developing epilepsy (15). Similar to humans, Matb also have a relatively severe AHC phenotype, particularly in terms of motor function as episodes of hind-limb dragging have been previously described (50). This motor impairment may therefore provide an explanation for the hypoactivity.

Whilst the majority of models have displayed hyperactivity, the mania phenotype has been most characterised in *Myshkin* mice (34). Patients with bipolar disorder, who have manic episodes similar to those observed in AHC, are particularly sensitive to amphetamine which exacerbates hyperactivity (68), and also have a reduced need for sleep (69). Consistent with this, *Myshkin* mice were likewise more sensitive to amphetamine and had altered circadian rhythms compared to WTs – they spent a significantly longer time awake and had less REM and non-REM sleep (34, 45).

Symptoms of mania in humans also include increased risk-taking behaviours alongside reduced anxiety levels (45). Anxiolytic-like phenotypes were revealed in *Myshkin* and

Atp1a3$^{D801Y/+}$ mice via the elevated plus maze (EPM), where they entered and spent more time in the open arms compared to WT mice (34, 52). Additionally, *Myshkin* mice displayed more head dips in the EPM and showed a preference for the light side in the light-dark box, which are both indicative of exploratory and risk-taking behaviours. It was also noted that *Atp1a3*$^{D801Y/+}$ mice jumped off platforms during behavioural tests despite the risk of injuring themselves, again supporting this manic phenotype (52).

1.1.3.5 Modelling other manifestations

1.1.3.5.1 Seizures and SUDEP

AHC is often comorbid with epilepsy, a debilitating condition of the brain characterised by recurrent seizures (70). Approximately 50% of AHC patients have been reported to have epilepsy and experience seizures characterised by tonic-clonic activity (70). Among epilepsy patients as a whole, up to 70% are able to fully control their seizures with medication but many are still unresponsive, therefore there is a high demand for more effective treatments (71).

Seizures manifest from the hyper-synchronisation of cortical neurons which arise from the disruption of ion homeostasis, and genetic mutations in ion channels and transporters can contribute to this imbalance (72). 65% of all forms of epilepsy are considered idiopathic (73), and are therefore believed to have a genetic basis (72). The NKA pump is essential for the maintenance of Na^+ and K^+ gradients across the plasma membrane and is required for the resting membrane potential, action potentials, and secretion of neurotransmitters (20). Mutations in NKA α3 can perturb the electrochemical gradient and cause a reduction in NKA activity, which supposedly facilitate seizures (74). Inhibition of NKA activity is shown to produce seizure activity, as shown by experiments using the NKA inhibitor, ouabain (75).

Seizures have been observed at the age of weaning in *Myshkin* mice and these were characterised by a plethora of behaviours including jumping, jerking, freezing, salivating, and hind limb extension (42). The mice are highly susceptible to seizures – even vestibular stress, such as shaking of the cage, induces them. Sudden death or SUDEP was observed in *Myshkin* mice, and also in Matb, and Mashl mice (42, 50, 51). Interestingly, *Myk*/+/BAC transgenic mice, which carry an extra copy of WT NKA α3, showed a 16% increase in NKA activity and no seizures were observed (62). This is consistent with the hypothesis that reduced NKA activity is correlated with seizure activity and also highlights the importance of α3 isoform specificity in epileptic activity and seizures.

Mashl displayed spontaneous seizures and showed a predisposition to flurothyl-induced seizures and kindling (51). This resembles AHC patients who are also predisposed to focal and generalised seizures (7). Similarly, *Atp1a3*$^{D801Y/+}$ mice displayed a lower threshold for pentylenetetrazole-induced seizures compared to WT mice, but no spontaneous seizures were observed (52). No seizures were seen in *Atp1a3*^{tm2Kwk} mice either (49).

1.1.3.5.2 Body weight

AHC patients tend to be smaller and have a lower body weight, which has been hypothesised to be due to feeding and swallowing difficulties, therefore resulting in reduced calorie consumption (7). It is hard to investigate swallowing capabilities of mice; therefore, it is no surprise that few AHC mouse models have addressed this symptom. Despite this, *Myshkin*, Mashl, and Matb mice weighed less than their WT littermates, which is consistent with observations in AHC patients (33, 42, 50, 51, 62). One study found body weight reductions of 18% in males and 16% in females of *Myshkin* mice compared to WT mice (62). *Myshkin* mice were also observed to have a shorter trunk length (distance between the forelimbs and hindlimbs) compared to WT mice (62). A study of energy metabolism using comprehensive lab animal monitoring system (CLAMS) cages revealed that *Myshkin* mice have elevated basal metabolic rates and decreased hopper visits, suggesting their low weight may be attributed to both feeding deficits and a high metabolic rate (45). *Myk*/+/BAC transgenic mice were of normal body size and weight, therefore showing that NKA activity levels likely correlate with body weight amongst other symptoms (62).

1.1.4 D923Y Mutation

There are AHC and DYT12 causing mutations that target the same residue, namely positions in the NKA α3 subunit, Ile274, Asp801, and Asp923 (15, 76). Asp923 mutants, which are located in M8, include D923N, which is associated with DYT12 and familial AHC, and mutant D923Y, which is associated with AHC. Interestingly, this could suggest that amino acid changes may determine the severity of clinical phenotype between AHC and DYT12, and may therefore explain the comparatively mild and late onset phenotype of DYT12 compared with AHC (76).

As previously mentioned, NKA α3 E1 binds Na^+ at three different sites, first site III, then sites I and II (25). It has been shown that mutation D923N reduces Na^+ site III affinity which results in K^+ binding impairment (77). One study showed that reduced Na^+ affinity, caused by D928N (α1 equivalent of D923N), was rescued by the introduction of a second site mutation, E314D (E309D in α3) – a glutamate located in the M4 extracellular helix (78). Remarkably, this mutation increased Na^+ affinity 10-fold and resulted in K^+ uptake higher than that of WT. AHC D923Y mutation also likely disturbs the Na^+ site III given its bulky tyrosine residue (20). In an unpublished study, our collaborator, Bente Vilsen, found that D923Y reduced NKA α3 activity to 15% of WT levels in transfected COS cells, and interestingly, the introduction of second-site mutation, E309D, caused a 2-fold increase in α3-D923Y activity, but not to WT levels (Fig. 4). Mutant E309D is thought to prevent E309 and N119 in M2 from forming a hydrogen bond, thus causing M4 reorientation which may consequently affect Na^+ site II binding (20, 78). Together, these findings suggest that introduction of second-site mutation E309D to D923N/Y may rescue reduced Na^+ affinity and restore NKA pump function. Targeted breakage of this hydrogen bond through drug administration may therefore yield therapeutic potential as a treatment for AHC.

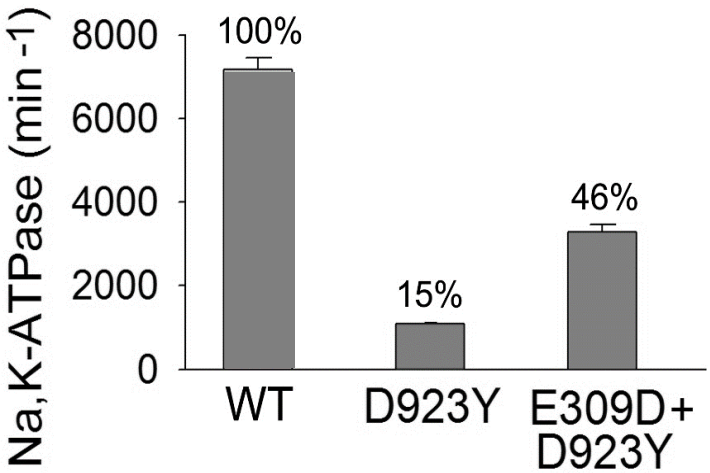

Figure 4. The introduction of second site mutation E309D causes a ~ 2-fold increase in D923Y NKA α3 activity in transfected COS cells, from 15% of WT (D923Y) to 46% of WT (E309D+D923Y) (B. Vilsen, unpublished).

1.1.5 Aims and objectives

1. Generate a novel AHC mouse model with mutation D923Y (*Atp1a3*$^{D923Y/+}$)
2. Assess locomotor activity using the open field test in *Atp1a3*$^{D923Y/+}$ mice
3. Assess anxiety-like behaviours using the EPM and EMM *Atp1a3*$^{D923Y/+}$ mice
4. Assess learning and memory using delay and trace cued fear conditioning *Atp1a3*$^{D923Y/+}$ mice
5. Assess whether forced swimming induces hemiplegia or dystonia in *Atp1a3*$^{D923Y/+}$ mice

1.2 Methods and Materials

1.2.1 Animals

1.2.1.1 Generation of *Atp1a3*$^{D923Y/+}$ mice

Conditional *Atp1a3*$^{D923Y/+}$ knock-in mice were generated by homologous recombination (Cyagen US Inc.). The DNA targeting construct was generated from C57BL/6 genomic DNA. The targeting construct was flanked by 5' and 3' homologous arms, which were generated by PCR using BAC clones RP23-284H16 and RP24-208E13 from the C57BL/6 library as template. The 5' arm contained homologous genomic sequence with a promotor sequence, upstream from the cDNA insertion. The targeting construct contained two cDNA knock-in sequences. The first sequence was inserted into intron 6 and included the coding sequence (CDS) of exon 7-23 with the AHC-causing point mutation, D923Y (GAC to TAC) (Fig. 5). The second sequence was inserted 5' of the first sequence in intron 6 and contained the CDS of exon 7-23 with both the D923Y mutation and the second site rescue mutation, E309D (GAG to GAC). In between both of these sequences was the neomycin phosphotransferase gene (neo) flanked by self-deletion anchors. The 3' homologous arm was inserted downstream of the second cDNA knock-in sequence. PolyA tails were added to the end of both sequences and loxP sites were incorporated to flank the cDNA containing the D923Y mutation and neo. Neo and diphtheria toxin A (DT-A) were used for positive and negative selection, respectively, to help select successfully targeted clones. C57BL/6N ES cells were used for gene targeting and the transgene expression cassette was introduced through homologous recombination into the *Atp1a3* locus on chromosome 7.

The targeting vector was electroporated into embryonic stem cells and the resultant targeted allele was partially transcribed. The D923Y point mutation was transcribed and the polyA tail downstream of this mutation prevented transcriptional read through, so the E309D/D923Y mutation was not transcribed. Modified embryonic stem cells were injected into blastocysts which were then implanted into female mice for gestation to create *Atp1a3*$^{D923Y/+}$ transgenic mice yielding a D923Y mutation and an inactive D923Y/E309D mutation. *Atp1a3*$^{D923Y/+}$ mice were backcrossed for one generation to C57BL/6NCrl females (Charles River, Margate, UK) to yield wild-type (+/+) and *Atp1a3*$^{D923Y/+}$ littermates. These mice were used for the behavioural studies later discussed.

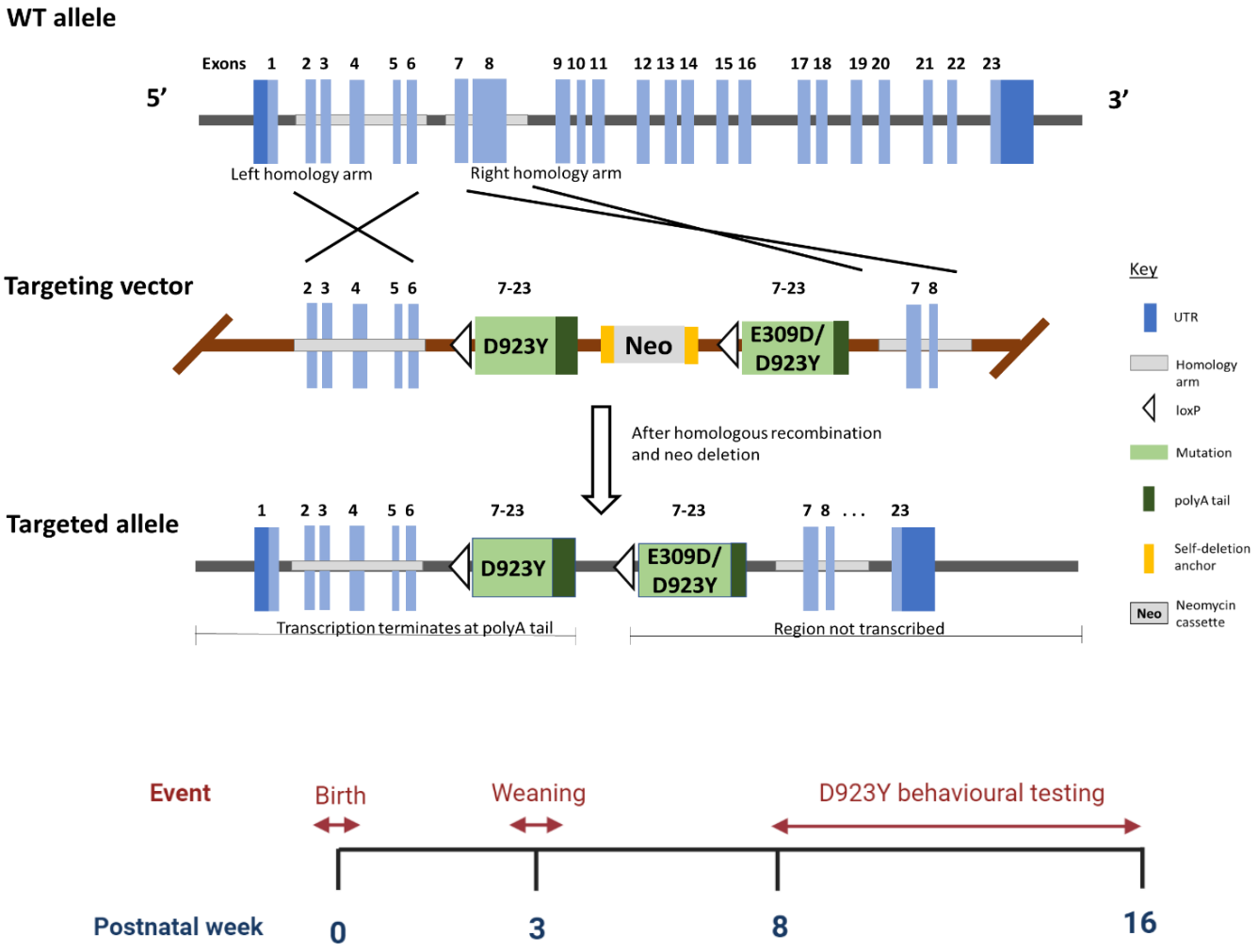

Figure 5. Vector design for the generation of conditional *Atp1a3*$^{D923Y/+}$ knock-in mice. The WT allele, with 23 exons, is shown at the top, the targeting vector on the following line, the correctly targeted allele on the next line after homologous recombination and neo cassette deletion, and on the last line is the knockin allele after Cre recombination. The targeting vector was designed to have a D923Y mutation in exons 7-23, E309D/D923Y mutation (also in exons 7-23) downstream of the first mutation, loxP sites, polyA tails, and a neomycin cassette. This targeting vector was flanked by two homologous arms. After homologous recombination, the resultant targeted allele was partially transcribed – the polyA tail prevented transcriptional read through so that the D923Y mutation, but not E309D/D923Y, was expressed.

1.2.1.2 Mouse genotyping

Atp1a3$^{D923Y/+}$ and WT (+/+) mice were genotyped by PCR using DNA from tail or ear samples. For routine genotyping, the primers were as follows: forward primer, 5'-GACAACTCCTCCCTGACTG-3' in exon 7; reverse primer, 5'-GCCACAATGATGCCGATGA-3' in exon 8 (Fig. 6). The target region was amplified and cycled through different conditions using the thermocycler. See table 3 for PCR reagents and cycling conditions. After amplification, products were electrophoresed through a 3% agarose gel. The expected band size is 462 bp for the WT sample and 350 bp and 462 bp for the HET sample.

1.2.1.3 Animal husbandry

Mice were weaned at 3-4 weeks of age and group housed in cages of up to five with same-sex littermates. Mice were tested at 2-6 months of age and both sexes were used. Mice were housed under a 12h:12h light/dark cycles and had access to food and water ad libitum. Efforts were made to minimize both suffering and the number of animals used. All animal procedures were carried out in accordance with the Animals (Scientific Procedures) Act 1986, and were approved by the University of Leeds Ethical Review Committee.

PCR mixture		PCR cycling conditions	
Reagent	Volume (µL)	Step	Temperature, time
dH_2O	19.55	1	95°C, 3 min
10X buffer	2.5	2	94°C, 30 s
$MgCl_2$ (50mM)	0.8	3	57°C, 1 min
dNTPs (25mM each)	0.2	4	72°C, 40 s
Primer mix (5µM each)	0.75	5	Go to 2, 34 times
Taq polymerase	0.2	6	72°C, 10 min
DNA (50ng)	1.0	7	4°C, hold
TOTAL	25.0	8	End

Table 3. PCR mixture and cycling conditions

Wild-type (462 bp – genomic)

GACAACTCCTCCCTGACTGgcgaatctgagcctcagacccgctccccggactgcacacacgacaacccccctggagactcggaacatcacct
tcttttccaccaactgcgtggaaggtgaaggggaggggacccccaagggcacaaaaccagagatgctgctcaggaggtggggtgcctgcagc
cttctgaggcccagcagacctgagcccctccctttgttcctgcaggcaccgctcggggtgtggtggtagccacaggtgaccgcaccgtcat
gggccgcattgccaccctggcctcgggcttggaggtgggcaagacgcccatcgccattgagattgagcatttcatccagctcattacgggc
gtggccgtgttcctgggcgtgtccttcttcatcctctctctcattctgggttacacctggctcgaGgcagtcatcttccTCATCGGCATCA
TTGTGGC

Mutant (350 bp – cDNA)

GACAACTCCTCCCTGACTGGCGAATCTGAGCCTCAGACCCGCTCCCCGGaCTGCACACACGACAACCCCCTGGAGACTCGGAACATCACCT
TCTTTTCCACCAACTGCGTGGAAGGCACCGCTCGGGGTGTGGTGGTAGCCACAGGTGACCGCACCGTCATGGGCCGCATTGCCACCCTGGC
CTCGGGCTTGGAGGTGGGCAAGacGCCCATCGCCATTGAGATTGAGCaTTTCATCCAGCTCATTACGGGCGTGGCCGTGtTCCTGGGCGTG
TCCTTCTTCATCCTCTCTCTCATTCTGGGTTACACCTGGCTCGAcGCAGTCATCTTCCTCATCGGCATCATTGTGGC

Exon 7
Intron 7
Exon 8
E309

Figure 6. Sequence of the PCR amplified region. Underlined regions represent the forward and reverse primers.

1.2.2 Behavioural Experiments

The study consisted of 4 cohorts of mice; cohorts 1 and 2 were tested at 5-6 months of age, and cohorts 3 and 4 were tested at 2 months of age. Cohort 1 (*Atp1a3*$^{D923Y/+}$ n=21 (9 female, 12 male) and WT n=21 (11 female, 10 male)) were tested in the open field, cohort 2 (*Atp1a3*$^{D923Y/+}$ n=18 (5 female, 13 male), WT n=8 (3 female, 5 male)) were tested in delay fear conditioning and the forced swim test, and cohorts 3 (*Atp1a3*$^{D923Y/+}$ n=6 (1 female, 5 male) and WT n=10 (4 female, 6 male)) and 4 (*Atp1a3*$^{D923Y/+}$ n=7 (5 female, 2 male) and WT n=7 (5 female, 2 male)) were tested in the following test sequence: elevated plus maze → elevated minus maze → trace fear conditioning → forced swim test. Results were pooled for cohorts 3 and 4. Mice were removed from analyses if they fell off the apparatus (elevated plus maze, elevated minus maze) or if the video froze during recording (fear conditioning). All experiments were recorded using a video camera and subsequently analysed using AnyMaze software (Stoelting Co, Wood Dale, IL, USA). All behavioural apparatuses were cleaned with 70% alcohol between experiments.

1.2.2.1 Open Field

The open field (OF) test was used to measure general locomotor activity, anxiety-like and exploratory behaviour. Each mouse was placed into the centre of the open field arena (40 x 40 x 40 cm) and given 10 minutes to explore freely. For analysis, the arena was divided into three zones: centre, intermediate and outer using AnyMaze (79). The outer zone was designated as the area 8 cm from the outer walls and the centre zone was designated as the centre of the open field measuring 6.4 cm^2. The intermediate zone was the remaining area between the outer and centre zone. Spontaneous locomotor activity, quantified as distance travelled, time spent in each zone, number of entries into each zone, and number of rears, was analysed.

1.2.2.2 Elevated Plus Maze

The elevated plus maze (EPM) was used to test for anxiety-like and exploratory behaviours. The EPM consisted of two opposing open arms (25 x 5 cm), two opposing closed arms (25 x 5 x 30 cm) and a centre square (5 x 5 cm) elevated 50 cm from the floor. Each mouse was placed onto the centre square, facing an open arm, and was recorded for 5 minutes. The number of entries into each arm, the time spent in each arm, overall distance, and number of head dips were analysed. Mice that fell off an arm were immediately returned to the same arm. These mice were excluded from analysis, but we

continued to test them to ensure they had the same amount of exposure to the EPM as the other mice.

1.2.2.3 Elevated Minus Maze

The elevated minus maze (EMM) was carried out as previously described (80). Like the EPM, the EMM tests for anxiety-like behaviours using thigmotactic cues; the EPM consists of three closed walls in each closed arm, whereas the EMM has just one wall. The maze consisted of a clear Perspex platform (42 x 42 cm), elevated 45 cm from the floor. The platform was divided into nine equal squares (14 x 14 cm) labelled 1-9, with a clear Perspex wall (12 x 14 x 0.5 cm) in the centre. Outer squares (all squares but number 5) were designated the outer zone, and the inner square (number 5) with the wall was designated the inner zone. Each mouse was placed on the bottom right square and recorded for 5 minutes. Time spent in the zones, distance travelled, and head dips were analysed.

1.2.2.4 Fear Conditioning

Fear conditioning was used to test fear memory (Fig. 7). Experiments took place in a fear-conditioning chamber (26 x 26 x 30 cm; Ugo Basile, Model 46004, Varese, Italy). During training, mice were exposed to the conditioning context, comprised of a stainless-steel shock grid and grey walls (context A), for 180s. This was then followed by a 30s tone exposure (3.6KHz, 80dB) which was used as the conditioned stimulus (CS). This was then followed immediately (delay conditioning) or after 15s (trace conditioning) by a foot shock (1.00mA, 2s) as the unconditioned stimulus (US). Mice were kept in the chamber for an additional 30s before returning to their home cage. White background noise (19.25dB) played throughout.

24h after training, mice were placed in the chamber to evaluate their tone-dependent memory. The context from the training phase was altered; white flooring replaced the shock grid, checkerboard walls replaced the grey walls, and lemon juice was added to change the odour (context B). To test tone-dependent memory, mice were first exposed to the novel context for 180s and then 180s of the tone. The chamber was cleaned between experiments with scented alcohol wipes.

AnyMaze software was used to record videos, administer foot shocks, control sound and light, and measure freezing (minimum freezing detection: 1000ms).

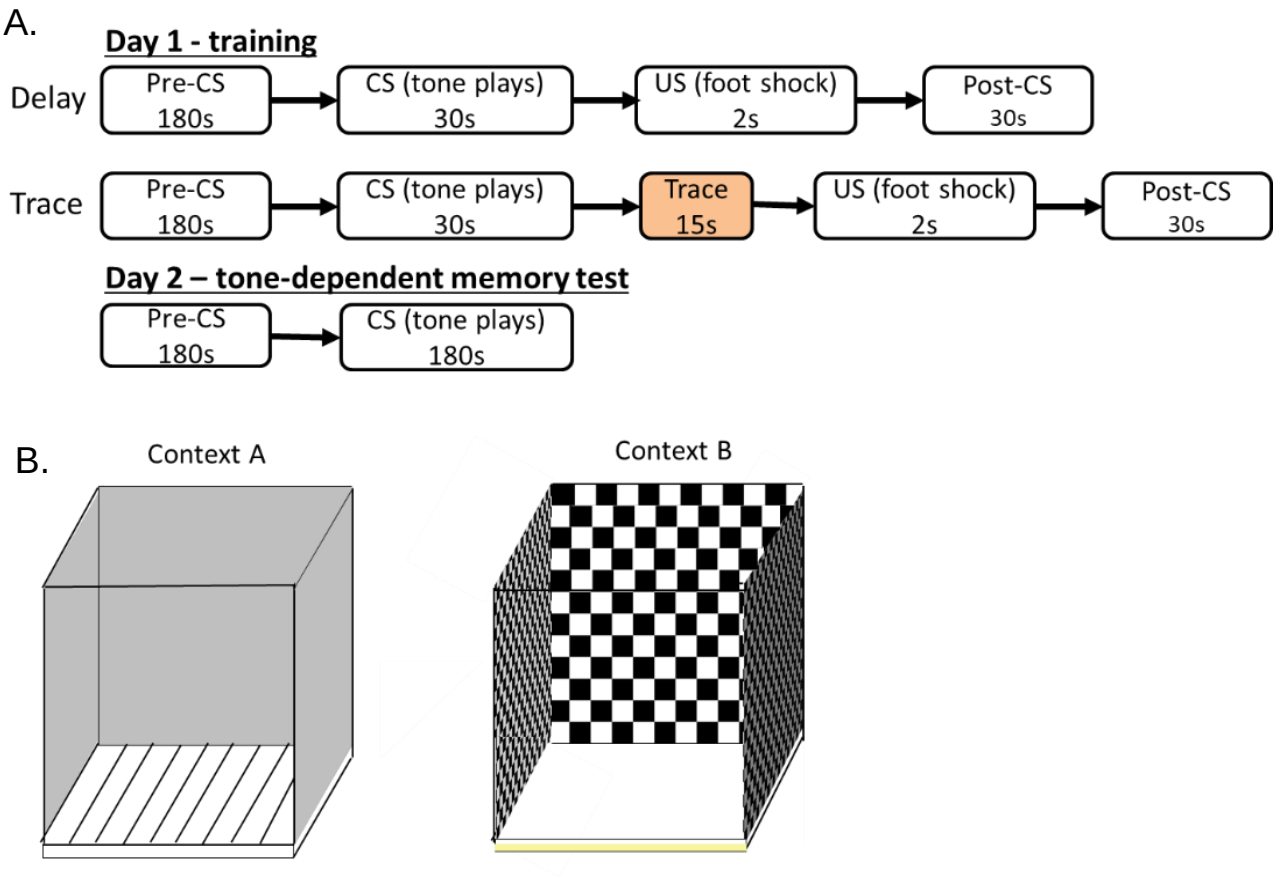

Figure 7. Fear conditioning experimental protocol is outlined in which describes 180s of pre-CS, 30s of CS, a footshock, and 30s of post-CS for both types of conditioning, with trace conditioning consisting of an additional trace interval of 15s. On day 2, the cue test consisted of 180s pre-CS and 180s CS (A). Two different contexts were used - Context A comprised of 3 grey card inserts and a stainless-steel shock grid through which the electric foot-shock was delivered. Context B comprised of 3 checkerboard card inserts, white flooring, and lemon juice in the compartment below the flooring (normally used to collect faecal matter) (B).

1.2.2.5 Porsolt Forced Swim Test

Traditionally, the forced swim test (FST) is used to test the effectiveness of anti-depressants and the latency for the mice to stop swimming and begin floating is used an indicator of motivation and therefore depressive-like behaviours (81). Additionally, hemiplegic attacks are commonly induced by stimuli such as water and stress in AHC patients, so we therefore used the FST to see whether such attacks can be induced in these mice. Each mouse was put into a 5000ml glass container (17 cm diameter) filled with 3000ml of water at 25 ± 1°C for 6 minutes. Containers were filled deep enough so that mice were unable to touch the bottom of the container, and water was changed between mice. After each FST experiment, mice were taken out of the water, dried with tissue paper, observed and monitored closely for at least 10 minutes before returning to the home cage. Latency to first immobile episode, immobility (AnyMaze parameters: 65% immobility, 500ms) and distance travelled were analysed automatically using AnyMaze.

1.2.3 Statistical Analysis

Videos were scored and analysed by an experimenter blind to the genotypes. All statistics were calculated using GraphPad Prism and SPSS. The Shapiro-Wilk test was used to test for normality and Levene's test was used to test for homoscedasticity. If data were normal and homoscedastic, we used two-way ANOVA with Sidak's multiple comparisons post hoc test and unpaired t-tests. If data did not pass these assumptions, Mann Whitney U tests and Friedman ANOVA were used with the Wilcoxon signed-rank test as a post hoc test. Where there was no sex x genotype interaction (using ANOVA), data were pooled together by genotype. Data are presented as mean ± standard error of the mean (SEM) and $p < 0.05$ was considered significant. Graphs were created using GraphPad Prism and figures were generated using BioRender and Microsoft PowerPoint.

1.3 Results

1.3.1 Gait

During behavioural testing, *Atp1a3*$^{D923Y/+}$ mice occassionally displayed unusual gait, in which the hind limbs were splayed (Fig. 8). This was particularly evident during stressful tasks such as the EPM and EMM. Attempts were made to quantify this observation (footprint and video analysis), but methods to do this were not deemed reliable enough to assess gait.

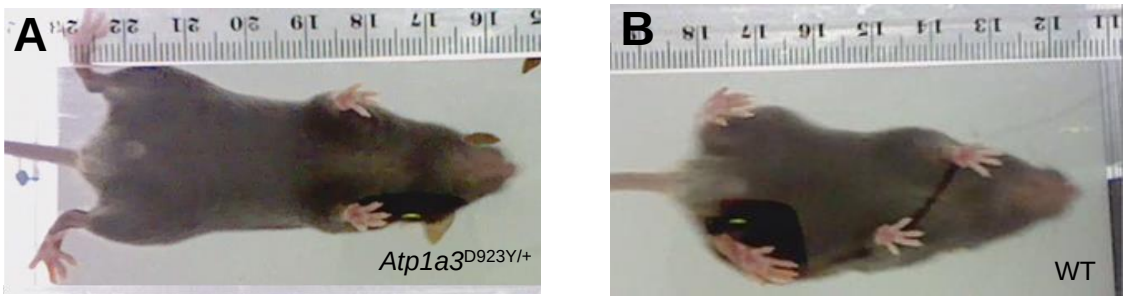

Figure 8. Screenshots from videos showing *Atp1a3*$^{D923Y/+}$ and WT mice gait. Some *Atp1a3*$^{D923Y/+}$ mice displayed hind limbs during behavioural tests (A), whereas WT mice showed normal gait (B).

1.3.2 Open field

The open field was used to measure general locomotor activity, anxiety-like and exploratory behaviours (Fig. 9). Upon analysis, the open field was divided into three zones: centre, intermediate and outer, and time, entries, and distance travelled within these zones were measured. *Atp1a3*$^{D923Y/+}$ mice spent significantly less time in the intermediate zone (*Atp1a3*$^{D923Y/+}$ mean rank = 15.67; WT mean rank = 27.33; U = 98, p = 0.002) and more time in the outer zone (*Atp1a3*$^{D923Y/+}$ mean rank = 27.24; WT mean rank = 15.76; U = 100, p = 0.002). Although *Atp1a3*$^{D923Y/+}$ mice were observed to spend less time than WT mice in the centre zone, this did not reach significance.

Entries into each zone were also analysed and results showed *Atp1a3*$^{D923Y/+}$ mice entered the centre (*Atp1a3*$^{D923Y/+}$: M = 17.14, SD = 8.24; WT: M = 25.00, SD = 9.08; t(40) = -2.937, p = 0.005) and intermediate zones (*Atp1a3*$^{D923Y/+}$: M = 105.71, SD = 26.15; WT: M = 126.67, SD = 26.91; t(40) = -2.559, p = 0.014) fewer times than WT mice. There was no significant difference between genotypes in outer zone entries.

Atp1a3$^{D923Y/+}$ mice covered significantly less distance in the centre zone (*Atp1a3*$^{D923Y/+}$: M = 1.27, SD = 0.62; WT: M = 1.87, SD = 0.69; t(40) = -3.022, p = 0.004) and more distance in the outer zone compared to WT mice (*Atp1a3*$^{D923Y/+}$ mean rank = 27; WT mean rank = 16; U = 105, p = 0.004), whilst distance in the intermediate zone and overall distance travelled was similar between the genotypes.

Rearing behaviour, which describes an exploratory vertical posture, was also assessed. We scored two different types of rears: unsupported and supported rears. Supported rears were scored when mice were seen rearing, i.e. standing on hind limbs with forelimbs off the ground, with the support of a wall. In contrast, unsupported rears were counted when mice reared away from the wall without support. *Atp1a3*$^{D923Y/+}$ mice displayed significantly fewer unsupported rears than WT mice (*Atp1a3*$^{D923Y/+}$ mean rank = 15.55; WT mean rank = 27.45; U = 95.5, p = 0.002), and there were no differences in supported rears.

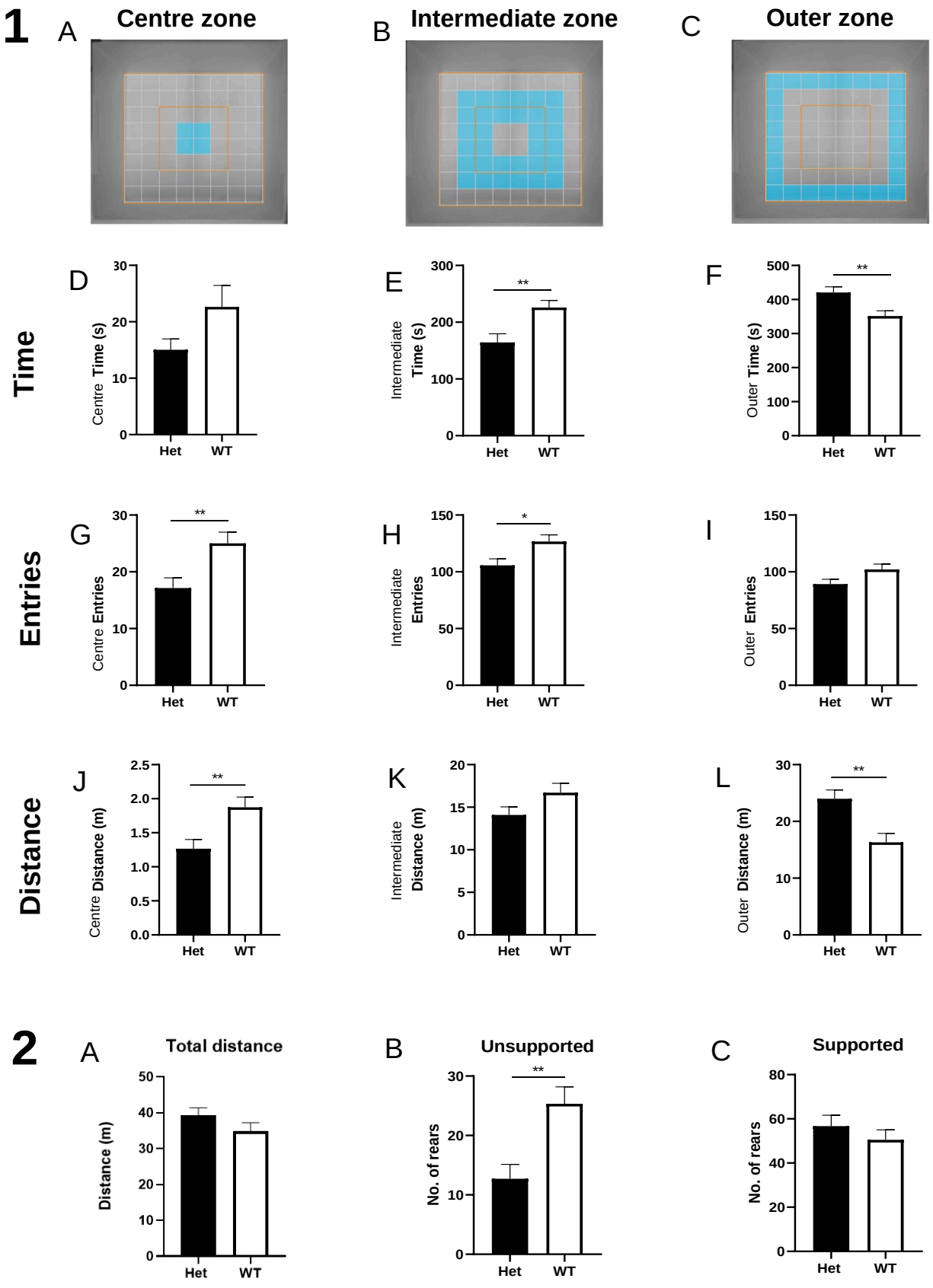

Figure 9. Open field. Graphs show comparisons between *Atp1a3*$^{D923Y/+}$ (n=21) and WT mice (n=21) in the open field on the following factors: time spent, number of entries, and distance travelled in the different zones. The OF was divided into centre (1A), intermediate (1B) and outer zones (1C) on AnyMaze for analysis. *Atp1a3*$^{D923Y/+}$ spent a similar amount of time in the centre zone, less time in the intermediate zone, and a greater amount of time in the outer zone relative to WT mice (1D, 1E, 1F). *Atp1a3*$^{D923Y/+}$ mice significantly entered the centre and intermediate zone less than WT mice but number of entries into the outer zone were similar (1G, 1H, 1I). *Atp1a3*$^{D923Y/+}$ mice also travelled less in the centre zone, similar amounts in the intermediate zone, and more in the outer zone compared to WT mice (1J, 1K, 1L), but total distance was not significantly different (2A). *Atp1a3*$^{D923Y/+}$ displayed fewer unsupported rears than WT mice (2B), but there was no difference in supported rears (2C). Data shown as mean ± SEM, *p<0.05; **p<0.01.

1.3.3 Elevated Plus Maze

In the EPM, mice were allowed to freely explore open and closed arms for 5 minutes. Preference towards open arms can be used as a measure of anxiety-like behaviour.

We identified a sex difference in time spent in open and closed arms. Female mice spent significantly longer on the open arms (female mean rank = 17.27; male mean rank = 9.64; U = 30, $p = 0.01$) and less on the closed arms (female mean rank = 8.18; male mean rank = 16.79; U = 24, $p = 0.004$) compared to male mice (Fig. 10*A,B*). *Atp1a3*$^{D923Y/+}$ mice appeared to spend longer in open arms and less in closed arms relative to WT mice, however time spent in open arms was not significantly different between genotypes (*Atp1a3*$^{D923Y/+}$ mean rank = 15.25; WT mean rank = 10.92; U = 51, ns), but time spent in closed arms was different (*Atp1a3*$^{D923Y/+}$ mean rank = 9.71; WT mean rank = 16.04; U = 38.5, $p = 0.032$).

To assess exploratory behaviour, we also analysed total distance travelled and number of head dips. *Atp1a3*$^{D923Y/+}$ mice appeared to show greater ambulatory activity, which was confirmed with a significant difference in total distance travelled (*Atp1a3*$^{D923Y/+}$ mean rank = 16.83; WT mean rank = 9.46; U = 32, $p = 0.012$) compared to WT mice (Fig. 10*C*). Head dips were counted when mice were seen moving their heads downwards over the side of open arm to observe the floor below. *Atp1a3*$^{D923Y/+}$ mice significantly displayed more head dips than WT mice ($t(23) = 2.215$, $p = 0.0370$) (Fig. 10*D*).

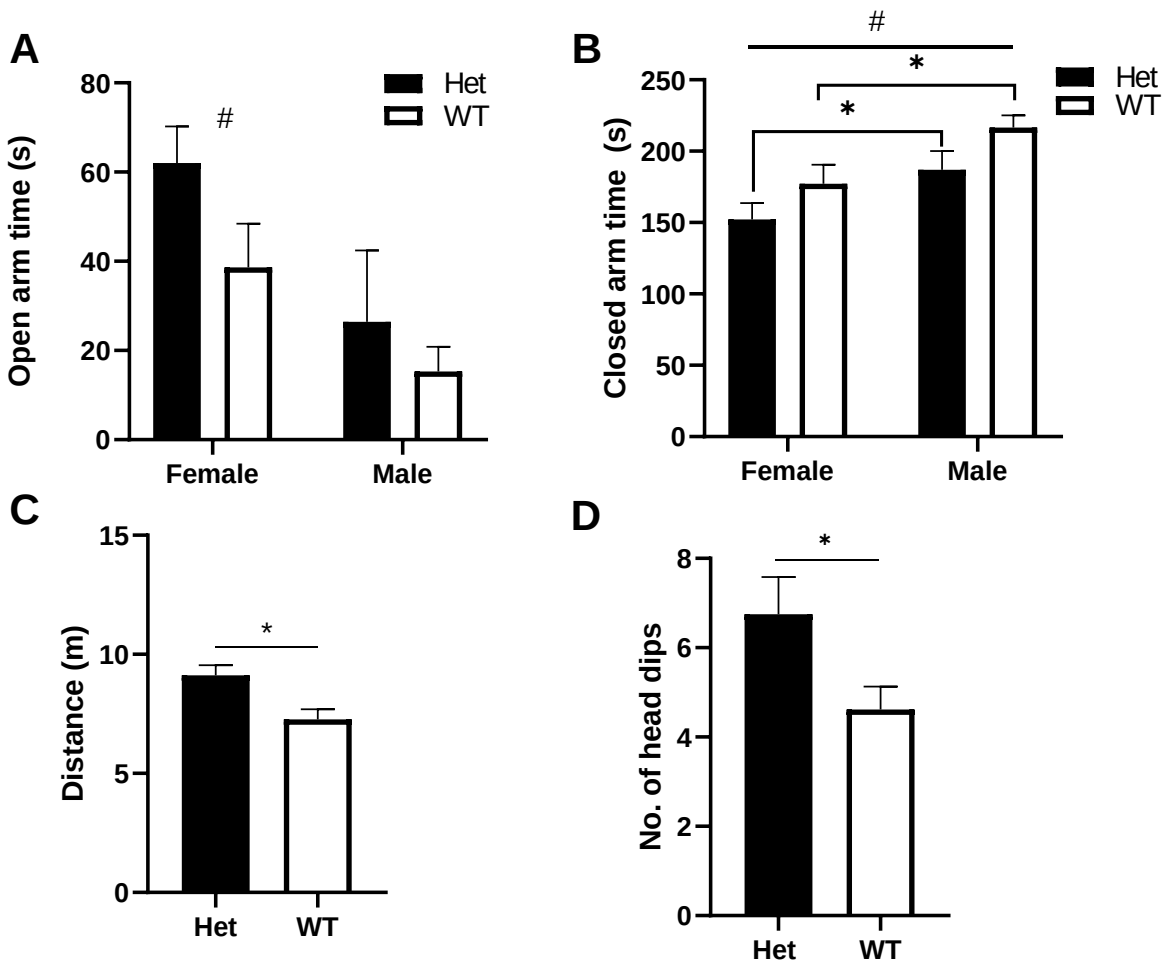

Figure 10. Elevated plus maze. Female mice spent significantly longer in open arms than male mice but there was no difference in genotype (A). Female mice spent less time in closed arms than male mice, and *Atp1a3*$^{D923Y/+}$ mice (n=12) spent significantly less time in closed arms compared to WT mice (n=12) (B). *Atp1a3*$^{D923Y/+}$ mice travelled a greater total distance in compared to WT mice (C). *Atp1a3*$^{D923Y/+}$ mice also displayed significantly more head dips than WT mice (D). Data shown as mean ± SEM, between genotypes *p<0.05, and between sexes #p<0.01.

1.3.4 Elevated Minus Maze

Similar to the EPM, we used the EMM to assess anxiety-like and exploratory behaviours in *Atp1a3*$^{D923Y/+}$ mice. *Atp1a3*$^{D923Y/+}$ mice spent significantly more time in the outer zone (*Atp1a3*$^{D923Y/+}$: mean rank = 21.92; WT mean rank = 10.12; U = 19, p = 0.000238) and less time in the inner zone (*Atp1a3*$^{D923Y/+}$ mean rank = 8.08; WT mean rank = 19.88; U = 19, p = 0.000238) relative to WT mice (Fig. 11*A*).

To further explore exploratory behaviours in a stressful environment, we measured distance travelled in the inner and outer zones (Fig. 11*B*). Corresponding to the increased time spent in the outer zone, *Atp1a3*$^{D923Y/+}$ mice also covered more distance in the outer zone than WT mice (*Atp1a3*$^{D923Y/+}$ mean rank = 20.58; WT mean rank = 11.06; U = 35, p = 0.002) (Fig. 11*C*). There was no difference in distance travelled in the inner zone. Consistent with the results of the EPM, *Atp1a3*$^{D923Y/+}$ travelled a greater overall distance than WT mice (t(27) = 2.198, p = 0.0367) (Fig. 11*D*).

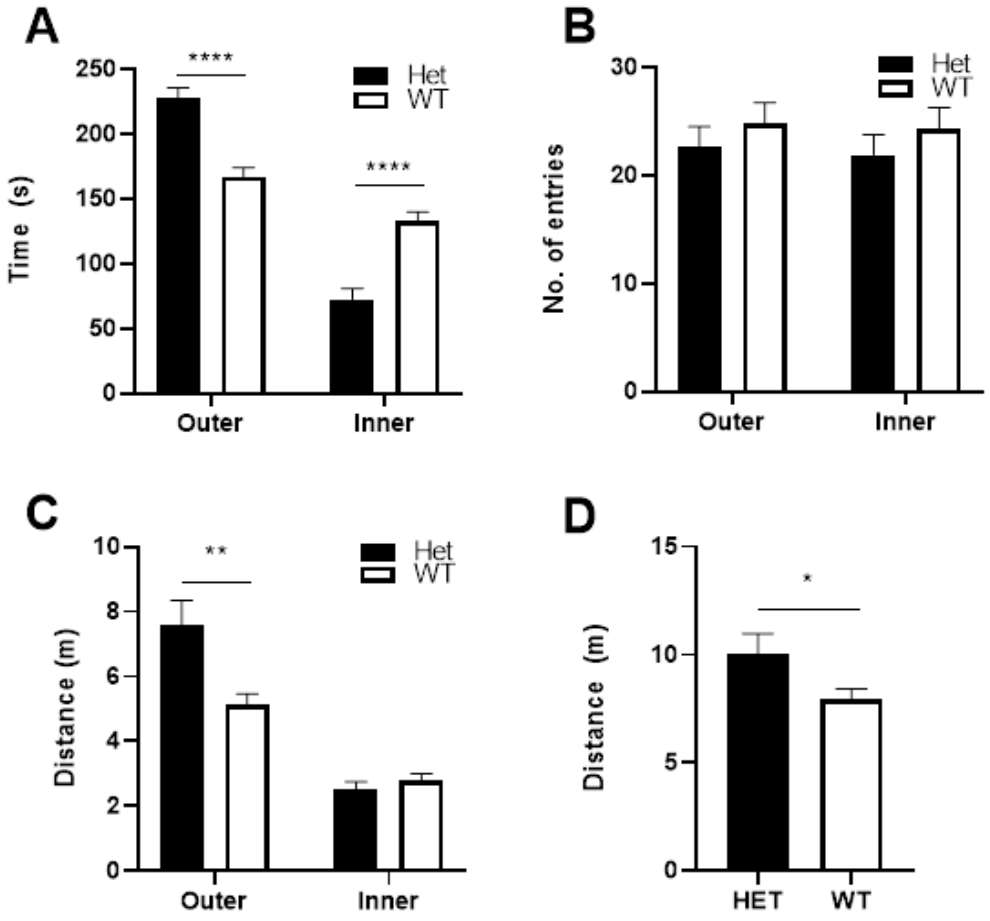

Figure 11. Elevated minus maze. *Atp1a3*$^{D923Y/+}$ mice (n=12) spent more time in the outer zone and less time in the inner zone compared to WT mice (n=17) (A). There was no difference in genotype in number of entries into outer and inner arms (B). *Atp1a3*$^{D923Y/+}$ mice travelled more within the outer zone compared to WT mice (C). Total distance travelled was greater in *Atp1a3*$^{D923Y/+}$ compared to WT mice (C). Data shown as mean ± SEM, *p<0.05; **p<0.01; ***p<0.001; ****p<0.0001.

1.3.5 Fear Conditioning

1.3.5.1 Delay Fear Conditioning

To test fear memory, we carried out delay fear conditioning. In the training phase of delay conditioning, the foot shock (US) was administered immediately after the termination of the tone (CS). There was no difference in baseline freezing between *Atp1a3*$^{D923Y/+}$ and WT mice (*Atp1a3*$^{D923Y/+}$ mean rank = 10.9; WT mean rank = 14.06; U = 43.5, ns) (Fig. 12*A*).

24h after the training phase, we carried out the cue test, in which mice were put in the fear conditioning box in a new context for a total of 6 minutes, with the CS starting at 3 minutes until the end. In the period before the CS was played (pre-CS), *Atp1a3*$^{D923Y/+}$ mice froze significantly less compared to WT mice (*Atp1a3*$^{D923Y/+}$ mean rank = 8.6; WT mean rank = 18.38; U = 18, $p = 0.001$), but when the CS was played, there was no difference in freezing between genotypes (*Atp1a3*$^{D923Y/+}$ mean rank =11.13; WT mean rank = 13.63; U = 40, ns) (Fig. 12*B*) . Moreover, both *Atp1a3*$^{D923Y/+}$ and WT mice froze significantly more to the CS compared to the pre-CS (*Atp1a3*$^{D923Y/+}$: pre-CS mean rank = 8.93;CS mean rank = 22.07; U = 14, $p = 0.00004$; WT : pre-CS mean rank = 4.5; CS mean rank = 12.50; U = 0, $p = 0.001$).

1.3.5.2 Trace Fear Conditioning

Given that both *Atp1a3*$^{D923Y/+}$ and WT mice froze more to the CS than the pre-CS in the cue test of delay fear conditioning, thereby suggesting successful conditioning of the CS to the footshock, we carried out trace fear conditioning with a trace interval of 15 seconds, to investigate potential subtle effects of fear memory impairment. Similar to delay fear conditioning, we found no significant differences in baseline freezing (*Atp1a3*$^{D923Y/+}$ mean rank = 14.33; WT mean rank = 15.47; U = 94, ns) (Fig. 12*C*).

In the cue test, we found that *Atp1a3*$^{D923Y/+}$ mice froze significantly less than WT mice during pre-CS (*Atp1a3*$^{D923Y/+}$ mean rank = 8.67; WT mean rank = 19.47; U = 26, $p = 0.001$) and CS (*Atp1a3*$^{D923Y/+}$ mean rank = 8.92; WT mean rank = 19.29; U = 29, p = 0.001) (Fig. 12*D*). Interestingly, in contrast to the delay fear conditioning results, we found that *Atp1a3*$^{D923Y/+}$ mice did not freeze significantly more in response to the CS compared to the pre-CS (new context mean rank = 10.17; cue test mean rank = 14.83; U = 44, ns), however WT mice did freeze significantly more to the CS (new context mean rank = 11.44; cue test mean rank = 23.56; U = 41.5, $p = 0.0004$).

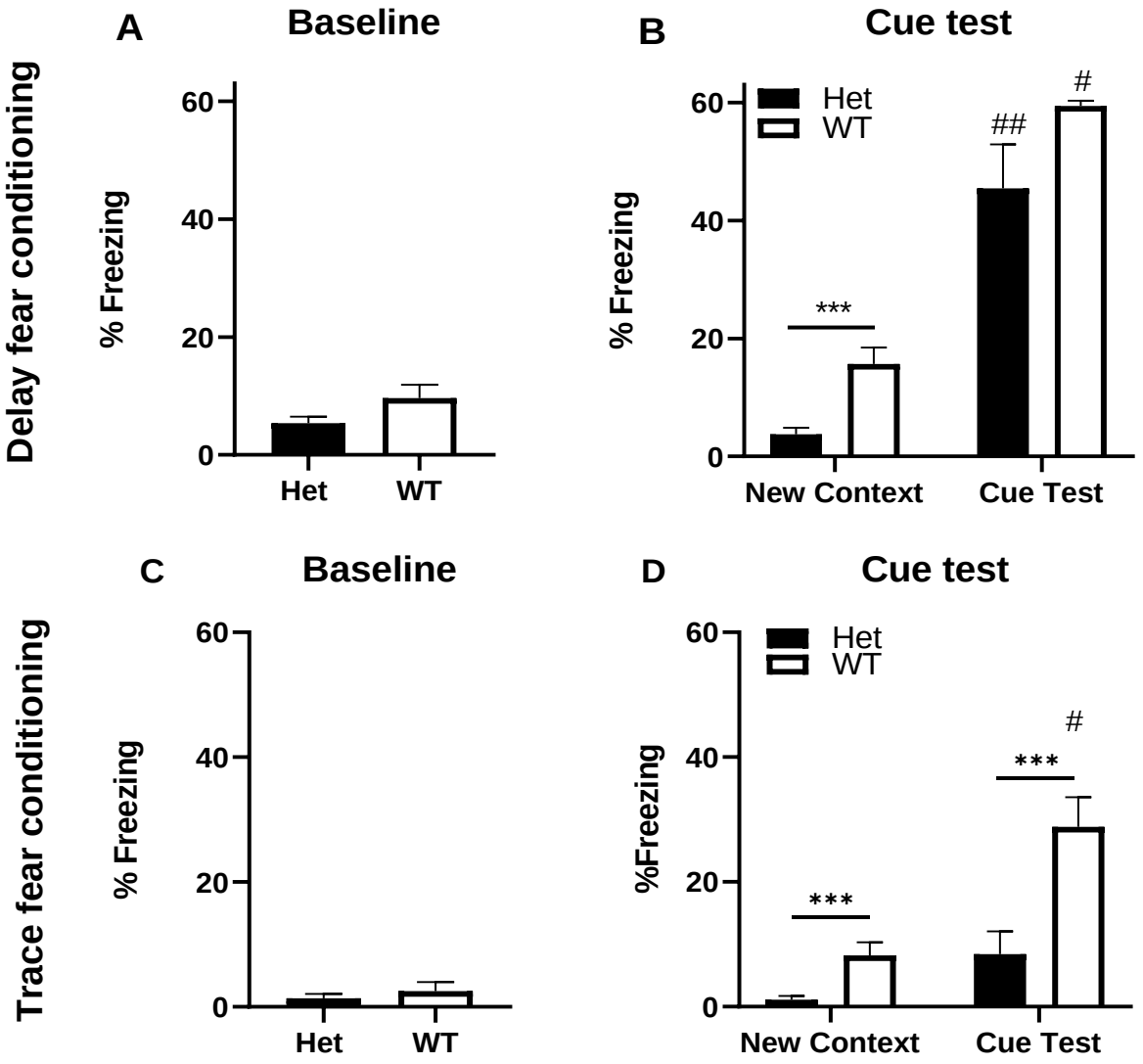

Figure 12. Fear conditioning. There was no difference in % freezing between *Atp1a3*$^{D923Y/+}$ (n=15) and WT (n=8) mice in the pre-CS, CS, or post-CS (A) and in the cue test both *Atp1a3*$^{D923Y/+}$ and WT mice significantly froze more in response to the CS (B). In trace conditioning, there was no difference in freezing between *Atp1a3*$^{D923Y/+}$ (n=12) and WT (n=17) mice in pre-CS, CS, TI, and post-CS (**C**). In the cue test, only WT mice froze significantly more in response to the CS compared to the new context and froze more than *Atp1a3*$^{D923Y/+}$ mice in response to the CS (**D**). Data shown as mean ± SEM; between genotype **p*<0.05, ***p*<0.01, ****p*<0.001; and between pre-CS and CS #*p*<0.001. #*p*<0.001, ##*p*<0.0001.

1.3.6 Forced Swim Test

In the forced swim test, latency to the first immobile episode was not significantly different between *Atp1a3*$^{D923Y/+}$ and WT mice (*Atp1a3*$^{D923Y/+}$ mean rank = 13.23; WT mean rank = 13.77; U = 81, *ns*) (Fig. 13*A*). However, *Atp1a3*$^{D923Y/+}$ mice had a significantly lower immobility time in the last 4 minutes of the FST compared to WT mice (*Atp1a3*$^{D923Y/+}$ mean rank = 7.85; WT mean rank = 19.15; U = 11, $p = 0.0002$) (Fig. 13*B*). In accordance with these results, *Atp1a3*$^{D923Y/+}$ mice travelled a greater overall distance (*Atp1a3*$^{D923Y/+}$ mean rank = 18.92; WT mean rank = 8.08; U = 14, $p = 0.0003$) (Fig. 13*C*).

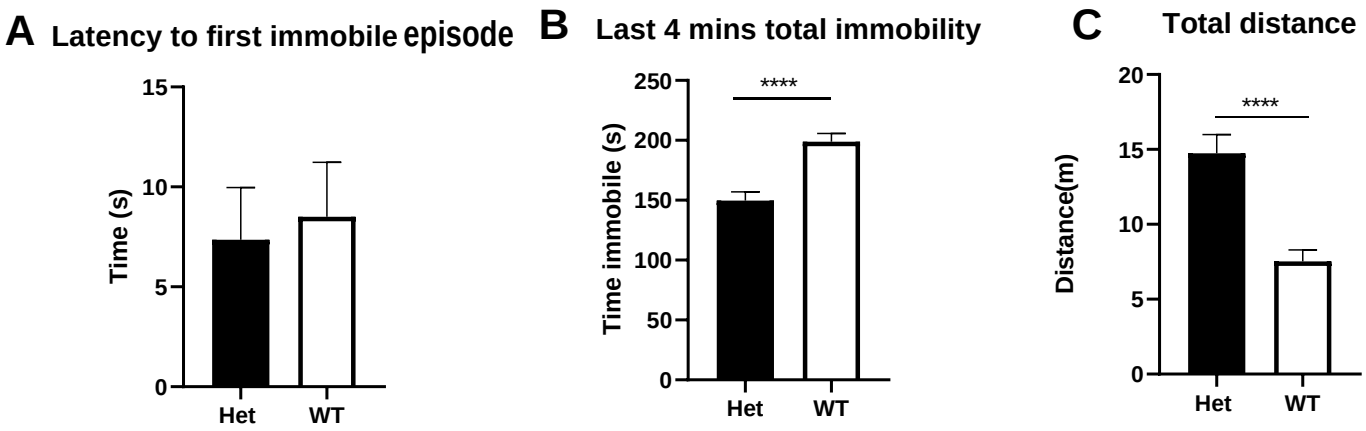

Figure 13. Forced swim test. Latency to first immobile episode was not significantly different between WT (n=13) mice and *Atp1a3*$^{D923Y/+}$ (n=13) (A). *Atp1a3*$^{D923Y/+}$ spent less time immobile (B) and travelled an overall greater distance than WT mice (C). Data shown as mean ± SEM, ****p<0.0001.

1.4 Discussion

In the present study, we generated a novel AHC mouse model with mutation D923Y (Aim 1), in which we assessed activity level (Aim 2), anxiety-like behaviours (Aim 3), cognitive impairments (Aim 4), and motor deficits (Aim 5). Results from these behavioural tests are summarised in Table 4 and indicate that *Atp1a3*$^{D923Y/+}$ mice are hyperactive, have an anxiolytic-like phenotype, exhibit increased risk-taking behaviour, and have subtle learning and memory impairment.

Behavioural Test		*Atp1a3*$^{D923Y/+}$ vs WT	Significance
Open field	Time in centre zone	ND	*ns*
	Time in outer zone	↑	**
	Distance in centre zone	↓	**
	Distance in outer zone	↑	**
	Unsupported rears	↓	**
EPM	Time in open arms	ND	*ns*
	Time in closed arms	↓	*
	Overall distance travelled	↑	*
	Number of head dips	↑	*
EMM	Time spent in outer zone	↑	****
	Time spent in inner zone	↓	****
	Distance travelled in outer zone	↑	**
	Distance travelled in inner zone	ND	*ns*
	Overall distance travelled	↑	*
Delay fear conditioning	Freezing in response to the CS in the cue test	ND	*ns*
Trace fear conditioning	Freezing in response to the CS in the cue test	↓	***
Forced swim test	Latency to first immobile episode	ND	*ns*
	Last 4 minutes of total immobility	↓	****
	Overall distance travelled	↑	****

Table 4. Table summarising the results of behavioural tests, comparing *Atp1a3*$^{D923Y/+}$ mice to WT mice. N.D, no difference; ↑, statistically significant increase in behaviour of *Atp1a3*$^{D923Y/+}$ mice relative to WT mice, ↓ statistically significant decrease in behaviour of *Atp1a3*$^{D923Y/+}$ mice relative to WT mice. Significance: *ns*, not significant, *p<0.05, **p<0.01, ***p<0.001, ****p<0.0001.

1.4.1 Phenotype

Atp1a3$^{D923Y/+}$ mice were noticeably smaller than WT mice, reflecting the small stature seen in AHC patients, but this was not quantified (7). Moreover, *Atp1a3*$^{D923Y/+}$ mice also displayed abnormal gait in short bouts notably in stressful situations (EMM, EPM), in which the hind limbs were splayed, but not to the extent exhibited by *Myshkin* mice (33). However, this was not quantified and should be further characterised in future studies. *Atp1a3*$^{D923Y/+}$ mice were also hyperactive, suggesting that their abnormal gait did not impair movement.

1.4.2 ATPase activity

Typically, AHC-causing mutations reduce NKA activity without affecting protein expression, unlike DYT12 mutations in which NKA α3 protein expression is reduced considerably (15). AHC-causing mutations – S137F, C333F, D801N, S811P and E815K – were shown to cause reduced ATPase activity in COS-7 cells by ~54-90% relative to WT (15). Consistent with *in vitro* studies, *in vivo* studies have also reported reductions in NKA activity – *Myshkin* mice showed normal protein expression of NKA α3 but the enzyme was inactive and caused reductions of ~40% of total NKA activity (α1 + α2 + α3) in the brain (42). In the present study, we generated a mouse model (*Atp1a3*$^{D923Y/+}$) with the mutation D923Y, retaining partial function (15% of WT) as shown from in-vitro studies.

1.4.3 Hyperactivity

Besides the paroxysmal manifestations of AHC, many patients additionally have neuropsychiatric diagnoses such as ADHD and disruptive behaviour, with one of the core symptoms being hyperactivity (6). Consistent with the human AHC phenotype, *Atp1a3*$^{D923Y/+}$ mice were hyperactive as they travelled a greater overall distance in the EPM and EMM. Increased locomotor activity seen in *Atp1a3*$^{D923Y/+}$ mice is consistent with most AHC mouse models.

1.4.4 Anxiolytic-like phenotype

AHC patients are prone to behavioural problems, consistent with ADHD symptoms (6). Impulsivity in particular has been seen in AHC patients, which is associated with reduced anxiety and greater risk-taking behaviour (6). To assess whether *Atp1a3*$^{D923Y/+}$ mice have abnormal behavioural symptoms such as risk-taking behaviour, we used the EPM, EMM and OF.

Atp1a3$^{D923Y/+}$ and WT mice spent longer in the closed arms than the open arms of the EPM, suggesting a preference towards the closed arms for both genotypes. However, *Atp1a3*$^{D923Y/+}$ mice spent significantly less time in the closed arms compared to WT mice. *Atp1a3*$^{D923Y/+}$ mice therefore displayed relatively less thigmotaxis, which suggests that they are less anxious than WT mice. This is because rodents tend to avoid open areas and prefer to stay close to walls (thigmotaxis) when introduced to new environments, therefore the degree of thigmotaxis can be used as a measure of anxiety-like behaviour.

Ethological behaviours such as head dips can also be used as a complementary parameter to assess anxious phenotypes. Anxious mice are less likely to explore the open arms of the EPM given the increased chance of falling off, moreover they are exposed on the open arms, so are more at risk of predation, e.g. a bird of prey. We found that *Atp1a3*$^{D923Y/+}$ mice displayed significantly more head dips than WT mice. Video recordings were taken above the apparatus, which made scoring head dips rather difficult, therefore it would be beneficial to additionally record side views of the EPM in future studies to allow for more accurate scoring. Nevertheless, the results of the EPM indicate that *Atp1a3*$^{D923Y/+}$ mice are less anxious, as they spent less time in the closed arm of the EPM and displayed more risk-taking behaviours.

To further explore whether *Atp1a3*$^{D923Y/+}$ mice have an anxiolytic-like phenotype as suggested by reduced thigmotaxis, mice underwent the EMM. Similar to the EPM, time spent in contact with the wall or in close proximity to the wall (located in the inner zone), is indicative of an anxiety-like state, and decreases in this measure are consistent with anxiolysis. We therefore measured time spent and distance travelled in the zones. *Atp1a3*$^{D923Y/+}$ mice spent significantly more time and travelled a greater distance in the outer zone versus the inner zone compared to WT mice. *Atp1a3*$^{D923Y/+}$ mice spent less time by the wall and therefore exhibited less thigmotactic behaviour relative to WT mice, which is suggestive of an anxiolytic-like phenotype.

These results contrast those of the OF, in which increased anxiety-like behaviour in *Atp1a3*$^{D923Y/+}$ mice compared to WT mice was found. To test for general locomotor activity and anxiety-like behaviours, we divided the open field into three zones for analysis (centre, intermediate, and outer). We found that *Atp1a3*$^{D923Y/+}$ mice spent significantly longer and travelled a greater distance in the outer zone, demonstrating increased thigmotaxis. The number of entries into the centre zone was also analysed as a measure of risk-taking behaviour, as mice generally display aversion to open areas. Given that *Atp1a3*$^{D923Y/+}$ mice were more anxious in the OF, as suggested by increased thigmotaxis, we expected

to see fewer entries into the centre zone, and therefore less risk-taking behaviours than WT mice, which was confirmed as *Atp1a3*$^{D923Y/+}$ mice made significantly fewer entries and travelled less in the centre zone compared to WT mice. Collectively, these OF results suggest that *Atp1a3*$^{D923Y/+}$ mice are more anxious than WT mice; they exhibited more thigmotactic behaviour and made significantly fewer entries into the centre zone. *Atp1a3*$^{D923Y/+}$ mice also displayed fewer unsupported rears but no differences were found in supported rears, which may suggest a balance deficit as the mice require the wall support for rearing. Whilst these results are not consistent with the results of the EPM and EMM, it is again important to note that the mice which underwent the OF were significantly older than the mice used in the EPM and EMM, although this may not explain the differences found.

1.4.5 Learning and memory

Children with AHC are prone to cognitive and language delay (6). Studies have shown that AHC patients experience difficulties in reading and writing, and have poor memory, resulting in lower academic performance relative to other children. In the present study, we therefore assessed cognitive functioning, such as learning and memory, in *Atp1a3*$^{D923Y/+}$ mice using delay and trace fear conditioning.

Fear can be measured as freezing, which is a natural defence response seen in rodents, therefore in fear conditioning, rodents with normal functioning memory will freeze in response to the re-presentation of the cue previously paired with a footshock. One cohort of mice (5-6 months of age) underwent delay fear conditioning (0s trace interval). We found no differences in freezing levels in the training phase or cue test between *Atp1a3*$^{D923Y/+}$ mice and WT mice. Moreover, in the cue test, both genotypes froze significantly more in response to the cue compared to the pre-CS, suggesting that mice were able to successfully associate the CS with the US, therefore demonstrating intact fear memory. The cue test is amygdala dependent; lesions of the amygdala affect cued and contextual fear conditioning, and lesions of the hippocampus affect contextual fear conditioning (82, 83). Therefore, hippocampal and amygdalar function in *Atp1a3*$^{D923Y/+}$ mice can be assessed using contextual and cued fear conditioning. In the present study, we did not assess delay contextual conditioning; however, this would have been an interesting comparison with trace fear conditioning as both are hippocampal dependent.

Trace fear conditioning can be used to reveal subtle memory impairments in mice that have not been found previously in delay fear conditioning by introducing a trace interval.

Moreover, lesions and pharmacological manipulations in the hippocampus impair the ability of animals to associate the CS and US in trace fear conditioning (84-86), whereas delay fear conditioning is unaffected (87, 88). We used a trace interval of 15 seconds between the termination of the CS and the start of the US. No differences in baseline freezing were found between *Atp1a3*$^{D923Y/+}$ and WT mice. In the cue test, *Atp1a3*$^{D923Y/+}$ mice were unable to associate the CS with the US, as they did not freeze significantly more to the CS relative to the pre-CS, and they froze significantly less to the CS compared to WT mice. Together, these suggest that *Atp1a3*$^{D923Y/+}$ mice have subtle impairments in fear memory. However, though WT mice were able to associate the CS with the US, we observed low levels of freezing (~30%) in the cue test. This is considerably lower than in a study of *Myshkin* mice, in which WT mice showed ~65% freezing with a 3-second trace interval (43), therefore suggesting a trace interval of 15 seconds may have been too long.

Interestingly, *Atp1a3*$^{D923Y/+}$ mice showed intact fear memory in delay fear conditioning, but not trace fear conditioning, which may indicate deficits in hippocampal function. Attention and the anterior cingulate cortex is also thought to be necessary for forms of associative learning, such as trace conditioning, but not delay conditioning (89), suggesting deficient attention required for fear trace conditioning in *Atp1a3*$^{D923Y/+}$ mice – this inattentiveness is consistent with ADHD symptoms seen in some AHC patients (6).

To further assess cognitive and motor functioning in *Atp1a3*$^{D923Y/+}$ mice, we used the FST, which has previously been used in other AHC mouse models to assess motivation (34) and induce hemiplegic or dystonic episodes (34, 50, 53). The latency for the mice to begin floating is used an indicator of motivation; the shorter the latency, the less motivated the mice are, which is therefore suggestive of a depressive-like state (90).

Although we did not find any significant differences in latency to start of first immobile episode between *Atp1a3*$^{D923Y/+}$ and WT mice, we found that in the last 4 minutes of immobility, *Atp1a3*$^{D923Y/+}$ mice spent significantly less time immobile than WT mice. Correspondingly, *Atp1a3*$^{D923Y/+}$ mice travelled a greater overall distance. These results are similar to *Myshkin* mice who were also active longer in the FST compared to WT mice (34), however we did not observe forced swimming induced hemiplegia or dystonia in *Atp1a3*$^{D923Y/+}$ mice.

The validity of the FST has been controversial as immobility can be interpreted in many ways. Immobility in the FST is traditionally thought to be representative of a depressive-like phenotype because anti-depressant drugs reduce immobility (91), however it has also

been argued that it is a learned process (also known as learned helplessness), in which mice may remain passive until removed from the water – although the latter is suggestive of anthropomorphism (81). It is unclear whether these results show that *Atp1a3*$^{D923Y/+}$ mice have a less depressive-like phenotype compared with WT mice, however this can be confirmed by behavioural tests such as the sucrose preference test. The immobility displayed by *Atp1a3*$^{D923Y/+}$ mice could also be explained by hyperactivity, which was seen in the EPM and EMM and may therefore confound these results.

1.5 Conclusion

In summary, we found that *Atp1a3*$^{D923Y/+}$ mice containing an NKA α3 missense mutation display a phenotype similar to that of AHC patients and other AHC mouse models. We observed that *Atp1a3*$^{D923Y/+}$ mice display an unusual gait (albeit unquantified) and have deficits in memory and learning. Moreover, we observed hyperactivity, reduced anxiety-like behaviours, and increased risk-taking behaviours in *Atp1a3*$^{D923Y/+}$ mice, which may be likened to neuropsychiatric diagnoses in AHC patients. This mouse line is the first to model the D923Y mutation *in vivo*, therefore behavioural characterisation of *Atp1a3*$^{D923Y/+}$ mice in the present study will provide a good foundation in exploring the hypothesised rescuing effects of the E309D mutation and rostafuroxin treatment. We therefore highlight *Atp1a3*$^{D923Y/+}$ mice as a promising model to investigate disease mechanisms and potential treatments for AHC.

1.6 Future Directions

The present study focused largely on basic phenotyping and assessing cognitive functioning such as behaviour and memory. Given that motor impairments such as hemiplegia and dystonia are defining symptoms of AHC, and *Atp1a3*$^{D923Y/+}$ mice displayed an unusual gait, the motor phenotype of *Atp1a3*$^{D923Y/+}$ mice should be quantified in future studies. Although the footprint test and gait analysis were carried out on *Atp1a3*$^{D923Y/+}$ mice, the methodology used was not reliable enough.

Regrettably, due to COVID-19, I was unable to complete all the experiments I would have liked to have done. Nevertheless, the work in this study has helped identify targetable phenotypes which will be useful in testing rostafuroxin and investigating the effect of the second-site rescue mutation (E309D) in *Atp1a3*$^{D923Y/+}$ mice.

In future studies, we can quantify the behavioural and biochemical effects of chronic rostafuroxin treatment in *Atp1a3*$^{D923Y/+}$ mice and *Myshkin* mice. To achieve the latter, brains will be sent to Prof. Bente Vilsen at Aarhus University, Denmark, for NKA functional assays. Prior to the closure of the lab, Paul Armstrong (postdoc in Clapcote lab) and I had started preparation of rostafuroxin. I also practiced “scruffing” of mice in preparation for oral gavage and received initial oral gavage training.

Moreover, in a separate study, we can determine effects of E309D *in vivo* by phenotyping E309D/D923Y mice bred from D923Y mice injected with tamoxifen (recombination in germ cells), which will express E309D throughout development. D923Y/Cre mice have recently been bred and can be injected with tamoxifen, which will induce Cre recombination and concomitant expression of the E309D mutation. Therefore, the *Atp1a3*$^{D923Y/E309D}$ mice bred from these mice can be behaviourally phenotyped.

Chapter 2:

Effects of genetic ablation of PDZD8 in mice

2.1 Introduction

2.1.1 Intellectual disability

2.1.1.1 Background

Brain development is a highly intricate and regulated process, and its disruption can result in neurodevelopmental disorders (NDDs) (92). NDDs are a collection of heterogeneous conditions which are characterised by cognitive, social, language and motor impairments, which manifest before the age of 18 (93). The most common NDDs are autism spectrum disorder (ASD), attention deficit/hyperactivity disorder (ADHD), and intellectual disability (ID) (93). According to the Diagnostic and Statistical Manual of Mental Disorders, Fifth Edition (DSM-5) criteria, ID is characterised by substantial deficits in intellectual functioning, which refer to mental abilities (problem solving, abstract thinking, and reasoning), and adaptive behaviours, which refer to age-appropriate behaviours required for daily living (93). Intellectual functioning is measured by IQ tests and adaptive behaviours are classified by severity (mild, moderate, severe, or profound) (93, 94). Consequently, treatments for ID are personalised and aim to help maximise an individual's ability and functioning (94).

ID is comorbid with other disorders, including mental health disorders (95), epilepsy (96), and gastroesophageal reflux disease (97). Given the overlap between ID and other disorders, it can be subdivided into non-syndromic ID and syndromic ID (98). Non-syndromic ID classifies intellectual deficits as the sole feature without other associated pathology, whereas syndromic ID is characterised by intellectual deficits occurring with other clinical features. However, syndromic symptoms may include subtle deficits that are undetected, thus blurring the distinction between the two classifications (98).

The prevalence of ID is estimated to be 1% worldwide, but this is highly variable across regions due its heterogeneity, and has a higher incidence in males and children of low socioeconomic status (99). Not only does it affect the wellbeing of the affected individual and their family, ID is also a socio-economic burden due to support services and unemployment costs – it is estimated the average lifetime cost for a person with ID totals up to more than $1 million (100).

2.1.1.2 Non-genetic causes of ID

ID is associated with a range of genetic factors and non-genetic factors, but up to 60% of cases have unknown aetiology (101). Non-genetic causes include environmental factors and risk factors that exert their effects during the vulnerable prenatal, perinatal and postnatal stages of development (102).

A common risk factor that has particular effect during prenatal exposure is alcohol consumption by the mother during pregnancy (103). This causes the transfer of alcohol from the mother's blood to the baby via the placenta, resulting in foetal alcohol spectrum disorder in the offspring, which is characterised by growth deficiency, dysmorphic features, ID and behavioural changes (104). Other prenatal risk factors also include exposure to toxic chemicals during pregnancy such as tobacco or drug abuse and maternal diseases (diabetes, placental disease) (102, 105, 106). Perinatal factors, which take effect in the period immediately before and after childbirth, include delivery-related complications, such as pre-term birth, perinatal asphyxia, low birth weight, and post-natal effects include brain trauma (102, 107).

2.1.1.3 Genetic causes of ID

Genetic causes of ID can occur on different scales, from single nucleotide mutations to cytogenetically visible chromosomal abnormalities, and can be inherited by autosomal recessive, autosomal dominant, and X-linked modes of inheritance (108). Down syndrome, a chromosomal aberration resulting from an extra copy of chromosome 21 (trisomy 21), is one of the most common causes of ID, with an estimated incidence of 1 in 1000 births (109). X-linked intellectual disability (XLID) account for 5-10% of male ID patients and may therefore explain why the incidence of ID is higher in males than females (110). Due to its mode of inheritance, males with a mutation in the X chromosome will express the phenotype, whereas females will only express the phenotype if they are homozygous for the mutation. Fragile X syndrome is the most common XLID, and is caused by the dysfunction of fragile X mental retardation protein (FMRP), a protein involved in the regulation of synaptic plasticity (111). In most cases, this dysfunction is the result of >200 trinucleotide repeats in the promotor region of *FMR1*, which reduces the expression of FMRP (112). In outbred populations, the cause of ID is largely attributed to autosomal dominant mutations, which contrasts with consanguineous (inbred) populations where ID is predominantly caused by recessive mutations (113).

2.1.1.4 Critical time windows

Synaptic plasticity is the ability of the brain to modify its structure and function in response to environmental stimuli and experience (114). This process facilitates learning and memory by altering the strength or efficacy of synaptic transmission, and is therefore essential in early stages of neurodevelopment (114, 115). The capacity for synaptic plasticity is variable throughout one's lifetime, but is particularly enhanced in the period after birth, allowing children to learn rapidly (116). Critical time windows describe a timeframe in which neuronal connections are highly receptive to certain stimuli which help to initiate the development of neuronal circuits in different areas of the brain (114). Changes during these critical time windows are essential as they have long lasting effects throughout life, therefore disruption to these circuits in this period can be detrimental to brain function (115).

2.1.1.5 Animal models of ID

ID treatments often focus on maximising an individual's functioning as few therapeutic treatments exist (117). This is likely due to the fact that ID disease mechanisms are poorly understood, which may be due to its complex aetiological overlaps with various disorders. Although ID is currently uncurable, animal models can be used to replicate cognitive impairment and have therefore been vital in ID research. Moreover, it is easier to study pathophysiology in animals than humans due to low costs, high throughput, and genomic similarity (118). In particular, mice are often used to study human disease due to their ease of manipulation (118).

2.1.2 Membrane contact sites, ERMES and PDZD8

2.1.2.1 Membrane Contact Sites

Although organelles have distinctive functions, they also crosstalk with each other at specialised domains to work collaboratively in performing additional functions. Organelles are highly interconnected and can communicate by forming membrane contact sites (MCSs), in which organelles are brought close together (10-30nm) via tethers (119).

One well-characterised interaction is between the endoplasmic reticulum (ER) and mitochondria (120). Both organelles are essential for cellular functions; the ER, the largest membrane-bound organelle, is involved in cellular protein synthesis, folding, maturation, transport, lipid synthesis and calcium (Ca^{2+}) homeostasis, and mitochondrion have a vital role in energy metabolism. These organelles connect and interact via a complex of proteins at junctions known as mitochondrial-associated membranes (MAMs). There are several tethering complexes described at these junctions, including a Ca^{2+} channel known as inositol 1,4,5-tripohsophate receptor (IP3R) found in the endoplasmic reticulum, voltage-dependent anion channel 1 (VDAC1) located on the outer mitochondrial membrane, and glucose-regulated protein 75 (GRP75) which links the two together (Fig. 14) (120). Yeast also has an ER-mitochondria tethering complex, known as the ER-mitochondrial encounter structure (ERMES), with no identifiable mammalian orthologue (121).

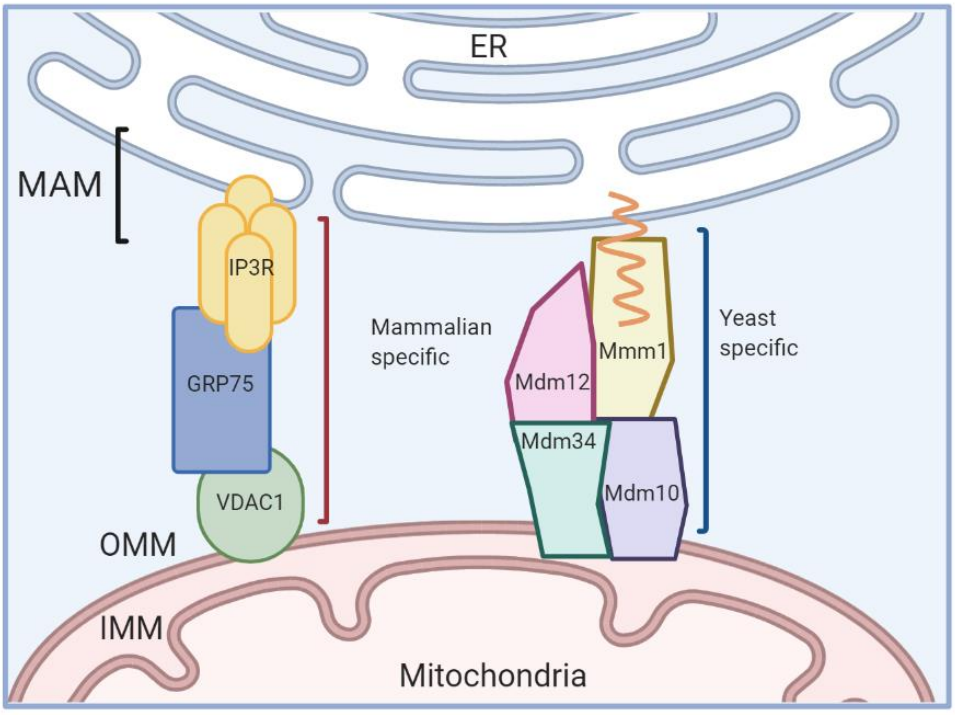

Figure 14. There are multiple tethers found at MAMs, one example of a complex involved in Ca^{2+} transport between the ER and mitochondria is the IP3R-VDAC1-GRP75 tether. ERMES is also a yeast specific ER-mitochondria tethering complex, composed of four proteins Mm1, Mdm12, Mdm34 and Mdm10.

2.1.2.2 ER-mitochondrial encounter structure (ERMES)

An ER-mitochondria tethering complex has also been described in yeast, known as the ER-mitochondrial encounter structure (ERMES) which tethers the two organelle membranes together and most notably aids in the exchange of phospholipids (121). ERMES is composed of four proteins: maintenance of mitochondrial morphology protein 1 (Mmm1) which is integral to the ER membrane; mitochondrial distribution and morphology protein 12 (Mdm12) which is a cytosolic linker; mitochondrial distribution and morphology protein 34 (Mdm34) and 10 (Mdm10), both of which are outer mitochondrial membrane proteins. These proteins localise at the contact sites, and are all required to form the complex (121). Synaptotagmin-like mitochondrial lipid-binding protein (SMP) domain proteins are localised at membrane contact sites (MCSs) and belong to the tubular lipid-binding protein (TULIP) superfamily, which dimerise to form a barrel-like structure with a hydrophobic cavity to allow for lipid exchange (122). Therefore, given that three of the four ERMES proteins contain a SMP domain, and lipid exchange occurs across the ER and mitochondria, it is proposed that the ERMES complex is likely involved in lipid transfer (123). To support this, ERMES structural analyses suggest Mmm1 and Mdm12 associate to form a tubular structure with a hydrophobic cavity (123). Moreover, in vitro studies show that mutations in either Mmm1 or Mdm12 impaired lipid transfer across the complex between the organelles (124). Despite its potential importance in lipid transfer, loss of the ERMES complex in yeast is not lethal and can be bypassed via redundant pathways (125).

It is thought that Mmm1, the only ERMES protein found in the ER membrane, is involved in extracting phospholipids from the ER membrane, which is then passed to Mdm34, located in the outer mitochondrial membrane, via Mdm12 (124). There are two suggested models for the transfer of phospholipids from Mmm1 to Mdm12: the lipid carrier model and the continuous conduit model (124). In the lipid carrier model, proteins Mmm1, Mdm12 and Mdm34 alter their orientations so that the outlet of the lipid binding pocket within each protein is in contact with other proteins. In contrast, the continuous conduit model suggests that there is one continuous hydrophobic tunnel through which the phospholipid travels from Mmm1 to Mdm34.

2.1.2.3 PDZD8

To date, an ERMES orthologue in metazoans has not been identified, however, bioinformatics predicted the existence of SMP-containing proteins, including PDZ domain

containing protein 8 (PDZD8) (126). Since this prediction, Hirabayashi et al. (127) identified PDZD8 as an SMP-containing ER protein mammalian orthologue of Mmm1, although more recently it has been argued it is a paralogue rather than orthologue (128). Both Mmm1 and PDZD8 contain an N-terminal transmembrane domain and an SMP domain (127) (Fig. 15). The PDZD8 protein is additionally followed by a PDZ domain, split C2 domain, C1 domain and a coiled coil region (127, 129). Prior to this discovery, little was known about PDZD8 function. The first report of PDZD8 outlined it as a candidate gene for a disorder seen in Japanese black cattle known as forelimb girdle muscular anomaly (130). Other studies discovered its role interacting with viruses; PDZD8 has been reported to bind to human immunodeficiency virus type 1 (HIV-1) Gag protein to facilitate HIV-1 infection and was highlighted as a potential target in treating the disease (131). PDZD8 was also found to interact with moesin, a cytoskeletal regulatory protein, and found to reduce microtubule stability and yield antiviral properties against herpes simplex virus type 1 (HSV-1) (132).

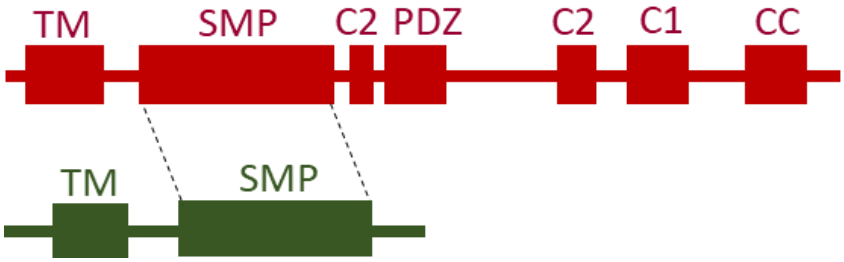

Figure 15. Yeast Mmm1 and mammalian PDZD8 protein domain organisation. Both proteins contain an N-terminal transmembrane domain (TM) and an SMP domain. The PDZD8 protein is additionally followed by a PDZ domain, split C2 domain, C1 domain and a coiled coil region (CC). Image modified from (127, 129).

Since the Hirabayashi et al. paper, it is now understood that PDZD8 is an SMP domain containing protein anchored to the membrane of the ER by a N-terminal transmembrane region with a PDZ domain (127). PDZD8 is suggested to be the paralogue of Mmm1 (ERMES protein) given the similarity of their SMP domains; moreover, they are functionally similar, as PDZD8 was required for the formation of MAMs in HeLa cells (127). The same study identified a role for PDZD8 in Ca^{2+} homeostasis in neurons. In the presence of PDZD8, synaptic activity caused the ER release of Ca^{2+}, which was taken up by mitochondria, whereas neuronal dendrites without PDZD8 resulted in an increase of

Ca^{2+} in the cytoplasm. It can therefore be assumed that PDZD8 is additionally involved in functional processes of ERMES such as lipid exchange.

PDZD8 had previously only been implicated in ER-mitochondria MSCs, but recently Elbaz-Alon et al. (133) discovered that PDZD8 is also enriched at ER-late endosome MCSs where mitochondria can also be recruited to form a three-way contact site. At these sites, PDZD8 is thought to interact with Rab7 and Protrudin (Fig. 16). Late endosomes are organelles that make up part of the endocytic pathway, in which selectively internalised cargo, such as cholesterol, is sorted for recycling or degradation (134). Endosomes undergo maturation from early endosomes to late endosomes and then fuse with the lysosome for degradation (134). Late endosome transport relies on motor proteins and cytoskeletal elements; the dynein motor mediates transport to the minus end of microtubules and kinesin motors are implicated in plus end transport (135). Movement in the late endocytic pathway is controlled by Rab7, a late endosomal Rab GTPase, and protrudin, an effector protein of Rab7 found in the ER; together, along with FYCO1, another Rab7 effector protein, they form ER-late endosome MSCs (136). Protrudin controls late endosome motility by forming a complex with FYCO1, and promotes late endosome transport via kinesin-1 to the cell periphery to fuse with the plasma membrane for neurite outgrowth (136). Although PDZD8 is implicated at this MSC with protrudin and Rab7, its precise role is unknown, but it is assumed to be involved in endosomal maturation and neurite outgrowth.

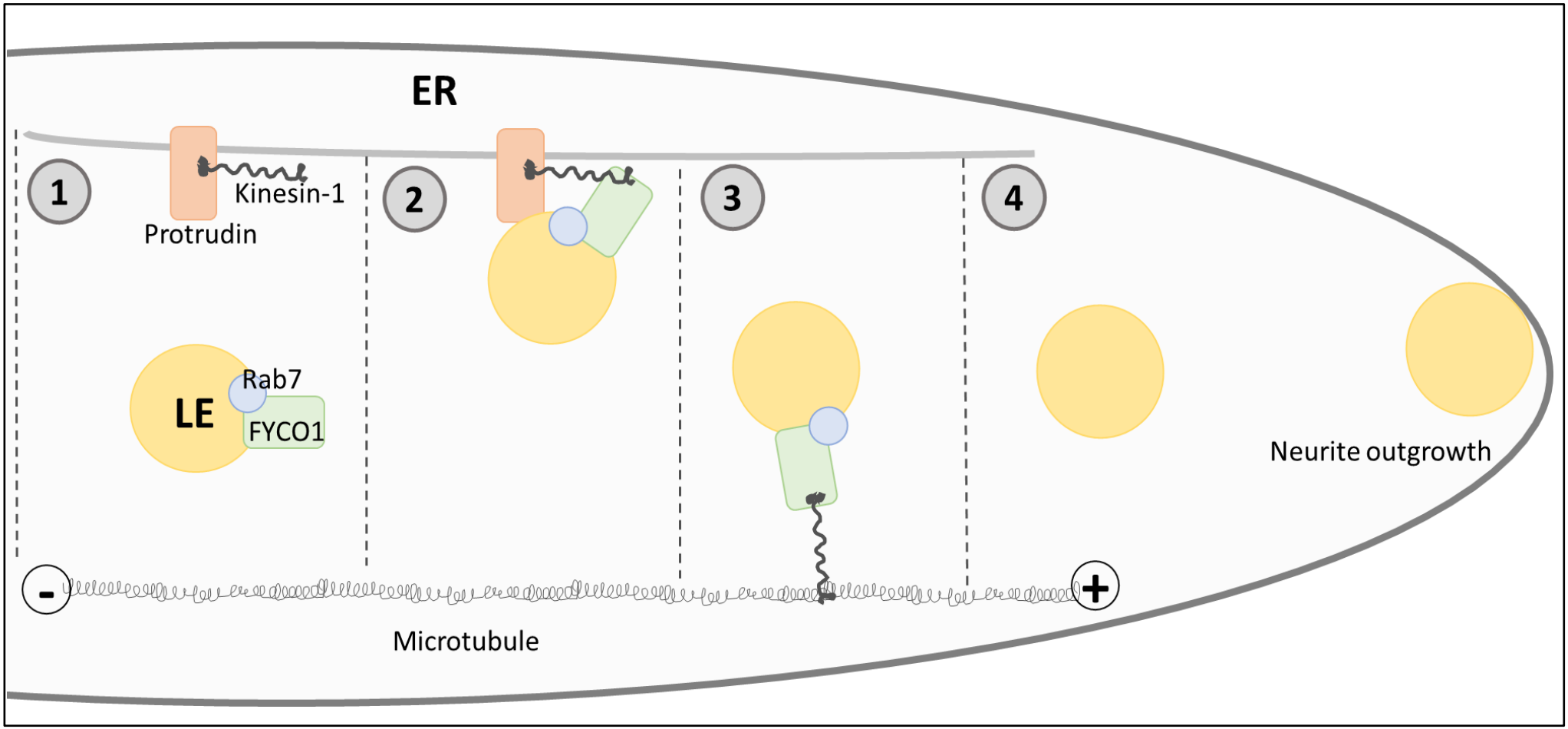

Figure 16. ER-late endosome MSCs are formed through the interaction between ER protein Protrudin, small GTPase Rab7, and late endosome protein FYCO1. Protrudin contacts late endosomes via the detection of Rab7. Protrudin promotes the association between kinesin-1 and FYCO1, which results in late endosome plus end transport along the microtubule towards the periphery of the cell. Late endosomes can then fuse with the plasma membrane for neurite outgrowth.

2.1.3 PDZD8 and intellectual disability (ID)

Consanguinity is a known risk factor for recessive genetic disorders as related parents (marriages between first cousins, double first cousins, or uncles and nieces) have an increased probability of carrying the same recessive variant from a common ancestor, and therefore their offspring are more likely to inherit copies of the recessive gene (113). This may therefore explain why autosomal recessive ID is studied less than other modes of ID inheritance as it has a comparatively lower incidence in western populations (113). ID remains a healthcare and socioeconomic problem, particularly in underdeveloped countries where consanguinity is common and diagnosis is low.

Within the last few years, many novel autosomal ID genes have been detected (137, 138). A study in the Clapcote lab identified a consanguineous Omani family, in which three of the five siblings (two male and one female) presented with ID, autistic features and dysmorphic features (unpublished). One of the male siblings was additionally diagnosed with obsessive compulsive disorder (OCD). Next generation sequencing identified a nonsense mutation in *PDZD8*, resulting in a premature stop codon and a truncated 732-aa PDZD8 protein, that co-segregated in the homozygous state with the ID in the affected siblings. Mutations in *PDZD8* have not previously been associated with ID or any disease to our knowledge.

The results from the Omani family study suggest that nonsense mutations in *PDZD8* can lead to ID, autistic features, and dysmorphic features, but no other cases of ID associated with homozygous null mutation of *PDZD8* have been confirmed, and the pathophysiological mechanisms causing these symptoms remain unknown. Moreover, besides its proposed function in Ca^{2+} dynamics in neurons, little is known about the physiological function of PDZD8 in cognition. Knockdown of a PDZD8 orthologue in Drosophila (CG10362) resulted in long term memory deficits, therefore we hypothesised that PDZD8 null mice may yield a similar phenotype. In the present study, we characterised a PDZD8 knockout (PDZD8KO) mouse model to better understand the consequences of functional loss of PDZD8, the pathophysiological mechanisms that lead to ID and autistic features, and evaluate whether PDZD8KO mice can be used as an animal model of ID.

2.1.4 Aims and Objectives

1. Assess repetitive behaviours by measuring grooming or stereotypic behaviours in the home cage of PDZD8KO mice

2. Assess social behaviour of PDZD8KO mice by measuring sociability and social novelty using the social recognition assay

3. Assess cognitive functioning of PDZD8KO mice by measuring recognition, spatial, and fear memory utilising the continual trial novel object recognition test, Y-maze, Barnes maze, and trace cued fear conditioning

2.2 Materials and Methods

2.2.1 Animals

C57BL/6NTac-Pdzd8$^{tm1b(EUCOMM)Wtsi}$ heterozygotes were supplied by MRC Harwell and intercrossed to generate PDZD8 knock out (PDZD8KO) and WT mouse littermates. Mice were weaned at 3-4 weeks of age and group housed in cages of up to five with same-sex littermates. Mice were tested at 2.5 months of age. Due to the availability of mice, only females were used. Mice were housed under a 12h:12h light/dark cycle and had access to food and water ad libitum. Efforts were made to minimize both suffering and the number of animals used. All animal procedures were carried out in accordance with the Animals (Scientific Procedures) Act 1986, and were approved by the University of Leeds Ethical Review Committee.

For most behavioural experiments, we used 15 PDZD8KO and 10 WT mice, besides the continual trial novel object recognition (10 PDZD8KO and 10 WT) and social interaction test (10 PDZD8KO and 5 WT). Mice were tested in the following sequence: CTNOR → Y maze spatial novelty preference → Barnes maze → social interaction → multiple trial trace fear conditioning. All experiments were recorded using a video camera and subsequently analysed using AnyMaze software (Stoelting Co, Wood Dale, IL, USA). All behavioural apparatuses were cleaned with 70% ethanol between experiments.

2.2.2 Continual Trial Novel Object Recognition

2.2.2.1 Apparatus

Continual trial novel object recognition (CTNOR) was carried out as described previously (139). CTNOR (CI.80514M-1, Campden Instruments Ltd) consisted of two rectangular chambers, a holding area and a larger object area, both with food reward dispensers and the chambers were divided by a small guillotine door (Fig. 17). The doors, food dispensers and overhead video camera were controlled by ABET II operant control software. Objects were placed in the corners of the object chamber (on the side closest to the door); given the angle of the camera, if the objects were placed away from walls, this may have created blind spots, making it difficult to score object exploration. Objects included Lego blocks, falcon tubes, paint tubes, glass bottles, light bulbs, shampoo bottles and lemon squeezy bottles. The apparatus was covered by a clear Perspex roof to prevent mice jumping out, reduce noise, and allow for video recording.

2.2.2.2 Habituation and shuttle training

Throughout CTNOR, mice were food deprived to 90-95% of their free feeding weight, with water available ad libitum. Three days prior to training, mice were given 50% condensed milk (Nestle) mixed with water, 2ml/mouse in home cages.

Mice were given one week of habituation and shuttle training. Mice from the same cage were habituated simultaneously for 30 minutes in two sessions, with the door open, allowing for exploration of both chambers. In a third session, mice were individually put in the apparatus to explore, again with doors open, but this time with access to liquid rewards in the food dispensers. Liquid rewards were automatically replenished after mice moved into the next chamber. Sessions occurred on different days.

Following habituation to the apparatus, mice underwent four sessions of shuttle training individually. Mice were first put in the holding chamber. Upon eating the food reward in the chamber, the door was opened to allow access to the holding area and closed again once the mouse entered the object area. Novel objects were present in the object chamber to allow for habituation to objects in the chamber. These objects were not re-used for the testing phase. After the food reward had been eaten, the door was opened again, allowing access back into the holding chamber – this counted as one trial. Shuttle training ended after 10 minutes or after the completion of 10 trials. Mice progressed onto the object recognition task if they managed to shuttle from one chamber to the other within ~10 seconds.

2.2.2.3 Object recognition task

In this task, like the shuttle training, mice were put in the holding chamber to begin. In the sample phase, two identical copies of an object were placed in the corners of the object chamber. After two minutes of exploration, the door was opened and mice shuttled into the holding chamber for one minute (inter-trial interval). During this interval, the experimenter changed one of the objects for a novel object, and both objects were sprayed with 70% ethanol. The novel object and novel object location were counterbalanced to minimise bias for a particular side or object. Mice were then allowed to explore the familiar object and novel object for 2 minutes, and again the door was opened for the mice to shuttle thorough. This process counted as one trial, and the session ended after 10 trials were completed (roughly 1 hr 20 minutes per mouse). When there were object problems or incomplete trials, mice were removed from analyses of CTNOR.

Discrimination ratios (D2) were calculated by the following:

$$\textbf{D2} = \frac{\text{time exploring novel object} - \text{time exploring familiar object}}{\text{total exploration}}$$

Using D2 values, two types of averages were calculated: cumulative D2 and averaged D2. Cumulative D2 scores were calculated as a 'running total' of the ratio recalculated after each trial for 10 trials within a session (this method ensures that the results are not skewed by individual trials where small amounts of object exploration occurred). For average D2 scores, all individual D2 scores over the 10 trials were averaged.

D2 scores fall between -1 and 1:

−1 = total exploration of the familiar object
0 = no object preference
+1 = total exploration of the novel object

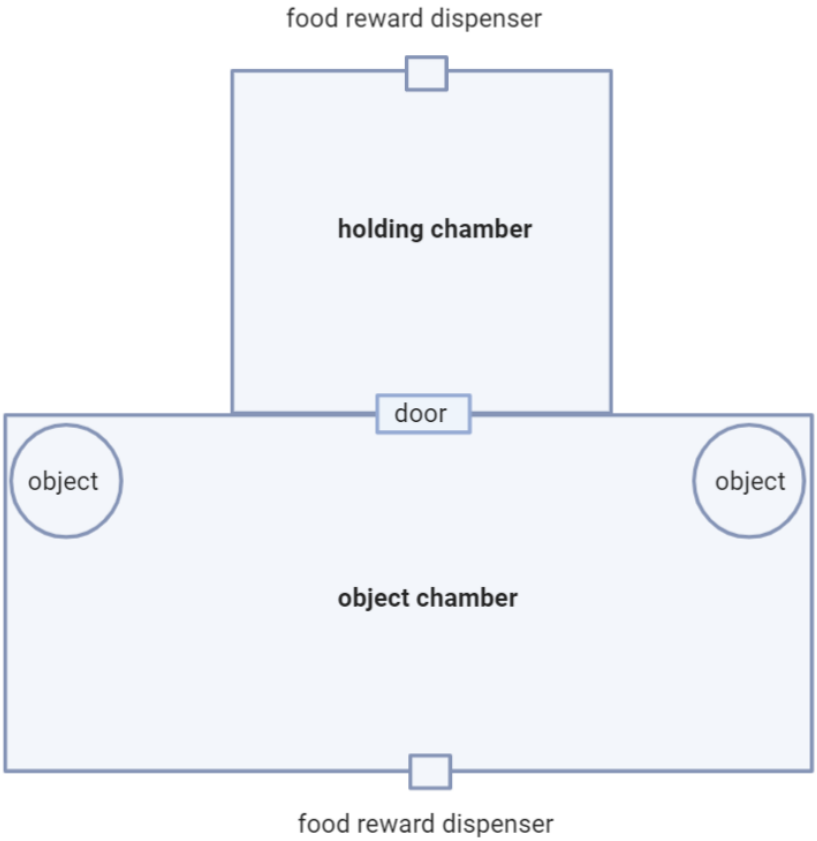

Figure 17. Continual trial novel object recognition apparatus consisted of two chambers (holding and object) separated by a door, and each had a food reward dispenser. Objects were placed in the object chamber for the experiment in the corners of the chamber.

2.2.3 Y-maze spatial novelty preference

The Y-maze was used to test spatial novelty preference, which is a test of stimulus-specific habituation to spatial cues, as previously described (140). The apparatus had three identical and equidistant arms (35cm x 5cm x 15cm), creating a “Y” shape. At the entrance of each arm, there was a slot to allow for the insertion of a door. Within each arm was an intra-maze cue, either black card, striped card or a polka dot card. The room additionally contained extra-maze cues.

During a 5-minute exposure phase, mice were allowed to freely explore two arms: the start arm and another arm (sample arm), leaving one arm (novel arm) blocked. During this time, mice could explore the two arms of the maze such that the allocentric cues associated with the arms became familiar. The start arm remained the same for all mice, but the novel arm was counterbalanced between the two other arms. After the exposure phase, mice were guided back into the start arm, and confined for 1 minute (inter-trial interval). This method reduced handling, to lessen any stress on the mice. In the test phase, all three arms were available for exploration for 3 minutes. Timing of the exposure and test phase began once the mouse had left the start arm. Entries into an arm were counted if the centre point of the mouse had crossed into the arm. The number of entries and the time spent in arms were measured.

Ratios were calculated by the following:

$$\textbf{Ratio} = \frac{\text{time or entries into the novel arm}}{\text{sum of time or entries of three arms}}$$

A ratio score above 33.33 reflected preferential exploration of the novel arm over the familiar and start arms.

2.2.4 Barnes Maze

The Barnes maze was used to study spatial memory. The maze consisted of a white circular PVC platform (diameter: 122cm) elevated ~40cm from the ground, with 20 equidistant holes (diameter: 5cm) around the periphery, and a black PVC escape tunnel which could be mounted under an escape hole. Extra-maze cues surrounded the platform and two lamps were used to provide bright illumination as an aversive stimulus to encourage the mice to find the escape box.

There were three phases: habituation, acquisition and probe. In the habituation trial, mice from the same cage were habituated simultaneously for 2 minutes to familiarise the

platform. The first acquisition trial took place after habituation. Acquisition lasted 4 days with 2 trials each day. The location of the escape box remained constant for each mouse (either northeast, northwest, southeast or southwest), but was counterbalanced between mice. During an acquisition trial, a mouse was put onto the centre of the platform facing north, and a cardboard box was placed on top of the mouse for several seconds. After removal of the box, the trial started and lasted for a maximum of 2 minutes. If a mouse located the escape box and entered it fully, the trial was terminated and the mouse was given an additional minute in the escape box before being returned to its home cage. Alternatively, if the trial was not completed within the 2 minutes, a large glass beaker was placed on top of the mouse, and it was guided into the escape hole. A probe trial began 24 hrs after the last acquisition trial. The escape hole was removed and mice were given 80 seconds to explore.

A video camera above the maze was used to record all trials. We measured latency for the animal to first enter its head into the escape hole, latency to enter the escape hole (whole body), and the distance travelled before first head dip into the escape hole (primary path length). For the probe trial, we measured the time spent in the quadrant of the escape hole, time spent in in the octant of the escape hole, and time spent immediately around the escape hole.

2.2.5 Social Interaction

Social interaction was assessed using a three-chambered box (60cm x 40cm); each compartment was of the same size (20cm x 40cm) and there were two moveable doors which allowed mice to access the left and right chamber. Mice were given 5 minutes to habituate to the apparatus, with all doors open, after which they were guided and kept in the centre compartment. Two empty cylinders were then placed into the left and right compartments, and in one of these cylinders an unfamiliar C57BL/6 female mouse (mouse 1) was placed. The doors were then removed again to allow the mouse to explore for 10 minutes. Thereafter, the mouse was guided and held in the middle compartment, and another unfamiliar C57BL/6 mouse (mouse 2) was introduced into the empty cylinder; the mouse was then released from the centre compartment to explore both cylinders for a further 10 minutes. When mice climbed on objects, they were removed from analyses. The time spent exploring mouse 1 vs the empty cylinder, and the time spent exploring mouse 1 vs mouse 2 were measured.

Ratios were calculated by the following:

Ratio = time spent by mouse 1 or mouse 2

total time spent exploring

A ratio score above 50 reflected preferential exploration of mouse 1 over the empty cylinder or mouse 2 over mouse 1.

2.2.6 Fear conditioning

Fear conditioning was performed as previously described (141). Experiments took place in a fear-conditioning chamber (26 x 26 x 30 cm; Ugo Basile, Model 46004, Varese, Italy). Within the chamber was a conditioning box made of plastic walls and stainless-steel bar flooring. Two different contexts were used, which differed in the internal walls, floor texture, and odour. Conditioning context A comprised a stainless-steel grid floor and walls covered with coloured card – white on the side walls and grey on the rear wall. For context B, white flooring replaced the grid floor, striped cards replaced the coloured cards, and the odour was changed by adding isoamyl acetate under the chamber floor. Mice were left in their home cage outside the experimental room, and individually brought in for testing.

Mice were first exposed to context A for 120 seconds, and then five consecutive trials. Each trial consisted of a 20s tone (CS) (80dB, 3600Hz), a 20s trace interval (defined as a temporal gap between the termination of the tone and start of the foot shock), a 2s foot shock (US) (0.65mA), and an inter-trial interval (ITI) of 60s, after which the process would start again and repeat until 5 trials were completed. Mice were kept in the chamber for an additional 30s before returning to their home cage. 24 hrs after exposure to context A, mice were introduced to context B, with a similar protocol but without the administration of foot shocks. 7 days later, mice were put back into context A for 3 minutes. AnyMaze software was used to record videos, administer foot shocks, control sound and light, and measure freezing (minimum freezing detection: 1000ms).

2.2.7 Statistical Analysis

Videos were scored and analysed by an experimenter blind to the genotypes. All statistics were calculated using GraphPad Prism and SPSS. Shapiro-Wilk test was used to test for normality and Levene's test was used to test for homoscedasticity. If data were normal and homoscedastic, we used 2-way ANOVA with Sidak's multiple comparisons post hoc test and unpaired t-tests. If data were not homoscedastic, t-tests with Welch's corrections

were used. If data were not normal, we used Mann Whitney U tests and Friedman ANOVA with the Wilcoxon signed-rank test. Data are presented as mean ± standard error of the mean (SEM) and $p < 0.05$ was considered significant. Graphs were created using GraphPad Prism and figures were generated using BioRender or Microsoft Powerpoint.

2.3 Results

2.3.1 Phenotype

PDZD8KO mice were visibly smaller in size than WT mice, although this became less distinguishable with age and was not quantified. PDZD8KO mice also engaged in repetitive and excessive vertical jumping behaviours while leaning against the wall of their home cage and occasionally during behavioural experiments (Fig. 18). The frequency of jumps and duration of jump bouts were observably high and long. A summer student in Clapcote lab, Kirstie Goodchild, quantified jumping in the open field and found that PDZD8KO mice jumped significantly more on average compared to WT mice (data not shown).

Figure 18. Screenshot from a video of a PDZD8KO mouse leaning against the wall of the home cage and jumping repetitively.

2.3.2 Continual trial novel object recognition

To assess recognition memory, we used continual trial novel object recognition (CTNOR), which is similar to the traditional novel object recognition, but involves multiple trials in one session. Two averages were calculated for the trials – a cumulative D2 and average D2 (Fig. 19 *A,B*). Although both averages tended to show that PDZD8KO mice had a higher discrimination index relative to WT mice, neither reached statistical significance (average D2: PDZD8KO M = 0.4034, SD = 0.15; WT M = 0.3444, SD = 0.19; t(12) = 0.644, ns; cumulative D2: PDZD8KO mean rank = 8.29; WT mean rank = 6.71; U = 19, ns). Moreover, both averages and individual trials for both genotypes had discrimination indexes above 0, which indicates increased exploration of the novel object relative to the familiar object. There were additionally no significant differences between genotype per trial, although PDZD8KO mice appear to have a higher discrimination index than WT mice at almost every trial (Fig. 19 *C*).

Regarding time exploring an object, mice generally spent longer time exploring novel objects relative to familiar objects, but there was no genotypic difference (main effect of object (F (1,24) = 15.72, p = 0.0006), with no main effect of genotype (F (1,24) = 1.360, ns) nor object x genotype interaction (F (1,24) = 0.08814, ns) (Fig. 19 *D*).

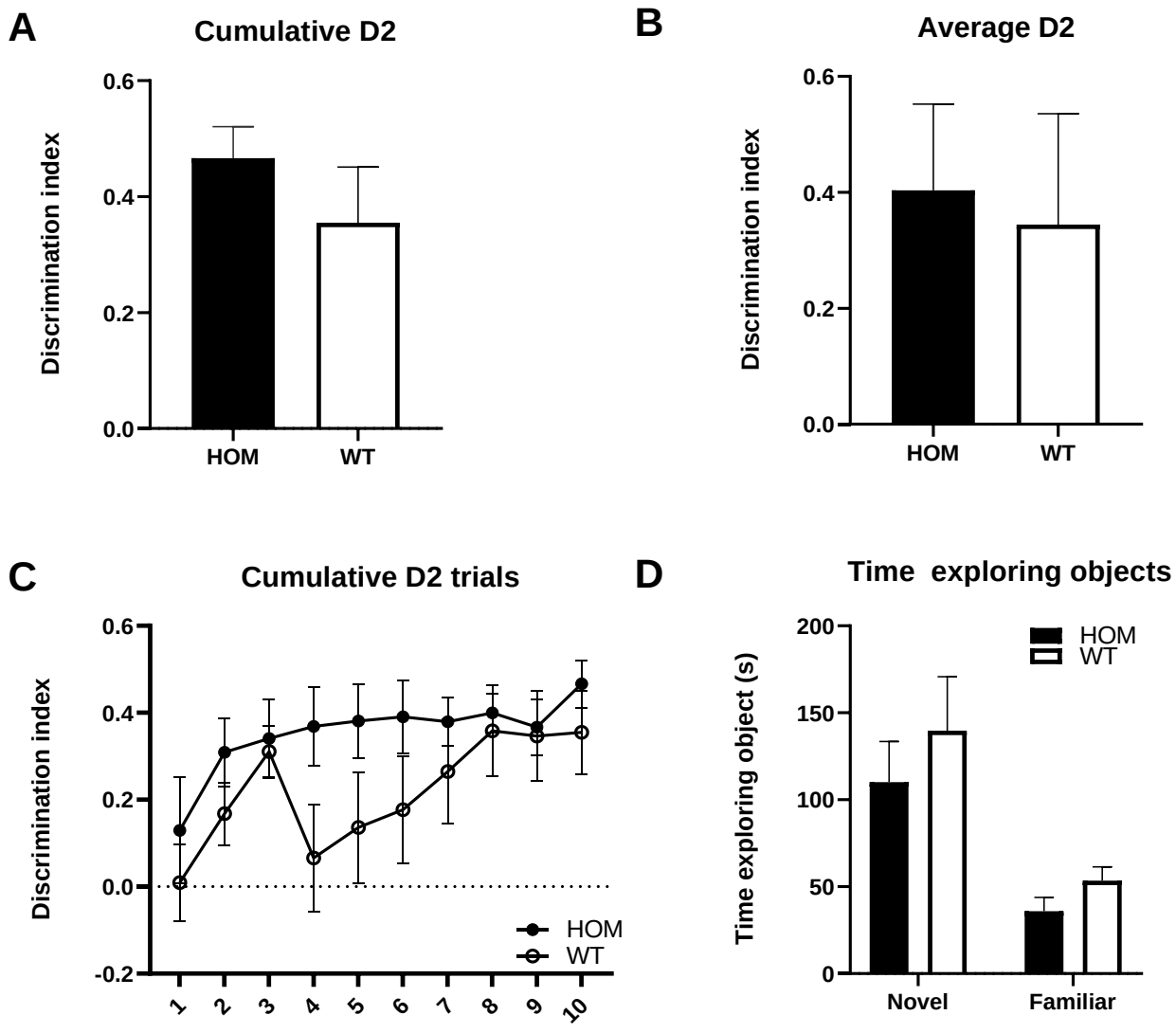

Figure 19. Continual trial novel object recognition. Cumulative and average D2 were calculated by averaging individual trials of each session for PDZD8KO (HOM; n = 7) and WT (n = 7) mice. There were no differences in genotype in cumulative D2 (**A**) and average D2 (**B**). Cumulative D2 index scores were not different between PDZD8KO and WT mice at every trial (**C**). There were no genotype differences between time exploring novel or familiar objects (**D**). Data shown as mean ± SEM.

2.3.3 Y Maze spatial novelty preference

The Y-maze was used to test spatial novelty preference, a test of stimulus-specific habituation to spatial cues. After the sample phase in which one arm was blocked, mice were given 3 minutes to explore all arms. There was a main effect of arm (F (2,69) = 24.25, p = 0.0001), with no main effect of genotype (F (1,69) = 0.1438, ns) nor arm x genotype interaction (F (2,69) = 1.820, ns) (Fig. 20 *A*). Post-hoc analysis showed that mice spent more time in the novel arm relative to the other arms (start arm: p = 0.000065, familiar arm: p = 0.00027). One sample t-tests revealed that both PDZD8KO and WT mice had a significant preference towards the novel arm (t (14) = 16.62, p=0.0001 and t (9) = 13.47, p=0.0001, respectively), but were not statistically different from each other (Fig. 20 *B*).

Although we did not find any statistically significant differences in short-term spatial novelty preference between PDZD8KO and WT mice, the slightly lower novel arm preference ratio and time in the novel arm of PDZD8KO mice compared to WT mice suggest that subtle deficits in spatial memory might be revealed in a harder task.

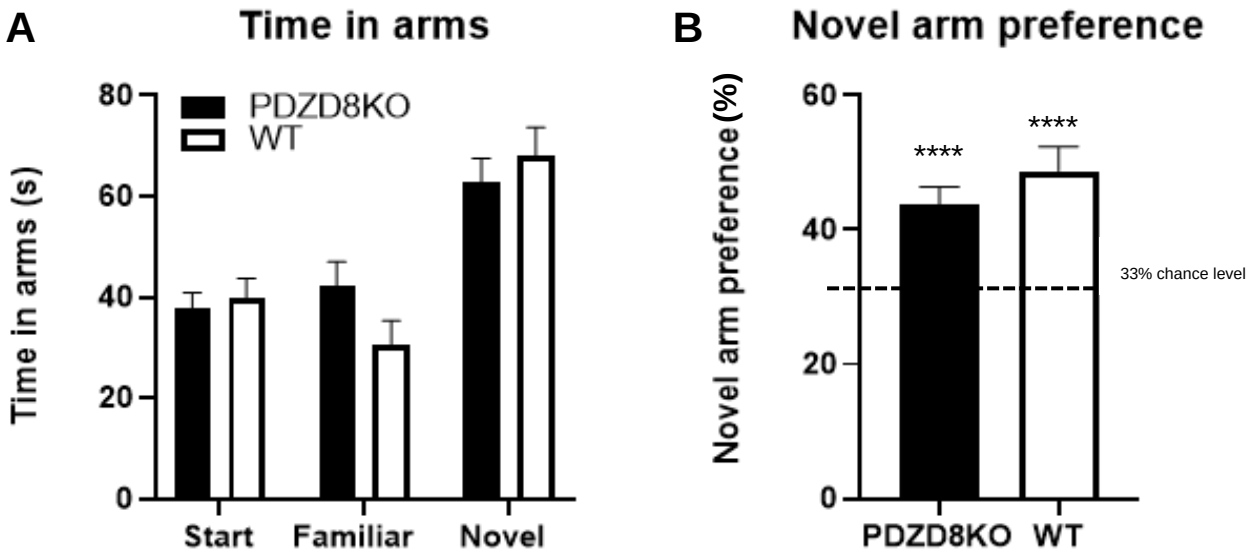

Figure 20. Y maze spatial novelty preference. PDZD8KO (n = 15) and WT (n = 10) mice spent more time in the novel arm relative to the start and familiar arm, but did not differ significantly from each other (A). Moreover, both genotypes had a preference for the novel arm over the start and familiar arm (preference index score above 33.33) (B). Data shown as mean ± SEM. Compared to chance level ****p<0.0001.

2.3.4 Barnes Maze

To further investigate spatial memory in PDZD8KO, we used the Barnes Maze to assess hippocampal-dependent spatial learning and memory. In the acquisition phase, mice were given 8 trials (2 trials per day) to learn the location of the escape hole. In the analysis, trials were averaged per day. PDZD8KO (n = 10) and WT (n = 15) mice performed similarly in the acquisition phase. The average latency for mice to first enter the escape hole (Friedman ANOVA, PDZD8KO: p = 0.002; WT: p = 0.00002 and Mann-Whitney U tests and t-tests: D1: U = 61, *ns*, D2: U = 71, *ns*, D3: t (23) = 0.899, *ns*, D4: U = 58, *ns*), first enter their head into the escape hole (Friedman ANOVA, PDZD8KO: p = 0.00009, WT: p = 0.0002 and Mann-Whitney U and t-tests: D1: U = 70.5, *ns*, D2: t (23) = -0.666, *ns*, D3: U = 72, *ns*, D4: t (23) = -1.248, *ns*) and their path efficiency (Friedman ANOVA, PDZD8KO: p = 0.00003, WT: p = 0.01 and Mann Whitney U and t-tests: D1: U = 60, *ns*, D2: t (23) = -0.569, *ns*, D3: U = 67, *ns*, D4: U = 58, *ns*) were not significantly different between genotypes, although they did decrease with increased trials (Fig. 21 *A,B,C*).

After the acquisition phase, mice underwent the probe trial, and results were analysed on AnyMaze in quadrants and sections (Fig. 21 *D,E*). During this trial, PDZD8KO mice spent less time in the target quadrant relative to WT mice (t-tests: PDZD8KO: M = 53.45, SD = 10.35; WT: M = 39.76, SD = 19.30, t (22.25) = 2.296, p = 0.031. Levene's test indicated unequal variances: F = 4.345, p = 0.048, so Welch's correction was used). Time spent in the left (t-tests: t (23) = -0.014, *ns*), right (t-tests: t (23) = -1.942, *ns*) and opposite (Mann Whitney U test: U = 44.5, *ns*) quadrants were not significantly different between genotypes (Fig. 21 *F)*. Time spent in the area immediately around the holes was also assessed (Fig. 21 *G)*. In Fig. 21 *G*, negative numbers represent the number of holes to the left of the target hole (e.g. -1 represents the first hole to the left of the target), and positive numbers represent the number of holes to the right of the target. PDZD8KO spent less time in the area surrounding the target (t (23) = 3.22, p = 0.004), -1 hole (t (23) = 3.78, p = 0.001), -2 hole (U = 28.5, p = 0.009), and more time at the +2 hole (U = 29, p = 0.011) compared with WT mice. Heat maps of the probe trial appear to show that WT mice were more concentrated near the target hole (west or east) compared to PDZD8KO mice (Fig. 21 *H,I*).Mice with deficits in spatial learning are more likely to utilise non-spatial than spatial methods to find the target hole. Non-spatial strategies include chaining around the maze, and non-spatial strategies can be identified by focal or direct movement to the target hole. Results show that both PDZD8KO and WT mice did not solve the Barnes maze using one strategy, but rather used both (Fig. 21 *J,K*).

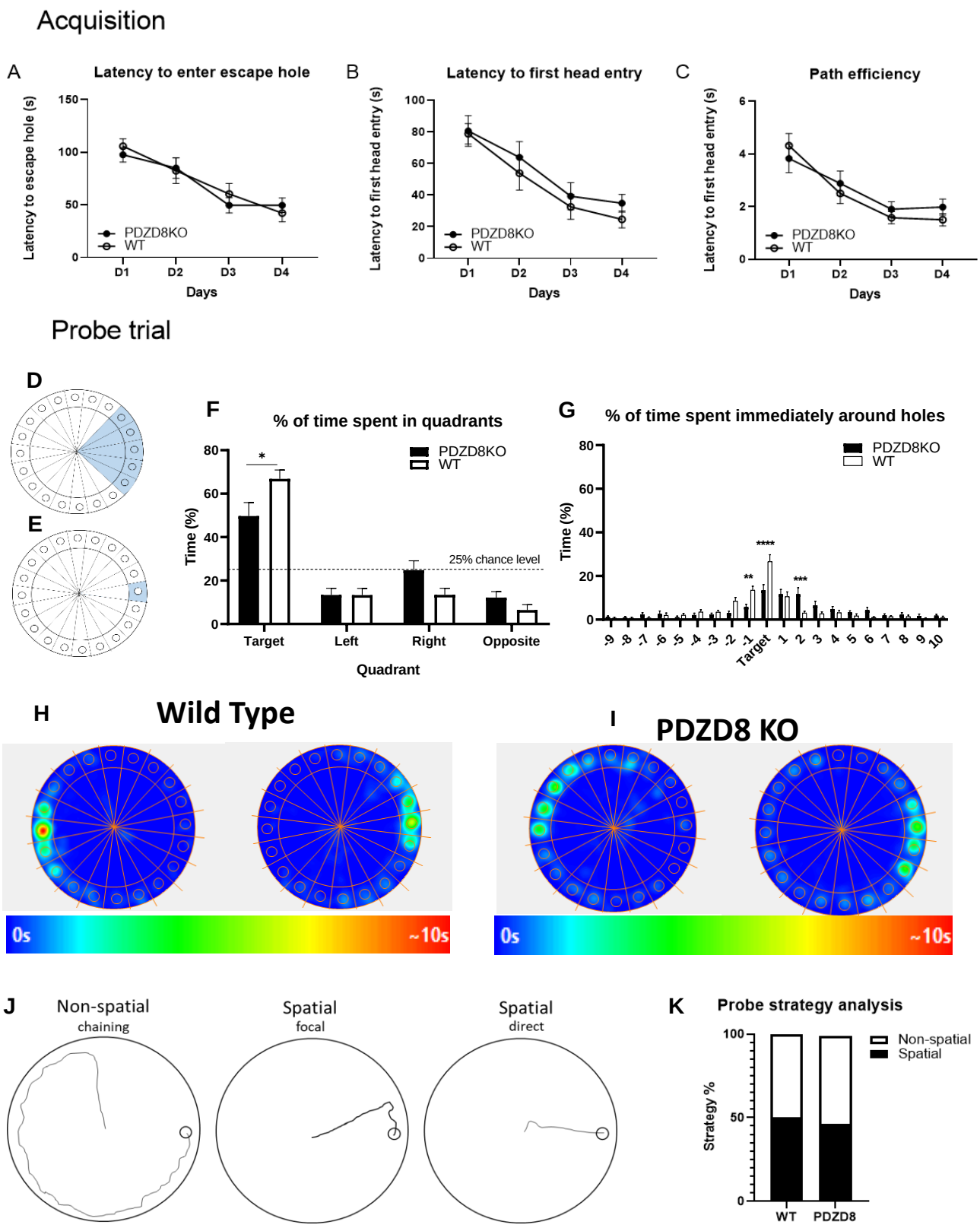

Figure 21. Latency to enter escape hole, latency to first head entry, and path efficiency were similar between PDZD8KO and WT mice in the acquisition stage and tended to decrease over the 4 days (A, B, C). For probe trial analysis, the Barnes maze was divided into quadrants (left, right and opposite the target quadrant, and the target quadrant) and sections as pictured (D,E). PDZD8KO mice spent significantly less time in the target quadrant than WT mice but similar amounts of time in other quadrants (F). Time spent immediately around the holes was also analysed and showed PDZD8KO mice spent significant less time in the area around the target zone (**G**). Heat maps of mice on the probe trial appear to show that WT mice were more concentrated near the target hole (west or east) than PDZD8KO mice (H,I). Mice can utilise different strategies, both non-spatial and spatial strategies, to find the escape hole (J); we found that PDZD8KO and WT mice used both strategies to a similar degree (K). Data shown as mean ± SEM, *p<0.05; **p<0.01; ***p<0.001; ****p<0.0001.

2.3.5 Social Interaction

We tested sociability of PDZD8KO mice by using the social interaction behaviour assay. After habituation, a novel mouse was introduced into one of the empty containers. Mice generally spent more time exploring mouse 1 relative to the empty container, but there were no genotypic differences in exploration of mouse 1 versus the empty container (main effect of mouse location: F (1,26) = 13.22, p = 0.0012; no main effect of genotype: F (1,28) = 1.016, *ns*); mouse location x genotype interaction: F (1,26) = 1.056), *ns*) (Fig. 22 *A*). Preference ratios also show that both PDZD8KO and WT mice had a preference towards the mouse compared to the empty container (one sample t-test: PDZD8KO p = 0.0001, WT p = 0.0012) but did not differ from each other (t(13) = 0.3778, *ns*) (Fig. 22 *B*).

Mouse 2 was then introduced into the empty container, and we assessed social novelty in PDZD8KO mice. Time spent exploring mouse 1 and mouse 2 were very similar between genotypes (no main effect of mouse location (F (1,26) = 0.4381, *ns*), no main effect of genotype (F (1,26) = 0.1115, *ns*), and no mouse location x genotype interaction (F (1,26) = 0.05523, ns)) (Fig. 22 *C*). Preference ratios show that PDZD8KO and WT mice did not significantly differ from each other, and neither genotype had a preference for mouse 2 over mouse 1 (t(13) = 0.1864, ns; one sample t-test: PDZD8KO and WT, *ns*) (Fig. 22 *D*). Distance travelled was measured for both the sociability and novel sociability stages of the test. Regardless of genotype, mice generally covered more distance in the sociability stage (mouse 1 vs container) relative to the novel sociability stage (mouse 1 vs mouse 2), but there was no interaction between genotype and stage (main effect of stage (F (1,26) = 4.884, p = 0.0361), no main effect of genotype (F (1,26) = 0.3039, *ns*), and no stage x genotype interaction (F (1,26) = 0.1853, *ns*)) (Fig. 22 *E*).

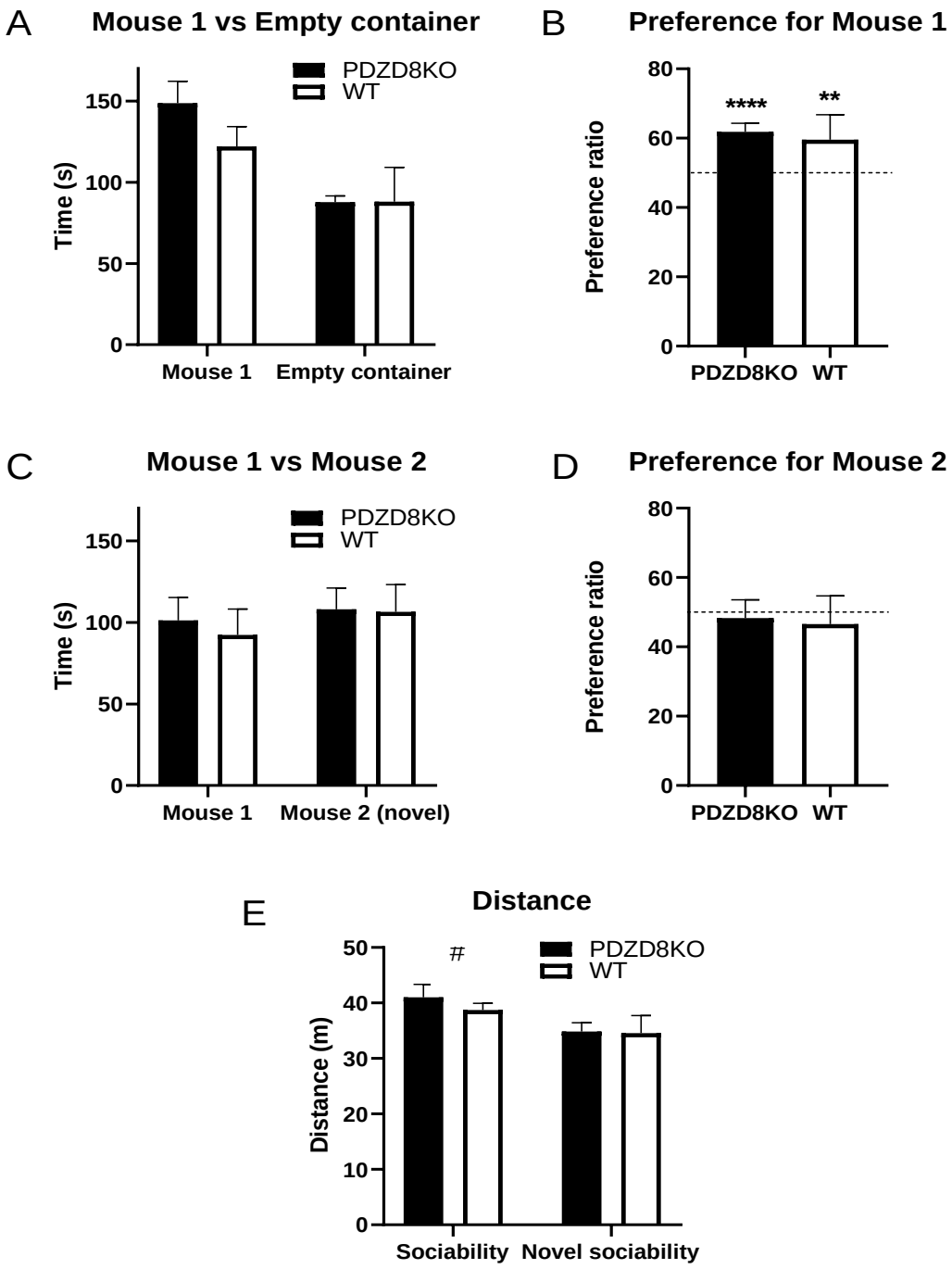

Figure 22. Social interaction. PDZD8KO (n = 10) and WT (n = 5) mice did not differ significantly in time spent exploring mouse 1 versus the empty container (A), and both genotypes had a preference towards mouse 1 over the empty container (B). After mouse 2 was introduced into the empty container, there was no difference in time spent between genotypes exploring mouse 1 (familiar) versus mouse 2 (novel) (C). Moreover, neither genotype showed a preference towards mouse 2 (D). Mice generally travelled more in the sociability stage than the novel sociability stage, but there were no genotypic differences at either stage (E). Data shown as mean ± SEM. Compared to chance *p<0.05; **p<0.01; ***p<0.001; ****p<0.0001, and between sociability and novel sociability #p<0.05.

2.3.6 Trace Fear Conditioning

In the training stage of fear conditioning, mice were exposed to context A for 120 seconds, and then five consecutive trials (20s tone, 20s trace interval, 2s foot shock, 60s intertrial interval). We measured freezing over the five consecutive CS presentations and trace intervals (TI). Freezing tended to increase with trials (CS trials: Friedman ANOVA, PDZD8KO: $p<0.0001$; WT: $p<0.0001$; TI trials: Friedman ANOVA, PDZD8KO: $p<0.0001$; WT: $p<0.0001$), however there were no differences in genotype at each trial (Pre-CS: U = 50.5, *ns*; CS1: U = 71, *ns*; TI1: U = 74, *ns*; CS2: U = 67.5, *ns*; TI2: U = 74.5, *ns*; CS3: U = 61.5, *ns*; TI3: U = 67.5, *ns*; CS4: U = 74, *ns*; TI4: U = 55, *ns* ;CS5: U = 73, *ns*; TI5: U = 38, *ns*) (Fig. 23*A*).

On the second day, mice were placed into a new context, and received the same CS. The cue test was similar to training but included no foot shock. Again, there were no differences in freezing between genotypes at each trial (Pre-CS: U = 68, *ns*; CS1: U = 64, *ns*; CS2: U = 75, *ns*; TI2: U = 55, *ns;* CS3: U = 66, *ns;* TI3: U = 75, *ns;* CS4: U = 39.5, *ns;* TI4: U = 62.5, *ns;* CS5: U = 72*, ns;* TI5: U = 45*, ns*) (Fig. 23*B*).

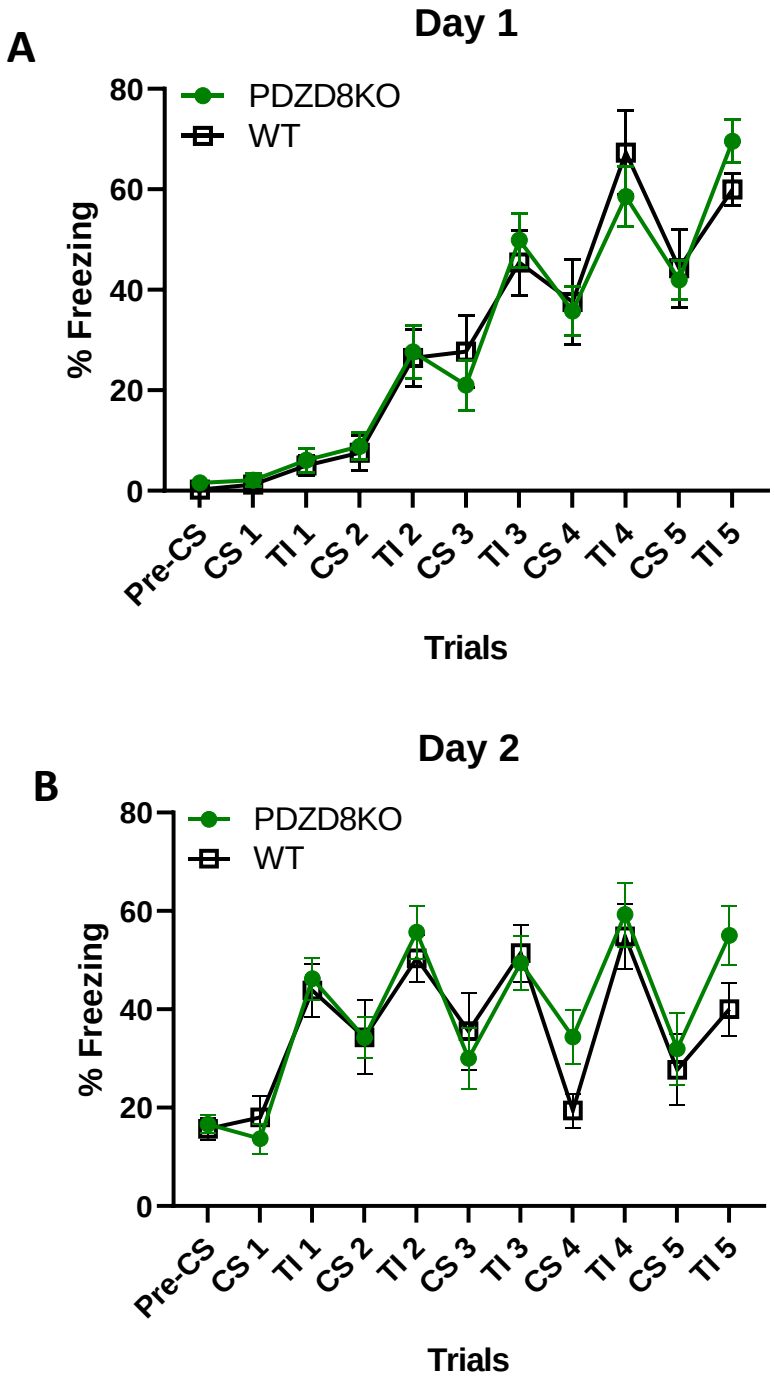

Figure 23. Trace Fear Conditioning. PDZD8KO (n = 15) and WT (n = 10) mice underwent 5 conditioning trials and froze similarly across all intervals (A). There were also no genotype differences at each trial on day 2 (B). Data shown as mean ± SEM.

2.4 Discussion

In the present study, we characterised a novel mouse model homozygous for a null mutation of PDZD8 (PDZD8KO), replicating the mutation seen in some members of the Omani family who exhibited autistic-like behaviours and had intellectual disability. Autism comprises variable deficits in two core symptom domains: social interaction and communication, and repetitive behaviours, therefore we assessed repetitive behaviours and sociability (Aim 1 and 2). Also, given that individuals of the Omani family had intellectual disability, we tested for cognitive impairments (Aim 3). Results from this study are summarised in Table 5 and indicate that PDZD8KO mice exhibit repetitive jumping behaviours and show subtle spatial memory deficits in the Barnes maze. The main limitation of this study was that only female mice were used – we therefore highlight the need for further behavioural testing on male PDZD8KO mice, particularly as there are sex differences in ASD and ID (142, 143).

Behavioural Test		PDZD8KO vs WT	Significance
CTNOR	Cumulative discrimination index scores	ND	*ns*
	Average discrimination index scores	ND	*ns*
	Time spent exploring novel object	ND	*ns*
Spatial novelty preference	Novel arm preference	ND	*ns*
Barnes maze	Acquisition – latency to first enter escape hole	ND	*ns*
	Acquisition – latency to first	ND	*ns*
	Acquisition – path efficiency	ND	*ns*
	Probe – time spent in target quadrant	↓	*
	Probe – time spent in area immediately around target hole	↓	****
Social interaction	Preference for mouse 1 over empty cylinder	ND	*ns*
	Preference for mouse 2 (novel) over mouse 1 (familiar)	ND	*ns*
Trace fear conditioning	Freezing in response to the CS in the cue test	ND	*ns*

Table 5. Table summarising the results of behavioural tests, comparing PDZD8KO mice to WT mice. N.D, no difference; ↑, statistically significant increase in behaviour of PDZD8KO mice relative to WT mice, ↓ statistically significant decrease in behaviour of PDZD8KO mice relative to WT mice. Significance: *ns*, not significant, **p*<0.05, ***p*<0.01, ****p*<0.001, *****p*<0.0001.

2.4.1 Autistic-like behaviours

The children of the Omani family in which *PDZD8* mutations were found have autistic-like behaviours, and one child additionally presented with OCD. PDZD8KO mice exhibited stereotypic jumping behaviour in the corners of their home cage, therefore we quantified this behaviour in the open field, and found that PDZD8KO mice significantly jumped more than WT mice. This stereotypic behaviour can be likened to repetitive motor behaviours and obsessive-compulsive mannerisms seen in people with autism spectrum disorder (ASD) and OCD (144).

In a separate unpublished study, PDZD8KO mice were also found to spend a significantly longer amount of time on the running wheel relative to WT mice, which can again reflect repetitive behaviours. However, the reliability of the data is uncertain as a small sample size was used (n=3). PDZD8KO mice were also observed to have fewer whiskers (vibrissae), which may have arisen due to excessive grooming – a behaviour often seen in ASD and OCD mouse models (144). Grooming behaviours were not analysed in the present study, but would be interesting to assess in the future.

ASD is characterised by hyposociability (145), and is often assessed in mouse models of ASD using the behavioural assay, the 3-chamber social interaction test. We found that PDZD8KO and WT mice both exhibited a preference for sociability (mouse over empty cylinder) but not a preference for social novelty (novel mouse over familiar mouse). Genotypic differences were not apparent, which may suggest that PDZD8KO mice do not have sociability deficits in this test, however interpreting the results of this data is limited by the small WT sample (n=5). Moreover, our WT mice did not show a preference for social novelty, which is unusual as WT mice in other studies tend to show a preference towards novel mice (146, 147). The overall distance travelled by mice in the social novelty stage was also significantly lower than in the sociability stage, suggesting that mice had habituated to the apparatus and became uninterested in new stimuli. This behavioural test requires the experimenter to shuttle mice into the centre chamber frequently between habituation, sociability, and novel sociability stages. Although mice were not physically handled during this, we cannot exclude the possibility that shuttling of mice may have introduced stress and confounded the results.

2.4.2 Memory

People with ID often have deficits in different domains of cognitive function, such as learning and memory. We therefore assessed different types of memories: recognition, fear and spatial memory. Our results show that PDZD8KO mice may have subtle deficits in spatial memory, which is partly consistent with the long-term memory deficits seen in the knockdown of a PDZD8 orthologue in Drosophila (CG10362).

2.4.2.1 Recognition memory

The novel object recognition (NOR) task is commonly used to assess recognition memory (148). Mice are first exposed to two identical objects in a sample phase, and then one is replaced with a novel object in the test phase. This task exploits the fact that mice tend to prefer novel objects over familiar objects. Preference towards the novel object suggests mice can discriminate between the two, and therefore have intact recognition memory. NOR usually consists of one trial (one sample and test phase), however more recently, CTNOR was developed in which mice undergo several trials within one session (139). Mice are taught to shuttle between a holding chamber and object chamber, therefore during the task mice do not need to be handled. Multiple trials allow for increased sensitivity and reliability of results; therefore, our sample size was relatively small. Moreover, CTNOR reduces handling compared with conventional NOR and therefore reduces stress and behavioural variability (139, 149).

Positive discrimination index values show that PDZD8KO mice had a preference towards the novel object over the familiar object, and also had similar D2 scores to WT mice. This suggests that recognition memory in PDZD8KO mice is intact. We had to remove some mice from the analysis as we encountered problems with objects during the testing sessions. Certain objects were made of materials that enabled mice to chew on them, causing mice to spend an increased time at the object, thus introducing bias. During scoring, it was therefore hard to distinguish between the mouse exploring the object or simply chewing it. In addition, we also observed stereotypic jumping behaviour of PDZD8KO mice in their home cages, which was also evident in the CTNOR apparatus. This resulted in some mice managing to jump high enough to get on top of some objects and consequently spending a large amount of time in that position. Again, this introduced bias and difficulties in scoring exploration. However, it can be argued that climbing on top

of objects is a form of exploration. Nevertheless, in the future, we shall use entirely climbable objects or entirely non-climbable objects.

2.4.2.2 Spatial memory

The Y-maze spatial novelty preference task was used to test spatial memory in PDZD8KO mice, and results show that they had a preference towards the novel arm. This preference appeared lower than that shown by WT mice, but this difference did not reach statistical significance. This task is similar in design to the novel object recognition task (148), in which mice tend to show a preference towards the novel object as a result of habituation to the familiar object. Our results are consistent with this as we did not find any genotypic differences in the Y-maze spatial novelty preference task or CTNOR.

Given our Y-maze spatial novelty preference task results, we hypothesised that PDZD8KO mice may have subtle deficits in spatial memory. As the Y-maze task is a measure of spatial working memory, we thought it would be interesting to assess long-term spatial memory using the Barnes maze. During acquisition training in the Barnes maze, we found no learning differences between PDZD8KO and WT mice. In the probe trial, both PDZD8KO mice and WT mice spent longer in the target quadrant relative to the other quadrants, but the PDZD8KO mice spent significantly less time in the quadrant zone compared to the WT mice. This was similarly found when analysing more specific Barnes maze parameters, such as the time spent immediately around the holes. These data suggest that PDZD8KO mice can locate the escape hole, just not as well as WT mice, thereby suggesting a mild spatial memory impairment. However, time spent in a zone may not necessarily be the best measure of spatial learning. It could be argued that the PDZD8KO mice may have noticed the absence of the escape box at the learnt location, and therefore decided to explore other parts of the maze. We also looked at the strategy mice used to locate the escape hole in the probe trial. Extra-maze visual cues were placed around the maze throughout training and the probe trial. We categorised the strategy to locate the target hole into spatial, non-spatial, and random. We expected that PDZD8KO mice were less likely to use spatial strategies, but this was not found. The Morris water maze, another behavioural test that assesses spatial memory, is thought to be more sensitive than the Barnes Maze and would be interesting to employ in future experiments (58).

2.4.2.3 Fear memory

Given that we found impairments, albeit subtle, in spatial memory in the Barnes maze but not the Y-maze, we used fear conditioning to further study memory in PDZD8KO mice. Rather than use delay fear conditioning, we used trace fear conditioning, in which a short temporal gap between the cue and the foot shock makes it harder for animals to form an association between the two. We used a protocol with multiple conditioning trials as reported in another study (141) to observe fear learning and memory over time.

During training, PDZD8KO and WT mice tended to freeze more with CS and TI trials, and there were no genotypic differences at each CS and TI trial. These suggest that PDZD8KO are able to sense the foot shock and hear the auditory tone like WT mice. On the second day, PDZD8KO mice, but not WT mice, froze significantly more to the CS at trials 2 and 4, and both PDZD8KO and WT mice froze significantly more at each TI trial compared to the pre-CS, indicating that they were able to associate the CS with the US. Moreover, there were again no differences between genotypes at each trial. These suggest that PDZD8KO fear memory is intact, however, given that there were 5 conditioning trials, this may have resulted in overtraining of the mice, which may have masked any subtle deficit. Future studies should use standard trace fear conditioning and contextual fear conditioning to study memory, as these are both hippocampal dependent.

2.4.3 Pathophysiological correlates

Since the Hirabiyashi et al. study (127), we know that ER-mitochondria MSCs are functionally important in cortical pyramidal neurons in maintaining Ca^{2+} homeostasis – a role already evident in non-neuronal cells. Interestingly, PDZD8 has been implicated at these sites as a tether. Its knockdown resulted in a significant reduction in ER-mitochondria contact sites despite structurally intact organelles, and also impaired Ca^{2+} mitochondrial import from the ER, resulting in increased cytoplasmic Ca^{2+}. Together these findings highly suggest that PDZD8 is involved in regulating Ca^{2+} dynamics in dendrites. Ca^{2+} is essential in physiological functioning; it is required for neurotransmission in which action potentials result in the intracellular influx of Ca^{2+} into the presynaptic neuron, causing the release of neurotransmitters into the synaptic cleft to bind to postsynaptic receptors for the transfer of electrical information (150). Moreover, Ca^{2+} plays an important role in synaptic plasticity. NMDA activation results in the influx of Ca^{2+} into the post synaptic neuron which is associated with long term potentiation – defined as the strengthening of synapses due to sustained stimuli (150). This is particularly interesting

as long-term potentiation is a process that underlies memory, and we found a deficit in spatial memory, although this does not explain why we did not find deficits in other types of memories. The pathophysiology is seemingly complex, therefore further elucidation of PDZD8 function is required before more hypotheses can be made.

PDZD8 is also implicated in ER-late endosome MSCs and interacts with Protrudin and Rab7, thereby highlighting its potential role in protrusions and neurite outgrowth (129, 133). Neurite outgrowth is the growth and extension of neural processes (dendrites and axons), which is particularly important in neuronal development and neuronal regeneration after nerve injury (151). Dendrites require growth and branching to form connections with target synapses, and this interaction determines the type of electrical information received by the neuron (152). Through this mechanism, complex neuronal networks are able to assemble across the brain to allow for normal nervous system functioning. It is therefore no surprise that dysfunction in neurite outgrowth can cause aberrant nervous system connectivity and is described in numerous disorders, including ID and ASD (153). Lipid transfer is known to occur at MSCs and is important in membrane expansion required for neurite outgrowth; this may therefore highlight a role for PDZD8 – particularly as it has an SMP domain (154, 155). A mechanism for lipid transfer at ER-late endosome sites has not been identified. At these sites, ORP1L, a cholesterol binding protein, and VAP, an integral ER VAMP-associated protein, have been suggested to act as cholesterol sensors, not transporters, which again may suggest a role for PDZD8 (156). Together, these suggest that mutations in PDZD8 could result in the impairment of neurite outgrowth and consequently disrupt neural connectivity which manifests as ID or ASD. Alternatively, rather than a disruption in neurite outgrowth causing disease, it may represent a secondary effect occurring during disease progression.

PDZD8 has an SMP domain and is a paralogue of Mmm1; therefore it can be assumed that it plays a role in lipid transport (127). ER-late endosome MSCs are involved in endosome maturation, and during this process, late endosomes determine whether cholesterol is targeted for degradation by lysosomes, recycled to the ER or Golgi apparatus, or brought to the plasma membrane (157). Therefore, cholesterol efflux from late endosomes is required. As PDZD8 is found at these MCS, and interact with molecules involved in endosomal maturation, it is conceivable that a mutation in *PDZD8* results in the impairment of cholesterol export from late endosomes. Niemann-Pick C disease is an example of the consequence of abnormal accumulation of cholesterol in late endosomes (158).

2.5 Conclusion

In summary, we have identified specific behavioural deficits in mouse model homozygous for a null mutation of PDZD8 that may have translational relevance to individuals with PDZD8 deletion, such as those in the Omani family who present with ID and autistic features. In this study, we found that PDZD8KO mice displayed deficits in one symptom domain of autism, repetitive jumping, and also had subtle impairment in long term spatial memory. These results highlight the potential of the PDZD8KO mouse model as a useful tool for investigating the underlying pathophysiology of PDZD8 dysfunction and provides useful information about which cognitive domains may be affected. Further characterisation of PDZD8 function, including male mice, is required and future studies should test other domains of cognitive functioning.

2.6 Future Directions

Further behavioural studies should be carried out to better characterise the PDZD8KO mouse model. Given that spatial impairment in the Barnes maze was found, further insight into spatial memory can be tested using the Morris water maze, especially as this test is thought to be more sensitive. Furthermore, autistic-like features should be quantified, especially as excessive jumping behaviours were observed without being quantified. Mice in home cages should be video-recorded and analysed for frequency and duration of jumping and self-grooming behaviours.

Moreover, PDZD8 is emerging as an important protein at MSCs, likely with roles in endosomal maturation, neurite outgrowth, and Ca^{2+} homeostasis. In particular, since the recent finding of PDZD8's interaction with Protrudin and Rab7 at ER-late endosomes, it is tempting to hypothesise on its involvement in neurite outgrowth. As PDZD8 contains an SMP domain and cholesterol is required for membrane expansion (and thus neurite outgrowth), it would be interesting to compare neurite outgrowth in PDZD8KO and WT mice.

References

1. Verret S, Steele JC. Alternating hemiplegia in childhood: a report of eight patients with complicated migraine beginning in infancy. Pediatrics. 1971;47(4):675-80.

2. Bourgeois M, Aicardi J, Goutieres F. Alternating hemiplegia of childhood. J Pediatr. 1993;122(5 Pt 1):673-9.

3. Sweney MT, Silver K, Gerard-Blanluet M, Pedespan JM, Renault F, Arzimanoglou A, et al. Alternating hemiplegia of childhood: early characteristics and evolution of a neurodevelopmental syndrome. Pediatrics. 2009;123(3):e534-41.

4. Maas R, Kamsteeg EJ, Mangano S, Vazquez Lopez ME, Nicolai J, Silver K, et al. Benign nocturnal alternating hemiplegia of childhood: A clinical and nomenclatural reappraisal. Eur J Paediatr Neurol. 2018;22(6):1110-7.

5. Silver K, Andermann F. Alternating hemiplegia of childhood: a study of 10 patients and results of flunarizine treatment. Neurology. 1993;43(1):36-41.

6. Jasien JM, Bonner M, D'Alli R, Prange L, McLean M, Sachdev M, et al. Cognitive, adaptive, and behavioral profiles and management of alternating hemiplegia of childhood. Developmental medicine and child neurology. 2019;61(5):547-54.

7. Panagiotakaki E, Gobbi G, Neville B, Ebinger F, Campistol J, Nevsimalova S, et al. Evidence of a non-progressive course of alternating hemiplegia of childhood: study of a large cohort of children and adults. Brain : a journal of neurology. 2010;133(Pt 12):3598-610.

8. Sasaki M, Ishii A, Saito Y, Morisada N, Iijima K, Takada S, et al. Genotype-phenotype correlations in alternating hemiplegia of childhood. Neurology. 2014;82(6):482-90.

9. Sasaki M, Ishii A, Saito Y, Hirose S. Progressive Brain Atrophy in Alternating Hemiplegia of Childhood. Mov Disord Clin Pract. 2017;4(3):406-11.

10. Saito Y, Sakuragawa N, Sasaki M, Sugai K, Hashimoto T. A case of alternating hemiplegia of childhood with cerebellar atrophy. Pediatric neurology. 1998;19(1):65-8.

11. Polanowska KE, Dziezyc K, Rosewich H, Ohlenbusch A, Seniow JB. Alternating Hemiplegia of Childhood in Two Adult Patients with a Mild Syndrome. Cogn Behav Neurol. 2018;31(4):214-9.

12. Panagiotakaki E, De Grandis E, Stagnaro M, Heinzen EL, Fons C, Sisodiya S, et al. Clinical profile of patients with ATP1A3 mutations in Alternating Hemiplegia of Childhood-a study of 155 patients. Orphanet J Rare Dis. 2015;10:123.

13. Morth JP, Pedersen BP, Toustrup-Jensen MS, Sorensen TL, Petersen J, Andersen JP, et al. Crystal structure of the sodium-potassium pump. Nature. 2007;450(7172):1043-9.

14. Roubergue A, Roze E, Vuillaumier-Barrot S, Fontenille MJ, Meneret A, Vidailhet M, et al. The multiple faces of the ATP1A3-related dystonic movement disorder. Mov Disord. 2013;28(10):1457-9.

15. Heinzen EL, Swoboda KJ, Hitomi Y, Gurrieri F, Nicole S, de Vries B, et al. De novo mutations in ATP1A3 cause alternating hemiplegia of childhood. Nature genetics. 2012;44(9):1030-4.

16. Neville BG, Ninan M. The treatment and management of alternating hemiplegia of childhood. Developmental medicine and child neurology. 2007;49(10):777-80.

17. Samanta D. Management of Alternating Hemiplegia of Childhood: A Review. Pediatric neurology. 2019.

18. Mikati MA, Kramer U, Zupanc ML, Shanahan RJ. Alternating hemiplegia of childhood: clinical manifestations and long-term outcome. Pediatric neurology. 2000;23(2):134-41.

19. Sasaki M, Sakuragawa N, Osawa M. Long-term effect of flunarizine on patients with alternating hemiplegia of childhood in Japan. Brain & development. 2001;23(5):303-5.

20. Holm R, Toustrup-Jensen MS, Einholm AP, Schack VR, Andersen JP, Vilsen B. Neurological disease mutations of alpha3 Na(+),K(+)-ATPase: Structural and functional perspectives and rescue of compromised function. Biochimica et biophysica acta. 2016;1857(11):1807-28.

21. Heinzen EL, Arzimanoglou A, Brashear A, Clapcote SJ, Gurrieri F, Goldstein DB, et al. Distinct neurological disorders with ATP1A3 mutations. The Lancet Neurology. 2014;13(5):503-14.

22. Harris JJ, Jolivet R, Attwell D. Synaptic energy use and supply. Neuron. 2012;75(5):762-77.

23. Kaplan JH. Biochemistry of Na,K-ATPase. Annu Rev Biochem. 2002;71:511-35.

24. Qiu LY, Krieger E, Schaftenaar G, Swarts HG, Willems PH, De Pont JJ, et al. Reconstruction of the complete ouabain-binding pocket of Na,K-ATPase in gastric H,K-ATPase by substitution of only seven amino acids. J Biol Chem. 2005;280(37):32349-55.

25. Kanai R, Ogawa H, Vilsen B, Cornelius F, Toyoshima C. Crystal structure of a Na+-bound Na+,K+-ATPase preceding the E1P state. Nature. 2013;502(7470):201-6.

26. Li Z, Langhans SA. Transcriptional regulators of Na,K-ATPase subunits. Front Cell Dev Biol. 2015;3:66.

27. Gadsby DC, Bezanilla F, Rakowski RF, De Weer P, Holmgren M. The dynamic relationships between the three events that release individual Na(+) ions from the Na(+)/K(+)-ATPase. Nat Commun. 2012;3:669.

28. Bassi MT, Bresolin N, Tonelli A, Nazos K, Crippa F, Baschirotto C, et al. A novel mutation in the ATP1A2 gene causes alternating hemiplegia of childhood. Journal of medical genetics. 2004;41(8):621-8.

29. Swoboda KJ, Kanavakis E, Xaidara A, Johnson JE, Leppert MF, Schlesinger-Massart MB, et al. Alternating hemiplegia of childhood or familial hemiplegic migraine? A novel ATP1A2 mutation. Annals of neurology. 2004;55(6):884-7.

30. Viollet L, Glusman G, Murphy KJ, Newcomb TM, Reyna SP, Sweney M, et al. Correction: Alternating Hemiplegia of Childhood: Retrospective Genetic Study and Genotype-Phenotype Correlations in 187 Subjects from the US AHCF Registry. PloS one. 2015;10(8):e0137370.

31. Capuano A, Garone G, Tiralongo G, Graziola F. Alternating Hemiplegia of Childhood: Understanding the Genotype-Phenotype Relationship of ATP1A3 Variations. Appl Clin Genet. 2020;13:71-81.

32. Yang X, Gao H, Zhang J, Xu X, Liu X, Wu X, et al. ATP1A3 mutations and genotype-phenotype correlation of alternating hemiplegia of childhood in Chinese patients. PloS one. 2014;9(5):e97274.

33. Kirshenbaum GS, Dawson N, Mullins JG, Johnston TH, Drinkhill MJ, Edwards IJ, et al. Alternating hemiplegia of childhood-related neural and behavioural phenotypes in Na+,K+-ATPase alpha3 missense mutant mice. PloS one. 2013;8(3):e60141.

34. Kirshenbaum GS, Clapcote SJ, Duffy S, Burgess CR, Petersen J, Jarowek KJ, et al. Mania-like behavior induced by genetic dysfunction of the neuron-specific Na+,K+-ATPase alpha3 sodium pump. Proceedings of the National Academy of Sciences of the United States of America. 2011;108(44):18144-9.

35. Li M, Jazayeri D, Corry B, McSweeney KM, Heinzen EL, Goldstein DB, et al. A functional correlate of severity in alternating hemiplegia of childhood. Neurobiology of disease. 2015;77:88-93.

36. Hamlyn JM, Blaustein MP, Bova S, DuCharme DW, Harris DW, Mandel F, et al. Identification and characterization of a ouabain-like compound from human plasma. Proceedings of the National Academy of Sciences of the United States of America. 1991;88(14):6259-63.

37. Bauer N, Muller-Ehmsen J, Kramer U, Hambarchian N, Zobel C, Schwinger RH, et al. Ouabain-like compound changes rapidly on physical exercise in humans and dogs: effects of beta-blockade and angiotensin-converting enzyme inhibition. Hypertension. 2005;45(5):1024-8.

38. Goto A, Yamada K, Nagoshi H, Terano Y, Omata M. Stress-induced elevation of ouabainlike compound in rat plasma and adrenal. Hypertension. 1995;26(6 Pt 2):1173-6.

39. Goldstein I, Levy T, Galili D, Ovadia H, Yirmiya R, Rosen H, et al. Involvement of Na(+), K(+)-ATPase and endogenous digitalis-like compounds in depressive disorders. Biological psychiatry. 2006;60(5):491-9.

40. Ferrari P, Ferrandi M, Valentini G, Bianchi G. Rostafuroxin: an ouabain antagonist that corrects renal and vascular Na+-K+- ATPase alterations in ouabain and adducin-dependent hypertension. Am J Physiol Regul Integr Comp Physiol. 2006;290(3):R529-35.

41. Song H, Karashima E, Hamlyn JM, Blaustein MP. Ouabain-digoxin antagonism in rat arteries and neurones. The Journal of physiology. 2014;592(5):941-69.

42. Clapcote SJ, Duffy S, Xie G, Kirshenbaum G, Bechard AR, Rodacker Schack V, et al. Mutation I810N in the alpha3 isoform of Na+,K+-ATPase causes impairments in the sodium pump and hyperexcitability in the CNS. Proceedings of the National Academy of Sciences of the United States of America. 2009;106(33):14085-90.

43. Kirshenbaum GS, Dachtler J, Roder JC, Clapcote SJ. Characterization of cognitive deficits in mice with an alternating hemiplegia-linked mutation. Behavioral neuroscience. 2015;129(6):822-31.

44. Kirshenbaum GS, Idris NF, Dachtler J, Roder JC, Clapcote SJ. Deficits in social behavioral tests in a mouse model of alternating hemiplegia of childhood. Journal of neurogenetics. 2016;30(1):42-9.

45. Timothy JWS, Klas N, Sanghani HR, Al-Mansouri T, Hughes ATL, Kirshenbaum GS, et al. Circadian Disruptions in the Myshkin Mouse Model of Mania Are Independent of Deficits in Suprachiasmatic Molecular Clock Function. Biological psychiatry. 2018;84(11):827-37.

46. Moseley AE, Williams MT, Schaefer TL, Bohanan CS, Neumann JC, Behbehani MM, et al. Deficiency in Na,K-ATPase alpha isoform genes alters spatial learning, motor

activity, and anxiety in mice. The Journal of neuroscience : the official journal of the Society for Neuroscience. 2007;27(3):616-26.

47. DeAndrade MP, Yokoi F, van Groen T, Lingrel JB, Li Y. Characterization of Atp1a3 mutant mice as a model of rapid-onset dystonia with parkinsonism. Behavioural brain research. 2011;216(2):659-65.

48. Kirshenbaum GS, Saltzman K, Rose B, Petersen J, Vilsen B, Roder JC. Decreased neuronal Na+, K+ -ATPase activity in Atp1a3 heterozygous mice increases susceptibility to depression-like endophenotypes by chronic variable stress. Genes Brain Behav. 2011;10(5):542-50.

49. Ikeda K, Satake S, Onaka T, Sugimoto H, Takeda N, Imoto K, et al. Enhanced inhibitory neurotransmission in the cerebellar cortex of Atp1a3-deficient heterozygous mice. The Journal of physiology. 2013;591(13):3433-49.

50. Helseth AR, Hunanyan AS, Adil S, Linabarger M, Sachdev M, Abdelnour E, et al. Novel E815K knock-in mouse model of alternating hemiplegia of childhood. Neurobiology of disease. 2018;119:100-12.

51. Hunanyan AS, Fainberg NA, Linabarger M, Arehart E, Leonard AS, Adil SM, et al. Knock-in mouse model of alternating hemiplegia of childhood: behavioral and electrophysiologic characterization. Epilepsia. 2015;56(1):82-93.

52. Holm TH, Isaksen TJ, Glerup S, Heuck A, Bottger P, Fuchtbauer EM, et al. Cognitive deficits caused by a disease-mutation in the alpha3 Na(+)/K(+)-ATPase isoform. Scientific reports. 2016;6:31972.

53. Isaksen TJ, Kros L, Vedovato N, Holm TH, Vitenzon A, Gadsby DC, et al. Hypothermia-induced dystonia and abnormal cerebellar activity in a mouse model with a single disease-mutation in the sodium-potassium pump. PLoS genetics. 2017;13(5):e1006763.

54. Gantois I, Fang K, Jiang L, Babovic D, Lawrence AJ, Ferreri V, et al. Ablation of D1 dopamine receptor-expressing cells generates mice with seizures, dystonia, hyperactivity, and impaired oral behavior. Proceedings of the National Academy of Sciences of the United States of America. 2007;104(10):4182-7.

55. Curzon P, Rustay NR, Browman KE. Cued and Contextual Fear Conditioning for Rodents. In: nd, Buccafusco JJ, editors. Methods of Behavior Analysis in Neuroscience. Frontiers in Neuroscience. Boca Raton (FL)2009.

56. Leger M, Quiedeville A, Bouet V, Haelewyn B, Boulouard M, Schumann-Bard P, et al. Object recognition test in mice. Nature protocols. 2013;8(12):2531-7.

57. Vorhees CV, Williams MT. Assessing spatial learning and memory in rodents. ILAR J. 2014;55(2):310-32.

58. Gawel K, Gibula E, Marszalek-Grabska M, Filarowska J, Kotlinska JH. Assessment of spatial learning and memory in the Barnes maze task in rodents-methodological consideration. Naunyn Schmiedebergs Arch Pharmacol. 2019;392(1):1-18.

59. Hughes RN. The value of spontaneous alternation behavior (SAB) as a test of retention in pharmacological investigations of memory. Neurosci Biobehav Rev. 2004;28(5):497-505.

60. Koehl M, Battle S, Meerlo P. Sex differences in sleep: the response to sleep deprivation and restraint stress in mice. Sleep. 2006;29(9):1224-31.

61. Gould TJ, Rowe WB, Heman KL, Mesches MH, Young DA, Rose GM, et al. Effects of hippocampal lesions on patterned motor learning in the rat. Brain research bulletin. 2002;58(6):581-6.

62. Kirshenbaum GS, Dachtler J, Roder JC, Clapcote SJ. Transgenic rescue of phenotypic deficits in a mouse model of alternating hemiplegia of childhood. Neurogenetics. 2016;17(1):57-63.

63. Brooks SP, Dunnett SB. Tests to assess motor phenotype in mice: a user's guide. Nat Rev Neurosci. 2009;10(7):519-29.

64. Zhao Y, DeCuypere M, LeDoux MS. Abnormal motor function and dopamine neurotransmission in DYT1 DeltaGAG transgenic mice. Experimental neurology. 2008;210(2):719-30.

65. Dang MT, Yokoi F, McNaught KS, Jengelley TA, Jackson T, Li J, et al. Generation and characterization of Dyt1 DeltaGAG knock-in mouse as a model for early-onset dystonia. Experimental neurology. 2005;196(2):452-63.

66. Carter RJ, Lione LA, Humby T, Mangiarini L, Mahal A, Bates GP, et al. Characterization of progressive motor deficits in mice transgenic for the human Huntington's disease mutation. The Journal of neuroscience : the official journal of the Society for Neuroscience. 1999;19(8):3248-57.

67. Smedemark-Margulies N, Brownstein CA, Vargas S, Tembulkar SK, Towne MC, Shi J, et al. A novel de novo mutation in ATP1A3 and childhood-onset schizophrenia. Cold Spring Harbor molecular case studies. 2016;2(5):a001008.

68. Anand A, Verhoeff P, Seneca N, Zoghbi SS, Seibyl JP, Charney DS, et al. Brain SPECT imaging of amphetamine-induced dopamine release in euthymic bipolar disorder patients. The American journal of psychiatry. 2000;157(7):1108-14.

69. Harvey AG. Sleep and circadian rhythms in bipolar disorder: seeking synchrony, harmony, and regulation. The American journal of psychiatry. 2008;165(7):820-9.

70. Kansagra S, Mikati MA, Vigevano F. Alternating hemiplegia of childhood. Handbook of clinical neurology. 2013;112:821-6.

71. Wahab A. Difficulties in Treatment and Management of Epilepsy and Challenges in New Drug Development. Pharmaceuticals. 2010;3(7):2090-110.

72. Stafstrom CE, Carmant L. Seizures and epilepsy: an overview for neuroscientists. Cold Spring Harbor perspectives in medicine. 2015;5(6).

73. Kammerman S, Wasserman L. Seizure disorders: Part 1. Classification and diagnosis. West J Med. 2001;175(2):99-103.

74. Krishnan GP, Filatov G, Shilnikov A, Bazhenov M. Electrogenic properties of the Na(+)/K(+) ATPase control transitions between normal and pathological brain states. Journal of neurophysiology. 2015;113(9):3356-74.

75. Pedley TA, Zuckermann EC, Glaser GH. Epileptogenic effects of localized ventricular perfusion of ouabain on dorsal hippocampus. Experimental neurology. 1969;25(2):207-19.

76. Rosewich H, Thiele H, Ohlenbusch A, Maschke U, Altmuller J, Frommolt P, et al. Heterozygous de-novo mutations in ATP1A3 in patients with alternating hemiplegia of childhood: a whole-exome sequencing gene-identification study. The Lancet Neurology. 2012;11(9):764-73.

77. Einholm AP, Toustrup-Jensen MS, Holm R, Andersen JP, Vilsen B. The rapid-onset dystonia parkinsonism mutation D923N of the Na+, K+-ATPase alpha3 isoform disrupts Na+ interaction at the third Na+ site. J Biol Chem. 2010;285(34):26245-54.

78. Holm R, Einholm AP, Andersen JP, Vilsen B. Rescue of Na+ affinity in aspartate 928 mutants of Na+,K+-ATPase by secondary mutation of glutamate 314. J Biol Chem. 2015;290(15):9801-11.

79. Dachtler J, Glasper J, Cohen RN, Ivorra JL, Swiffen DJ, Jackson AJ, et al. Deletion of alpha-neurexin II results in autism-related behaviors in mice. Transl Psychiatry. 2014;4:e484.

80. Pickles AR, Hendrie CA. Anxiolytic-induced attenuation of thigmotaxis in the Elevated Minus Maze. Behav Processes. 2013;97:76-9.

81. Yankelevitch-Yahav R, Franko M, Huly A, Doron R. The forced swim test as a model of depressive-like behavior. J Vis Exp. 2015(97).

82. Holland PC, Bouton ME. Hippocampus and context in classical conditioning. Curr Opin Neurobiol. 1999;9(2):195-202.

83. Phillips RG, LeDoux JE. Differential contribution of amygdala and hippocampus to cued and contextual fear conditioning. Behavioral neuroscience. 1992;106(2):274-85.

84. Bangasser DA, Waxler DE, Santollo J, Shors TJ. Trace conditioning and the hippocampus: the importance of contiguity. The Journal of neuroscience : the official journal of the Society for Neuroscience. 2006;26(34):8702-6.

85. Chowdhury N, Quinn JJ, Fanselow MS. Dorsal hippocampus involvement in trace fear conditioning with long, but not short, trace intervals in mice. Behavioral neuroscience. 2005;119(5):1396-402.

86. Misane I, Tovote P, Meyer M, Spiess J, Ogren SO, Stiedl O. Time-dependent involvement of the dorsal hippocampus in trace fear conditioning in mice. Hippocampus. 2005;15(4):418-26.

87. Quinn JJ, Oommen SS, Morrison GE, Fanselow MS. Post-training excitotoxic lesions of the dorsal hippocampus attenuate forward trace, backward trace, and delay fear conditioning in a temporally specific manner. Hippocampus. 2002;12(4):495-504.

88. McEchron MD, Bouwmeester H, Tseng W, Weiss C, Disterhoft JF. Hippocampectomy disrupts auditory trace fear conditioning and contextual fear conditioning in the rat. Hippocampus. 1998;8(6):638-46.

89. Han CJ, O'Tuathaigh CM, van Trigt L, Quinn JJ, Fanselow MS, Mongeau R, et al. Trace but not delay fear conditioning requires attention and the anterior cingulate cortex. Proceedings of the National Academy of Sciences of the United States of America. 2003;100(22):13087-92.

90. Castagne V, Porsolt RD, Moser P. Use of latency to immobility improves detection of antidepressant-like activity in the behavioral despair test in the mouse. Eur J Pharmacol. 2009;616(1-3):128-33.

91. Porsolt RD, Bertin A, Jalfre M. Behavioral despair in mice: a primary screening test for antidepressants. Arch Int Pharmacodyn Ther. 1977;229(2):327-36.

92. Levitt P, Eagleson KL, Powell EM. Regulation of neocortical interneuron development and the implications for neurodevelopmental disorders. Trends Neurosci. 2004;27(7):400-6.

93. Harris JC. New classification for neurodevelopmental disorders in DSM-5. Curr Opin Psychiatry. 2014;27(2):95-7.

94. Katz G, Lazcano-Ponce E. Intellectual disability: definition, etiological factors, classification, diagnosis, treatment and prognosis. Salud Publica Mex. 2008;50 Suppl 2:s132-41.

95. Cooper SA, Smiley E, Morrison J, Williamson A, Allan L. Mental ill-health in adults with intellectual disabilities: prevalence and associated factors. Br J Psychiatry. 2007;190:27-35.

96. Airaksinen EM, Matilainen R, Mononen T, Mustonen K, Partanen J, Jokela V, et al. A population-based study on epilepsy in mentally retarded children. Epilepsia. 2000;41(9):1214-20.

97. Bohmer CJ, Niezen-de Boer MC, Klinkenberg-Knol EC, Deville WL, Nadorp JH, Meuwissen SG. The prevalence of gastroesophageal reflux disease in institutionalized intellectually disabled individuals. Am J Gastroenterol. 1999;94(3):804-10.

98. Kaufman L, Ayub M, Vincent JB. The genetic basis of non-syndromic intellectual disability: a review. J Neurodev Disord. 2010;2(4):182-209.

99. Maulik PK, Mascarenhas MN, Mathers CD, Dua T, Saxena S. Prevalence of intellectual disability: a meta-analysis of population-based studies. Res Dev Disabil. 2011;32(2):419-36.

100. Centers for Disease C, Prevention. Economic costs associated with mental retardation, cerebral palsy, hearing loss, and vision impairment--United States, 2003. MMWR Morb Mortal Wkly Rep. 2004;53(3):57-9.

101. Rauch A, Hoyer J, Guth S, Zweier C, Kraus C, Becker C, et al. Diagnostic yield of various genetic approaches in patients with unexplained developmental delay or mental retardation. Am J Med Genet A. 2006;140(19):2063-74.

102. Huang J, Zhu T, Qu Y, Mu D. Prenatal, Perinatal and Neonatal Risk Factors for Intellectual Disability: A Systemic Review and Meta-Analysis. PloS one. 2016;11(4):e0153655.

103. Mattson SN, Riley EP. A review of the neurobehavioral deficits in children with fetal alcohol syndrome or prenatal exposure to alcohol. Alcohol Clin Exp Res. 1998;22(2):279-94.

104. Ornoy A, Ergaz Z. Alcohol abuse in pregnant women: effects on the fetus and newborn, mode of action and maternal treatment. Int J Environ Res Public Health. 2010;7(2):364-79.

105. Braun JM, Daniels JL, Kalkbrenner A, Zimmerman J, Nicholas JS. The effect of maternal smoking during pregnancy on intellectual disabilities among 8-year-old children. Paediatr Perinat Epidemiol. 2009;23(5):482-91.

106. Ross EJ, Graham DL, Money KM, Stanwood GD. Developmental consequences of fetal exposure to drugs: what we know and what we still must learn. Neuropsychopharmacology. 2015;40(1):61-87.

107. Bilder DA, Pinborough-Zimmerman J, Bakian AV, Miller JS, Dorius JT, Nangle B, et al. Prenatal and perinatal factors associated with intellectual disability. Am J Intellect Dev Disabil. 2013;118(2):156-76.

108. Chiurazzi P, Pirozzi F. Advances in understanding - genetic basis of intellectual disability. F1000Res. 2016;5.

109. Morris JK, Alberman E. Trends in Down's syndrome live births and antenatal diagnoses in England and Wales from 1989 to 2008: analysis of data from the National Down Syndrome Cytogenetic Register. BMJ. 2009;339:b3794.

110. Lubs HA, Stevenson RE, Schwartz CE. Fragile X and X-linked intellectual disability: four decades of discovery. Am J Hum Genet. 2012;90(4):579-90.

111. Coffee B, Keith K, Albizua I, Malone T, Mowrey J, Sherman SL, et al. Incidence of fragile X syndrome by newborn screening for methylated FMR1 DNA. Am J Hum Genet. 2009;85(4):503-14.

112. Hagerman RJ, Berry-Kravis E, Hazlett HC, Bailey DB, Jr., Moine H, Kooy RF, et al. Fragile X syndrome. Nat Rev Dis Primers. 2017;3:17065.

113. Jamra R. Genetics of autosomal recessive intellectual disability. Med Genet. 2018;30(3):323-7.

114. Hubener M, Bonhoeffer T. Neuronal plasticity: beyond the critical period. Cell. 2014;159(4):727-37.

115. Verma V, Paul A, Amrapali Vishwanath A, Vaidya B, Clement JP. Understanding intellectual disability and autism spectrum disorders from common mouse models: synapses to behaviour. Open Biol. 2019;9(6):180265.

116. Kuhl PK. Brain mechanisms in early language acquisition. Neuron. 2010;67(5):713-27.

117. Scorza CA, Cavalheiro EA. Animal models of intellectual disability: towards a translational approach. Clinics (Sao Paulo). 2011;66 Suppl 1:55-63.

118. Rosenthal N, Brown S. The mouse ascending: perspectives for human-disease models. Nat Cell Biol. 2007;9(9):993-9.

119. Prinz WA, Toulmay A, Balla T. The functional universe of membrane contact sites. Nat Rev Mol Cell Biol. 2020;21(1):7-24.

120. Lee S, Min KT. The Interface Between ER and Mitochondria: Molecular Compositions and Functions. Mol Cells. 2018;41(12):1000-7.

121. Kornmann B, Currie E, Collins SR, Schuldiner M, Nunnari J, Weissman JS, et al. An ER-mitochondria tethering complex revealed by a synthetic biology screen. Science. 2009;325(5939):477-81.

122. Kopec KO, Alva V, Lupas AN. Homology of SMP domains to the TULIP superfamily of lipid-binding proteins provides a structural basis for lipid exchange between ER and mitochondria. Bioinformatics. 2010;26(16):1927-31.

123. AhYoung AP, Jiang J, Zhang J, Khoi Dang X, Loo JA, Zhou ZH, et al. Conserved SMP domains of the ERMES complex bind phospholipids and mediate tether assembly. Proceedings of the National Academy of Sciences of the United States of America. 2015;112(25):E3179-88.

124. Kawano S, Tamura Y, Kojima R, Bala S, Asai E, Michel AH, et al. Structure-function insights into direct lipid transfer between membranes by Mmm1-Mdm12 of ERMES. J Cell Biol. 2018;217(3):959-74.

125. John Peter AT, Herrmann B, Antunes D, Rapaport D, Dimmer KS, Kornmann B. Vps13-Mcp1 interact at vacuole-mitochondria interfaces and bypass ER-mitochondria contact sites. J Cell Biol. 2017;216(10):3219-29.

126. Lee I, Hong W. Diverse membrane-associated proteins contain a novel SMP domain. FASEB J. 2006;20(2):202-6.

127. Hirabayashi Y, Kwon SK, Paek H, Pernice WM, Paul MA, Lee J, et al. ER-mitochondria tethering by PDZD8 regulates Ca(2+) dynamics in mammalian neurons. Science. 2017;358(6363):623-30.

128. Wideman JG, Balacco DL, Fieblinger T, Richards TA. PDZD8 is not the 'functional ortholog' of Mmm1, it is a paralog. F1000Res. 2018;7:1088.

129. Guillen-Samander A, Bian X, De Camilli P. PDZD8 mediates a Rab7-dependent interaction of the ER with late endosomes and lysosomes. Proceedings of the National Academy of Sciences of the United States of America. 2019;116(45):22619-23.

130. Masoudi AA, Uchida K, Yokouchi K, Ohwada K, Abbasi AR, Tsuji T, et al. Linkage mapping of the locus responsible for forelimb-girdle muscular anomaly of Japanese black cattle on bovine chromosome 26. Anim Genet. 2008;39(1):46-50.

131. Henning MS, Morham SG, Goff SP, Naghavi MH. PDZD8 is a novel Gag-interacting factor that promotes retroviral infection. J Virol. 2010;84(17):8990-5.

132. Henning MS, Stiedl P, Barry DS, McMahon R, Morham SG, Walsh D, et al. PDZD8 is a novel moesin-interacting cytoskeletal regulatory protein that suppresses infection by herpes simplex virus type 1. Virology. 2011;415(2):114-21.

133. Elbaz-Alon Y, Guo Y, Segev N, Harel M, Quinnell DE, Geiger T, et al. PDZD8 interacts with Protrudin and Rab7 at ER-late endosome membrane contact sites associated with mitochondria. Nat Commun. 2020;11(1):3645.

134. Scott CC, Vacca F, Gruenberg J. Endosome maturation, transport and functions. Semin Cell Dev Biol. 2014;31:2-10.

135. Hirokawa N. Kinesin and dynein superfamily proteins and the mechanism of organelle transport. Science. 1998;279(5350):519-26.

136. Raiborg C, Wenzel EM, Pedersen NM, Olsvik H, Schink KO, Schultz SW, et al. Repeated ER-endosome contacts promote endosome translocation and neurite outgrowth. Nature. 2015;520(7546):234-8.

137. Hu H, Kahrizi K, Musante L, Fattahi Z, Herwig R, Hosseini M, et al. Genetics of intellectual disability in consanguineous families. Mol Psychiatry. 2019;24(7):1027-39.

138. Harripaul R, Vasli N, Mikhailov A, Rafiq MA, Mittal K, Windpassinger C, et al. Mapping autosomal recessive intellectual disability: combined microarray and exome sequencing identifies 26 novel candidate genes in 192 consanguineous families. Mol Psychiatry. 2018;23(4):973-84.

139. Chan M, Eacott MJ, Sanderson DJ, Wang J, Sun M, Easton A. Continual Trials Spontaneous Recognition Tasks in Mice: Reducing Animal Numbers and Improving Our Understanding of the Mechanisms Underlying Memory. Front Behav Neurosci. 2018;12:214.

140. Sanderson DJ, Gray A, Simon A, Taylor AM, Deacon RM, Seeburg PH, et al. Deletion of glutamate receptor-A (GluR-A) AMPA receptor subunits impairs one-trial spatial memory. Behavioral neuroscience. 2007;121(3):559-69.

141. Wilmot JH, Puhger K, Wiltgen BJ. Acute Disruption of the Dorsal Hippocampus Impairs the Encoding and Retrieval of Trace Fear Memories. Front Behav Neurosci. 2019;13:116.

142. Lai DC, Tseng YC, Hou YM, Guo HR. Gender and geographic differences in the prevalence of intellectual disability in children: analysis of data from the national disability registry of Taiwan. Res Dev Disabil. 2012;33(6):2301-7.

143. Werling DM, Geschwind DH. Sex differences in autism spectrum disorders. Curr Opin Neurol. 2013;26(2):146-53.

144. Kim H, Lim CS, Kaang BK. Neuronal mechanisms and circuits underlying repetitive behaviors in mouse models of autism spectrum disorder. Behav Brain Funct. 2016;12(1):3.

145. Hill EL, Frith U. Understanding autism: insights from mind and brain. Philos Trans R Soc Lond B Biol Sci. 2003;358(1430):281-9.

146. Dachtler J, Ivorra JL, Rowland TE, Lever C, Rodgers RJ, Clapcote SJ. Heterozygous deletion of alpha-neurexin I or alpha-neurexin II results in behaviors relevant to autism and schizophrenia. Behavioral neuroscience. 2015;129(6):765-76.

147. Moy SS, Nadler JJ, Perez A, Barbaro RP, Johns JM, Magnuson TR, et al. Sociability and preference for social novelty in five inbred strains: an approach to assess autistic-like behavior in mice. Genes Brain Behav. 2004;3(5):287-302.

148. Ennaceur A, Delacour J. A new one-trial test for neurobiological studies of memory in rats. 1: Behavioral data. Behavioural brain research. 1988;31(1):47-59.

149. Seel SV, Eacott MJ, Langston RF, Easton A. Cholinergic input to the hippocampus is not required for a model of episodic memory in the rat, even with multiple consecutive events. Behavioural brain research. 2018;354:48-54.

150. Kawamoto EM, Vivar C, Camandola S. Physiology and pathology of calcium signaling in the brain. Front Pharmacol. 2012;3:61.

151. Miller KE, Suter DM. An Integrated Cytoskeletal Model of Neurite Outgrowth. Front Cell Neurosci. 2018;12:447.

152. McAllister AK. Cellular and molecular mechanisms of dendrite growth. Cereb Cortex. 2000;10(10):963-73.

153. Van Maldergem L, Hou Q, Kalscheuer VM, Rio M, Doco-Fenzy M, Medeira A, et al. Loss of function of KIAA2022 causes mild to severe intellectual disability with an autism spectrum disorder and impairs neurite outgrowth. Hum Mol Genet. 2013;22(16):3306-14.

154. Rowland AA, Voeltz GK. Endoplasmic reticulum-mitochondria contacts: function of the junction. Nat Rev Mol Cell Biol. 2012;13(10):607-25.

155. Petkovic M, Jemaiel A, Daste F, Specht CG, Izeddin I, Vorkel D, et al. The SNARE Sec22b has a non-fusogenic function in plasma membrane expansion. Nat Cell Biol. 2014;16(5):434-44.

156. Rocha N, Kuijl C, van der Kant R, Janssen L, Houben D, Janssen H, et al. Cholesterol sensor ORP1L contacts the ER protein VAP to control Rab7-RILP-p150 Glued and late endosome positioning. J Cell Biol. 2009;185(7):1209-25.

157. Eden ER. The formation and function of ER-endosome membrane contact sites. Biochimica et biophysica acta. 2016;1861(8 Pt B):874-9.

158. van der Kant R, Neefjes J. Small regulators, major consequences - Ca(2)(+) and cholesterol at the endosome-ER interface. J Cell Sci. 2014;127(Pt 5):929-38.